

FRESHM Zeeland

**FREsh Salt groundwater distribution by Helicopter
ElectroMagnetic survey in the Province of Zeeland**

Date	Author	Initials	Review	Initials	Approval	Initials
27 June 2017	Esther van Baaren (Deltares)		Perry de Louw (Deltares)			
	Joost Delsman (Deltares)					
	Marios Karaoulis (Deltares)					
	Pieter Pauw (Deltares)					
	Tommer Vermaas (Deltares)					
	Huite Bootsma (Deltares)					
	Perry de Louw (Deltares)					
	Gualbert Oude Essink (Deltares)					
	Willem Dabekaussen (TNO)					
	Jan Gunnink (TNO)					
	Wim Dubelaar (TNO)					
	Armin Menkovic (TNO)					
	Bernhard Siemon (BGR)					
	Annika Steuer (BGR)					
	Uwe Meyer (BGR)					

State**draft**

This is a draft report, intended for discussion purposes only. No part of this report may be relied upon by either principals or third parties.

Summary

Surrounded by estuaries and the North Sea, and with its limited fresh groundwater reserves, the availability of freshwater is not evident in the province of Zeeland in the Netherlands. The groundwater system is predominantly saline due to recent marine transgressions. Surface water on the islands is often salinised by saline groundwater seepage. There is some fresh groundwater available in fresh groundwater lenses, but the spatial variation in thickness of these lenses is high. Knowledge about the availability of the scarce fresh groundwater is essential for agriculture, water managers, drinking water companies, industry, environmental organisations and scientists. In order to have a reference situation, to know where the groundwater is fresh and where saline and to preserve and sustainable use the valuable fresh water, a three-dimensional mapping of the fresh-brackish-salt distribution of groundwater is important; such a mapping is made within the project FRESHEM Zeeland.

FRESHEM Zeeland is short for FRESH Salt groundwater distribution by Helicopter ElectroMagnetic survey in the Province of Zeeland. The FRESHEM project established a detailed, spatially consistent and validated image of the fresh-salt distribution of the groundwater system, based on helicopter-borne electromagnetic measurements (HEM). Compared to previous large scale HEM mapping campaigns, FRESHEM additionally provides (1) a quantitative translation of HEM-measured resistivity profiles to groundwater salinity, (2) a novel approach to interpolation of measurements to a 3D result, aimed at preserving small-scale linear features in the data (creek ridges), (3) a rigorous approach to quantitatively assess the uncertainty of the end-result and (4) a validation with different ground truth measurements.

The FRESHEM airborne surveys were flown within three two-week periods in 2014 and 2015, in addition to the two one-week surveys of the CLIWAT project flown in 2009. 9640 flight kilometres resulted in 14.4 million data points and 1700 km² of mapped chloride distribution of the groundwater.

The FRESHEM datasets consists of:

1. 2D results of probability of groundwater chloride concentration classes along flightlines, ~4m horizontal resolution, vertical resolution ranging from several decimetres to several metres,
2. 3D results of probability of groundwater chloride concentration classes, 50*50m² horizontal resolution, 0.5 m vertical resolution,
3. derived maps such as depth of 150 mg Cl/l and 1500 mg Cl/l boundary.

The depth range of the FRESHEM datasets varies between 30 metre in clay areas with saline groundwater up to 160 metres in sandy areas with fresh groundwater. There is no data above build-up areas: measurements would have been disturbed and low-level flights above urban areas were not allowed by the obtained permits.

For each dataset three values are available: the p50 value of the probability function of the groundwater chloride concentration is called the 'middle' value. The p25 value is the 'low' value and p75 the 'high' value. The uncertainty in the thickness of the fresh groundwater lens is represented by the difference between the 'low' and 'high' value. This uncertainty increases in areas with no-data: above power lines, railways, roads, build-up areas and radar installations. In most areas, where good data collection was possible, the uncertainty is generally less than 2 meter or less than 20% of the depth of the fresh-salt boundary of FRESHEM 'middle'.

The final 3D result was validated with the chloride concentration from 1294 monitoring wells, the thickness of the freshwater lens from 178 geophysical measurements and the presence of saline groundwater in the shallow subsurface from 41 TEC probe measurements. Using a classification of 'fresh' (< 1500 mg/L Cl), 'brackish' (1500 – 10000 mg/L Cl), and 'salt' (>10000 mg/L Cl), 78% of measured chloride points from monitoring wells are in agreement with the HEM 'middle' result (88% of measured chloride points fall within bounds given by HEM result 'low' and 'high'). These percentages increase with depth since local effects are often only present at shallow depth. The following should be kept in mind when using the FRESHEM result. The FRESHEM result gives accurate, but not perfectly accurate information on the chloride distribution in Zeeland. The result is more reliable in fresh and saline zones, and less reliable in brackish zones. The result should be interpreted cautiously when looking at local features: it should for example not be used to estimate the chloride distribution around ditches.

For Zeeland, the FRESHEM result gave more insight into the fresh-salt distribution of the groundwater. 20-30% of Zeeland has a fresh groundwater lens (<1500 mg Cl/l) with a thickness of more than 15 m. 35-50% of Zeeland has no or only a small fresh groundwater lens (<1500 mg Cl/l). Previously unknown fresh groundwater resources have been found, some freshwater lenses are smaller than previously assumed and large extents of freshwater occurring below saline groundwater and off-shore fresh groundwater were found. The detailed knowledge on the groundwater salinity distribution provided by FRESHEM Zeeland is a basis for improved groundwater management, such as licensing of groundwater extractions and designing measures for aquifer storage and recovery. The quantification of the uncertainty can guide the use of the FRESHEM results, for instance when planning and designing measures.

This study resulted in recommendations for future Airborne EM surveys for fresh-saline groundwater distribution. Since line kilometres are expensive it is recommended to carefully design the flight plan. In areas where no small freshwater lenses are expected, it is recommended to choose a bigger distance between the flightlines. In areas where differences are expected (for example large groundwater extractions, sandy creek ridges) it is recommended to fly across and perpendicular to the fresh or saline features. In areas where differences between fresh and saline groundwater are expected but the exact location is unknown (but important), 100 metre between the flightlines is recommended. Further research is necessary to apply the FRESHEM approach to other areas. It is recommended to extend the approach to characterise the surface conductivity and intrinsic formation factor to other areas, in order to translate resistivity data into groundwater salinity. Uncertainty is mainly caused by the inversion, surface conductivity, lithology and interpolation; more knowledge about each these factors can improve the uncertainty of the end-result.

Contents

1 Introduction	9
1.1 Background	9
1.1.1 Fresh water availability Zeeland	9
1.1.2 FRESHEM	10
1.1.3 FRESHEM Zeeland	10
1.2 Products	11
1.3 General methodology	11
1.4 Definition fresh-brackish-saline groundwater	13
2 Geological and hydrogeological genesis of Zeeland	15
2.1 Introduction	15
2.2 Geological setting of Zeeland	15
2.2.1 Pre-Holocene	15
2.2.2 Holocene	15
2.3 Hydrogeology and the current distribution of fresh and saline groundwater	18
2.3.1 Regional hydrogeology	18
2.3.2 Freshening and salinisation processes	19
3 Ground truth measurements	23
3.1 Theory and general procedure	23
3.1.1 TEC probe measurements	23
3.1.2 Cone penetration tests	23
3.1.3 Open hole geo-electrical borehole logging measurements	24
3.1.4 Vertical electrical sounding (VES)	24
3.1.5 Continuous Vertical Electrical Sounding (CVES)	24
3.1.6 EM-Slimflex	25
3.1.7 Chloride analyses groundwater	26
3.2 Measurements used for validation and calibration	26
4 3D geological model GeoTOP	28
4.1 Introduction	28
4.2 Data used	28
4.3 Method	28
5 Data acquisition: Helicopter-borne electromagnetics	31
5.1 Introduction	31
5.2 Airborne geophysical system	31
5.3 Airborne surveys	34
6 Data processing	38
6.1 Introduction	38
6.2 Calibration, phase & gain correction	39
6.3 Zero-level drift correction	39
6.4 Microlevelling	39
6.5 Data corrections, reduction of man-made effects	40
6.6 Data quality assessment	40
7 Data processing: Inversion	43

7.1	Introduction	43
7.2	Forward calculation	43
7.3	Inversion	43
7.3.1	Homogeneous half-space	44
7.3.2	Layered half-space	45
7.4	Selection of inversion approaches	47
7.4.1	Conclusions from pilot study Canal zone Gent-Terneuzen	47
7.5	Assessment of HEM inversion options using groundtruth data	47
7.5.1	Final selection of inversion methods	48
8	Transformation of bulk resistivity to groundwater chloride concentration	49
8.1	Theory	49
8.2	Determination of formation factors	51
8.2.1	Introduction	51
8.2.2	Methods	51
8.2.3	Results	53
8.2.4	Discussion	55
8.3	Calculation of groundwater chloride concentration within a Monte Carlo uncertainty approach	56
8.3.1	Inversion result: bulk conductivity	57
8.3.2	Obtain lithoclass from GEOTOP	57
8.3.3	Obtain formation factor and surface conductivity for lithoclass	57
8.3.4	Calculate pore water conductivity	58
8.3.5	Calculate chloride concentration	58
8.4	Results	59
9	3D interpolation	61
9.1	Introduction	61
9.2	Resampling the 2D dataset	61
9.3	Model boundaries	61
9.4	3D interpolation of chloride probability distribution	62
9.4.1	Interpolation method	62
9.4.2	Neighbourhood	64
9.4.3	The semivariogram	64
9.5	Anisotropy	66
9.5.1	Necessity	66
9.5.2	Quantifying anisotropy	69
9.5.3	Interpolation with anisotropy: a qualitative analysis	73
9.5.4	Interpolation with anisotropy: quantitative analysis	77
10	Parameter and interpolation uncertainty	79
10.1	Parameter contributions to uncertainty	79
10.1.1	Approach	79
10.1.2	Result	80
10.1.3	Relative contribution spatial uncertainty to complete uncertainty of the 3D model	83
10.2	Flightline resolution	85
11	Results	89
11.1	Uncertainty: 'low', 'middle' and 'high'	89
11.2	2D result FRESHEM Zeeland	89

11.3	3D result FRESHEM Zeeland	91
11.4	Boundary maps	92
11.4.1	Fresh groundwater	93
11.4.2	Saline areas	94
11.4.3	Uncertainty	95
11.5	Comparison with previous maps	96
11.5.1	Density dependent groundwater model	96
11.5.2	Map of Waterboard Scheldestromen used for groundwater extraction permits	98
11.6	Fresh below saline groundwater	99
11.6.1	Introduction	99
11.6.2	Method	99
11.6.3	Results	100
11.6.3.1	Fresh groundwater extending out into the sea	100
11.6.3.2	Flow of fresh groundwater below low permeable sediments along the landward side of the dunes and below the creek ridges.	101
11.6.3.3	Thin layer of saline groundwater in the clay and peat layer near Bruinisse (Schouwen-Duiveland), Tholen, St. Philipsland, East of Schelde-Rijnkanaal (Noord Brabant), and at the Brabantse Wal.	103
11.6.3.4	Saline groundwater on top of old marine deposits in Zeeuws-Vlaanderen	105
11.7	New insights in lithology	106
11.7.1	Resistivity differences within fresh water bodies	106
11.7.2	High chloride concentration as proxy for clay extent	108
11.7.3	Freshening of groundwater as a proxy for clay discontinuity	109
11.7.4	Width of the fresh water at creek ridges as an indication of clay occurrence	110
11.8	Comparison with fixed Ω_m boundary	111
12	Validation	115
12.1	Summary	115
12.2	Chloride measurements	116
12.2.1	Data and methods	116
12.2.2	Results	118
12.3	Geophysical ground measurements	120
12.3.1	Data and methods	120
12.3.2	Results	121
12.4	TEC probe	125
12.4.1	Data and methods	125
12.4.2	Results	125
12.5	Discussion	126
12.5.1	Chloride measurements	126
12.5.2	Geophysical ground measurements	126
12.5.3	TEC probe	127
13	Conclusions and recommendations	128
13.1	General conclusions	128
13.2	Conclusions regarding the result in Zeeland	128
13.3	How does the FRESHEM result compare to ground-truth measurements?	129
13.4	What methodological advances were made in FRESHEM?	129
13.5	Recommendations for freshwater management in Zeeland	131
13.6	Recommendations for future Airborne EM surveys	131

13 June 2017, draft

Deltares

13.7 Recommendations for further research	132
14References	134

1 Introduction

1.1 Background

1.1.1 Fresh water availability Zeeland

The availability of fresh water is not evident in the province of Zeeland in the Netherlands (Figure 1.1a). The groundwater system is predominantly saline due to old marine deposits and transgressions. The estuaries and the sea (Figure 1.1b) are saline and ditches are mainly saline due to seepage from the saline groundwater. There is some fresh groundwater available: larger (40 - 160 metres thick) freshwater lenses in the dunes, smaller (5 - 40 metre thick) freshwater lenses in creek ridges and thin (<5 metre thick) rainwater lenses in salty marshes. The spatial variation in thickness of freshwater lenses is high; therefore a three-dimensional mapping of the fresh-brackish-salt distribution of groundwater is desirable.

Agriculture is largely dependent on fresh water as saline water in the root zone causes salt damage to crops that are not salt tolerant. No irrigation causes drought damage to crops and irrigation with saline water causes salt damage. In environmental areas, the salt concentration of the water determines the ecological possibilities. The availability of fresh water is also important for drinking water and industry. Recently, the subsoil in Zeeland is used for freshwater storage: underground storage of fresh water in times of water surplus for use in times of water shortage (GO-FRESH.info, Oude Essink, 2014). An accurate mapping of the fresh-brackish-salt distribution of groundwater is essential for these functions and utilizing the opportunities of the subsurface.

Other applications of mapping the salinity of the groundwater are optimization of the surface water system (water supply, flushing) and calibration of groundwater models. Additionally, the awareness of the current salinity of the groundwater can be increased and the mapping provides knowledge of the influence of saltwater basins (eg Grevelingen) on the groundwater system. The latter provides knowledge for basins that can become saline in the future like the Volkerak Zoommeer.

Finally, the mapping of the current groundwater situation can be used as a reference situation for locations where interventions in the landscape or infrastructure may affect the fresh-salt-salt distribution of groundwater. Examples of interventions include the new lock at the Ghent Terneuzen Canal and nature development in Hedwigepolder, Perkpolder, Rammegors and Waterdunen. The mapping of the current situation can be compared with the post-intervention situation, which can determine whether salinisation of groundwater has taken place.

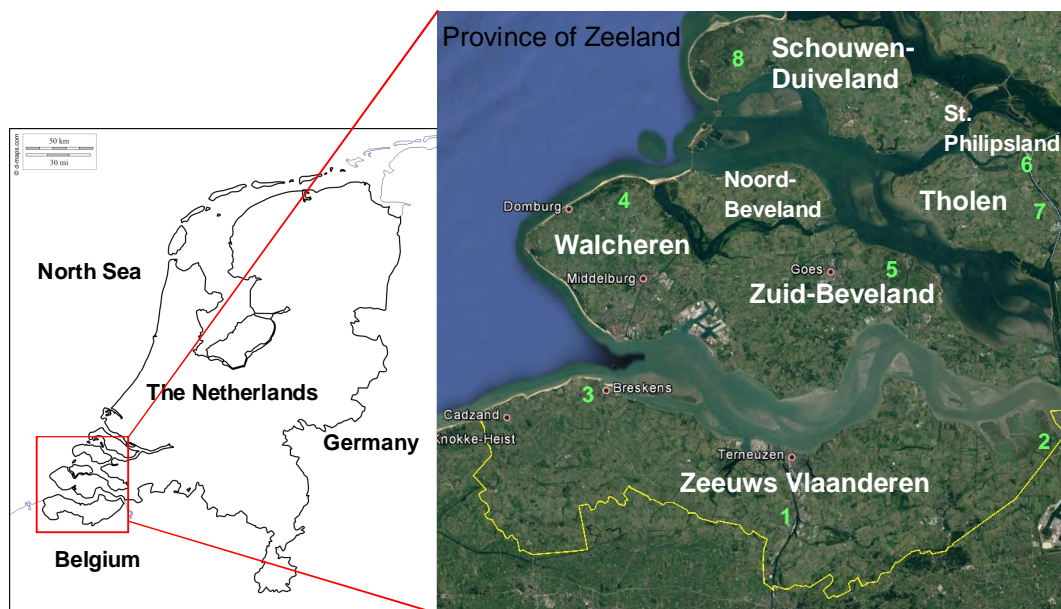


Figure 1.1 a. location of the Province of Zeeland in the Netherlands and b. the names of the islands and sub regions of Zeeland. The numbers in green correspond with the high resolution areas (section 1.1.3).

1.1.2 FRESHEM

FRESHEM stands for FRESH Salt groundwater distribution by Helicopter ElectroMagnetic survey.

The FRESHEM project aims to establish a detailed, spatially consistent and validated image of the fresh-salt distribution of the groundwater system, based on helicopter-borne electromagnetic measurements (HEM). HEM offers a relatively cheap (compared to ground measurements) and fast way to map the resistivity of the subsurface, a proxy for groundwater salinity, over large areas. FRESHEM results are presented in groundwater chloride concentration (mg/l), as chloride concentration is the parameter stakeholders (both water users and managers) are historically most familiar with and existing guidelines are based on.

Compared to previous HEM mapping campaigns, FRESHEM additionally provides (1) a quantitative translation of HEM-measured resistivity profiles to groundwater salinity and chloride concentration, (2) a novel approach to interpolation of measurements to a 3D result, aimed at preserving small-scale linear features in the data (creek ridges), (3) a rigorous approach to quantitatively assess the uncertainty of the end-result and (4) a validation with different ground truth measurements.

The final result of FRESHEM is the 3D density distribution of the chloride concentration of the groundwater. There is no data above build-up areas: the measurements will be disturbed and the permit does not allow flying low above these areas.

1.1.3 FRESHEM Zeeland

In October 2014, on behalf of the Province of Zeeland, Rijkswaterstaat, National government (Deltafonds), Evides, Waterboard Scheldestromen, Southern Agriculture and Horticulture Organization (ZLTO), the Flemish Dutch Scheldt Committee (VNSC) and the municipalities of Zeeland the research program FRESHEM Zeeland started. FRESHEM Zeeland stands for FRESH Salt groundwater distribution by Helicopter ElectroMagnetic survey in the province of

Zeeland. The executive knowledge organisations are the Dutch Deltares and TNO and the German Bundesanstalt für Geowissenschaften und Rohstoffe (BGR). They funded research aspects of the program and the scientific products. The final datasets are publicly available since May 2017 (scheldestromen.nl/zoetzout or zeeland.nl/zoetzout).

Above the entire province a survey was carried out in the years 2014 and 2015 with a resolution of 300 metres between the flightlines. A higher resolution (100 or 200 metres) has been used for some predetermined areas of interest (see Figure 1.1b):

1. Kanaalzone Gent-Terneuzen
2. Hedwigepolder
3. Waterdunen
4. Walcheren and Waterhouderij Walcheren
5. Kapelle-Wemeldinge
6. Rammegors
7. Eendracht
8. Kop van Schouwen

The measurements are carried out once since the fresh-brackish-saline distribution of the groundwater system is relatively constant in time. Seasonal differences in the thickness of the freshwater lens are small (De Louw, 2013; Pauw, 2015; Oude Essink, 1996; Eeman, 2012). Natural salinisation or freshening of the groundwater system is a slow process, but man-made effects can cause a speed-up of this process (f.e. extractions, changes in infrastructure, increase groundwater heads).

1.2 Products

FRESHEM Zeeland consists of three main products:

1. 3D chloride concentration voxel model entire province except build-up areas:
 - a. horizontal resolution 50*50m² and vertical resolution 0.5m;
 - b. every voxel has a value 'low', 'middle' and 'high'. Uncertainty is represented by 'middle' and 'high';
 - c. Digitally available for iMOD, GIS and as a *.csv file.
2. 2D chloride concentration along the flightlines:
 - a. horizontal resolution ~4m and vertical resolution varies from several decimetres up to several metres (increases with depth);
 - b. every cell has a value 'low', 'middle' and 'high'. Uncertainty is represented by 'middle' and 'high';
 - c. Digitally available as a *.csv file and in *.png for every flightline.
3. Boundary maps with depth of a certain chloride boundary:
 - a. boundaries 150, 300, 1000, 1500, 3000 and 10000 mg Cl/l;
 - b. referenced to surface level and to NAP (Dutch mean sea level).

1.3 General methodology

Procedural steps in the general methodology are outlined in Figure 8.1, each of these steps is further described in the following chapters of this report. A concise outline is presented here.

Helicopter-borne Electromagnetics (HEM) measures the response in the subsurface of an emitted electromagnetic field, using a measurement device carried by helicopter. The electromagnetic field is emitted (and measured) at 6 different frequencies, each penetrating to a different depth in the subsurface, providing vertical resolution. Flightlines cover the entire province of Zeeland, excluding build-up areas, roads and high-voltage power cables where no reliable measurement can be made. Measurements are taken approximately every four metres along a flightline. Flightline density is generally 300 m, while some areas were flown

with 200 and 100 m flightline separation (chapter 5). Raw measurement data are then elaborately processed to remove measurement errors and artefacts of e.g. drift in the instruments (chapter 6).

Processed raw measurements are then mathematically inverted to obtain vertical profiles of resistivity of the subsurface (reciprocal of electrical conductivity) for each measurement point. Mathematical inversion in short entails the fitting of the response of simple models (vertical layering and properties) of the subsurface to the measured data. The inversion process can be done in several ways and with different settings. The inversion process is ill-posed (more parameters to fit than available data) and non-unique, this step is therefore prone to uncertainty (chapter 7). Inversion of the HEM measurements yields a vertical profile of the *bulk* resistivity of the subsurface, i.e. the resistivity of the entire soil-groundwater matrix.

Bulk subsurface resistivity, or its reciprocal, bulk electrical conductivity, is a good proxy for groundwater salinity, but the presence of clay also contributes to the bulk electrical conductivity of the subsurface and must be accounted for. In addition, the effective porosity of the soil (what part of the soil is conductive groundwater, and what part is the solid) must be known to derive the electrical conductivity of the groundwater from the bulk electrical conductivity. Both the presence of clay particles (accounted for in the so-called surface conductivity of the soil), and the effective porosity (accounted for in the so-called formation factor) are lithological properties. In Zeeland, detailed information on the lithological build-up of the subsurface is present in the 3D GeoTOP lithological model. GeoTOP is presented in chapter 4. In FRESHEM, we developed a new dataset of values for the formation factor and surface conductivity for each of the lithological classes present in GeoTOP based on laboratory measurements of representative soil samples (chapter 8.2). Groundwater salinity is then calculated from vertical profiles of bulk resistivity by applying formation factor and surface conductivity values for the lithoclasses present in GeoTOP for that particular location. Groundwater chloride concentration is subsequently calculated from groundwater salinity using a well-established linear relation between chloride concentration and salinity (chapter 8). Groundwater chloride concentration is presented in classes, to facilitate interpolation (see further), and to not suggest unwarranted precision.

Up to this stage, results are generated for HEM measurement locations (4 m intervals along flightlines). These results are then interpolated to obtain a full 3D distribution of fresh and salt groundwater. This interpolation is, however, not straightforward. Both the distribution of measurement points (strongly clustered along flightlines), and the distribution of chloride concentration (strong bi-modal distribution of fresh and salt water, relatively low amount of brackish water) pose problems. This is especially problematic given the importance of small, linear features of fresh water present in creek ridges. An interpolation approach was developed based on indicator kriging to preserve the bi-modal distribution of fresh and salt, and the derivation of a laterally-varying anisotropy field to preserve small-scale linear features (chapter 9). End-result is a 50 x 50 x 0.5 m 3D voxel model of groundwater chloride concentration.

Many steps in this approach are to a certain extent uncertain, and hence so is the final outcome. To assess the uncertainty in the FRESHEM results, the above methodology is not performed deterministically, but in a probabilistic way. This entails using a Monte Carlo procedure to include the uncertainty in the inversion (three different inversion results were included chapter 7), the lithology (GeoTOP probabilities), formation factor and surface conductivity (distributions of both based on laboratory results), and the salinity-chloride conversion, and produce probabilities of chloride concentration at each measurement location

(chapter 8). The 3D interpolation then interpolates the probability of classes groundwater chloride concentration occurring in a given voxel (chapter 9). While full probabilities are available, presented most are the p25 (low), p50 (median) and p75 percentile results. This methodology is also used to assess the contributions of the different parameters to the uncertainty of the end-result, by sequentially treating each parameter as the only stochastic parameter. This analysis is performed for a study area located in the west of Walcheren (chapter 10).

In a final step, FRESHEM end-results are validated using available ground measurements, both groundwater chloride analyses and different types of geophysical measurements. Measurements were available both in provincial databases and at Deltares and TNO. Chapter 3 describes the available measurements and measurement techniques. The validation focuses on the parameters most of interest to stakeholders: the prediction of the groundwater chloride concentration class, and the depth of the fresh-saline boundary. For the former, a site-by-site comparison is made between available groundwater chloride analyses and the chloride class predicted in the 3D result. For the latter, start and end of the fresh-salt boundary of different geophysical measurement techniques (notably ECPT, borehole logging) is compared to the start and end of the fresh-salt boundary derived from the HEM measurements.

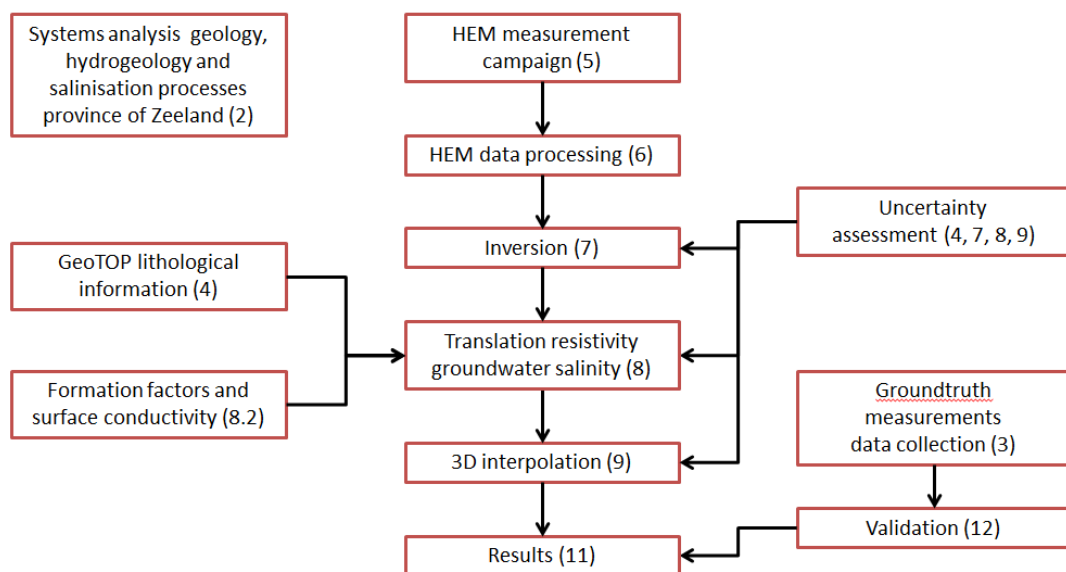


Figure 1.2 Procedural steps in the FRESHEM methodology, numbers between brackets refer to chapters in this report where these steps are further described.

1.4 Definition fresh-brackish-saline groundwater

Some common boundaries of the chloride concentration are shown in Table 1.1. This is the classification of (Stuyfzand, 1986) for drinking water and the salt damage thresholds according to (Maas, 1977) for agricultural crops. For more information about these salt damage thresholds of agricultural crops see (Stuyt, 2013). Saline ground- and surface water is so common in Zeeland that a different definition is used than for other parts of the Netherlands: the term agricultural fresh water is often used for water below 1500 mg Cl/l.

Table 1.1 Fresh-brackish-saline boundaries for drinking water and agriculture.

Description	Choloride concentration [mg Cl/l]
Classification from Stuyfzand (Stuyfzand, 1986)	
Fresh	< 150
Fresh-brackish	150 – 300
Brackish	300 – 1000
Brackish – saline	1000 – 10000
Saline	> 10000
Salt damage threshold agricultural (Maas, 1977)	
Sensitive crops	300
Moderately sensitive crops	600
Moderately tolerant crops	1200
Tolerant crops	2400
Reference concentrations	
Rhine waters that crosses the border	100
Most used limit for drinking water	150
Maximum salt content VZM, current situation	450
Limit between fresh and brackish groundwater as used in the province of Zeeland	1500

2 Geological and hydrogeological genesis of Zeeland

2.1 Introduction

This chapter describes the geological and hydrogeological genesis of the province of Zeeland, which has influenced the current distribution of fresh and saline groundwater to a large extent. Knowledge of the geological and hydrogeological genesis is important for the interpretation of the FRESHEM results. This knowledge is also indispensable for a sustainable use of the freshwater reserves in the province.

2.2 Geological setting of Zeeland

2.2.1 Pre-Holocene

The province of Zeeland is located at the edge of the subsiding North sea basin. Older deposits display a general dip towards the northeast, with an increasing angle for older deposits (Van Rummelen, 1965). The Paleogene and Neogene formations consist of shallow marine deposits, fine- to medium-grained sand and marine clays. Important for the local hydrology is the low conductivity Boom Member of the Rupel Formation, consisting of stiff marine clays. Because of the dip towards the northeast, Neogene and Paleogene marine units are present in Zeeuws-Vlaanderen at the surface up to some tens of metres below surface level, while they are present much deeper in the rest of Zeeland (see Figure 2.1). On top of the Paleogene and Neogene deposits several Pleistocene Formations are present. Among these are the Waalre Formation (estuarine sand and clay layers), the Eem Formation (marine fine- to medium-grained sand) and the Boxtel Formation (aeolian sands and silts). The youngest deposits belong to the Holocene Formations.

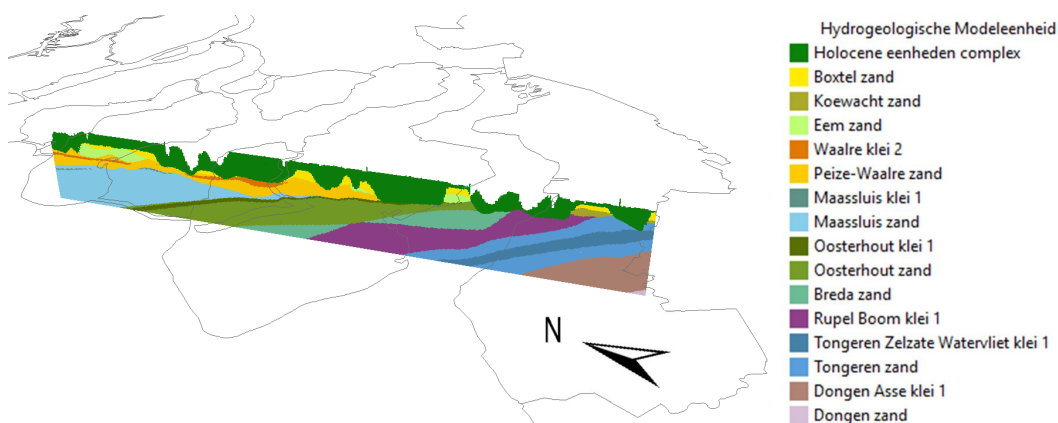


Figure 2.1: Birds-eye-view from the southwest on the deeper subsurface of Zeeland (TNO-GSN, in press). Displayed is a North-South cross-section with hydrogeological units to a depth of 100m below Dutch Ordnance Datum (NAP).

2.2.2 Holocene

The Holocene geological history of Zeeland is largely influenced by processes that are related to the rising sea level in the last 10.000 year (see Figure 2.2). In the period between 10.000 and 8000 BC the deeper parts of the North Sea were flooded. The land surface of Zeeland was still dry and consisted mainly of medium-grained sand forming an undulating relief with occasional ridges of dunes that reach several metres in height. The river Scheldt flowed in a northerly direction along the Brabantse Wal until the confluence with the Rhine-Meuse system south of Rotterdam. The rising sea level caused a rise of the groundwater level, inducing the

growth of peat bogs in the lower lying parts of Zeeland. The lateral growth of the peat bogs was congruent with the rising sea level in a southeast direction, towards higher lying areas (see Figure 2.4: a). The layer of peat that was formed is called Basal peat (Basisveen, see Figure 2.3).

The influence of the rising sea level was first noticeable in the lower lying parts in the north of Zeeland. Here, tidal channels and tidal flats were developing, with a lagoon just north of the peat bogs. The lagoon slowly spread on top of the Basal peat, and an approx. 2m layer of fine-grained sediments (silts and clays) was deposited on top of the peat. Sand, transported in the tidal channels, and the silt- and clay-layers belong to the Wormer member and are part of the Naaldwijk Formation (see Figure 2.3).

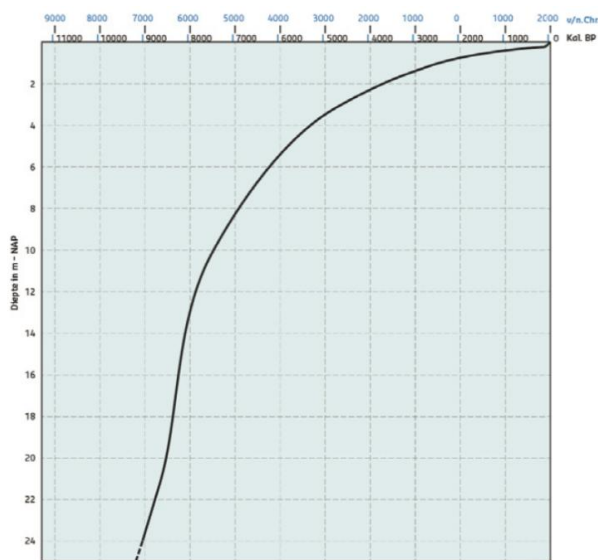


Figure 2.2: Sea level curve for the western Netherlands (from Vos & De Vries 2013).

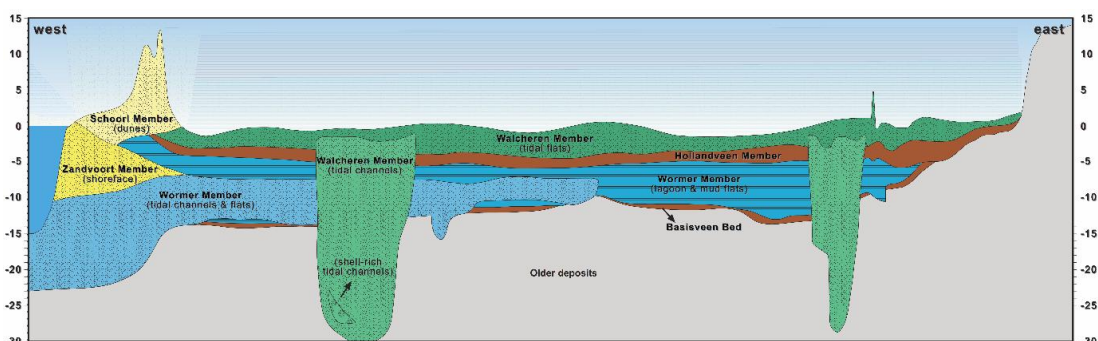


Figure 2.3: Conceptual West-East cross-section through Zeeland of holocene units (Stafleu et al. 2011).

At about 4500 BC the tidal area experienced significant changes. The open coast with broad tidal inlets was largely blocked by an elongated, relatively small zone of barrier beaches and low dunes. The basin behind the barrier beaches was filled in the next 500 years by sedimentation and extensive peat bogs developed on the higher Pleistocene grounds in the south and east, classified as Hollandveen (see Figure 2.3 and Figure 2.4b). The decreasing speed of sea level rise is an important factor in these events, as sedimentation is able to keep

up with the rising sea level, causing the filling of and subsequent formation of peat in the tidal basin. The river Scheldt was important for the drainage of the peat bogs that formed, flowing into the sea at the location of the current Oosterschelde.

From about 2500 BC the barrier beaches were breached during storm surges. The drainage of the peat bogs was improved and this made large parts of the area suitable for habitation. At the same time, improved drainage caused the process of lowering surface levels due to peat oxidation and compaction of the sediments. The lower surface elevation enabled the sea to spread across the land once again.

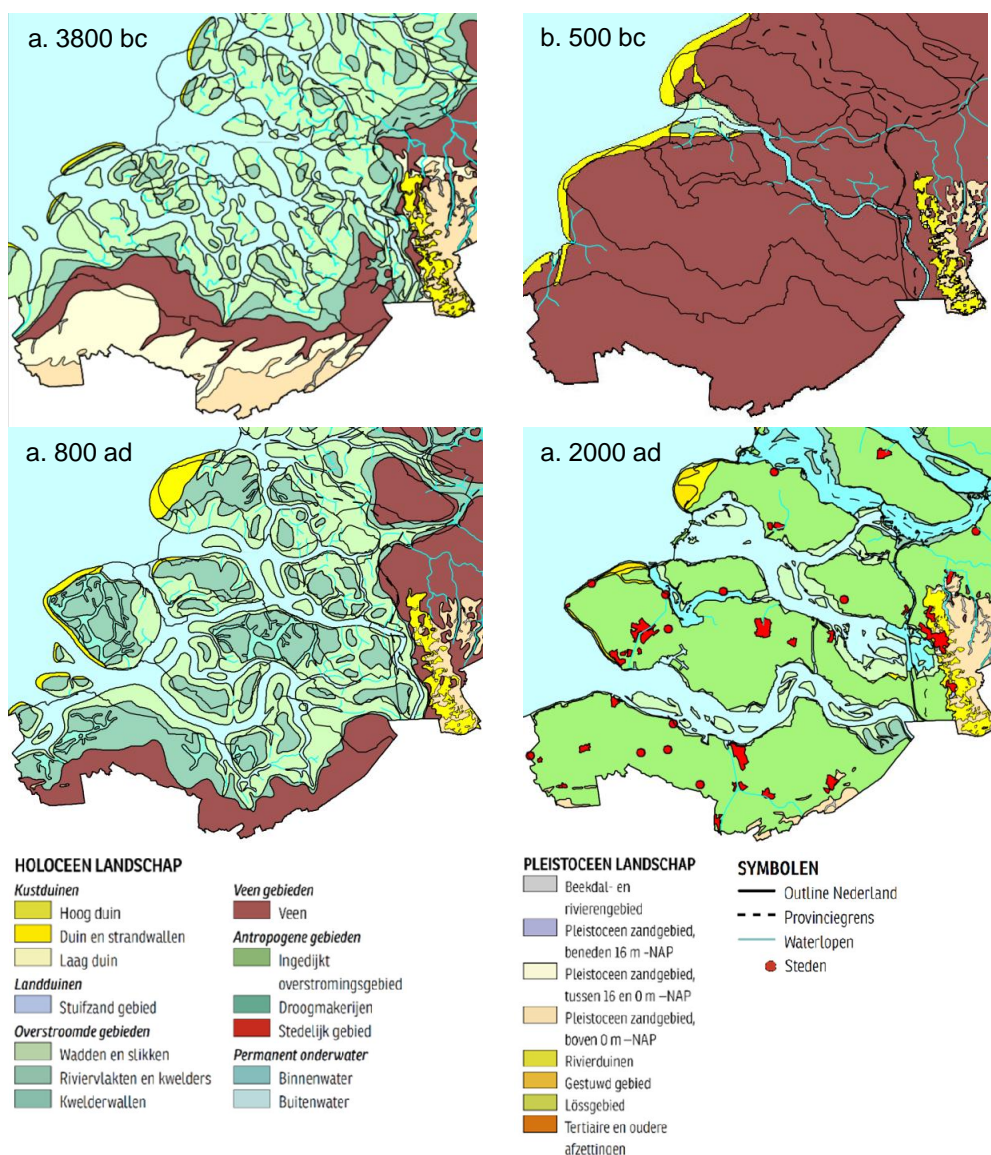


Figure 2.4: Palaeogeographical maps of Zeeland, from Vos & De Vries (2013).

At about 1000 BC Zeeland had become a large tidal basin where tidal channels eroded deep into the already present sediments (see Figure 2.4c). The sandy deposits that filled the tidal

channels and the clay that was deposited on the tidal flats belong to the Walcheren Member of the Naaldwijk Formation (see Figure 2.3). Through construction of mounds and later dikes on the relatively high tidal flats, inhabitants tried to defend themselves against the rising sea. Periods of storm surges and loss of land were compensated for by the embankment of new areas (see Figure 2.4). In the tidal clay dominated areas, sandy bodies of tidal channels can be present. Drainage has resulted in a lowering of surface level of the clay and peat on both sides of the creek system, which makes for the present pattern of creek ridges that are elevated relative to their surroundings (see Figure 2.5).

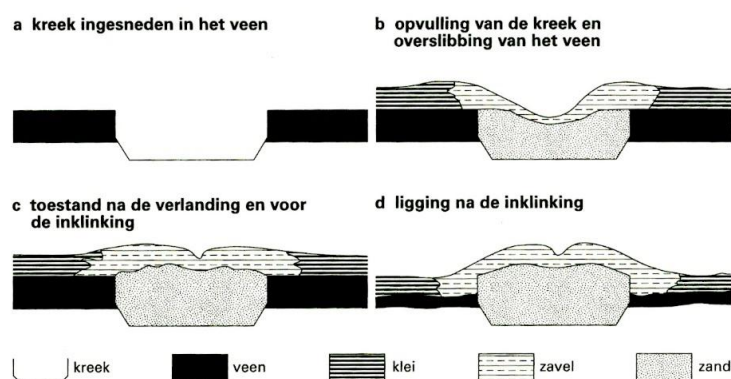


Figure 2.5: Development of a creek ridge (schematic). a) incision of a channel in underlying sediments; b and c) clay is deposited on the flats and sand fills the channel; d) a high creek ridge after drainage and settlement (naar Berendsen, 2000).

2.3 Hydrogeology and the current distribution of fresh and saline groundwater

2.3.1 Regional hydrogeology

In Figure 2.6 regional hydrogeological cross section extending from Zeeuws Vlaanderen to Zuid-Beveland is shown (Goes en Vernes, 2000). The dipping Neogene and Paleogene layers (denoted as 'deep') are clearly visible here. The clay-rich layers form the confining layers, the sandy layers the confined aquifers regional groundwater flow of fresh, brackish, and saline groundwater takes place, approximately from south (Belgium, the recharge area) to north. In the east, there is regional flow of fresh groundwater from the province Noord-Brabant into the direction of Zeeland.

On top of the dipping Neogene and Paleocene layers, shallow fresh and saline groundwater flow systems are present. The saline groundwater mainly originates from Holocene transgressions. Locally, saline surface water systems like the Oosterschelde recharge the saline groundwater flow systems. Discharge of the saline groundwater takes place in (deep) ditches and canals. The groundwater flow is in general relatively slow. Fresh groundwater flow systems are present below the dune areas and the creek ridges.

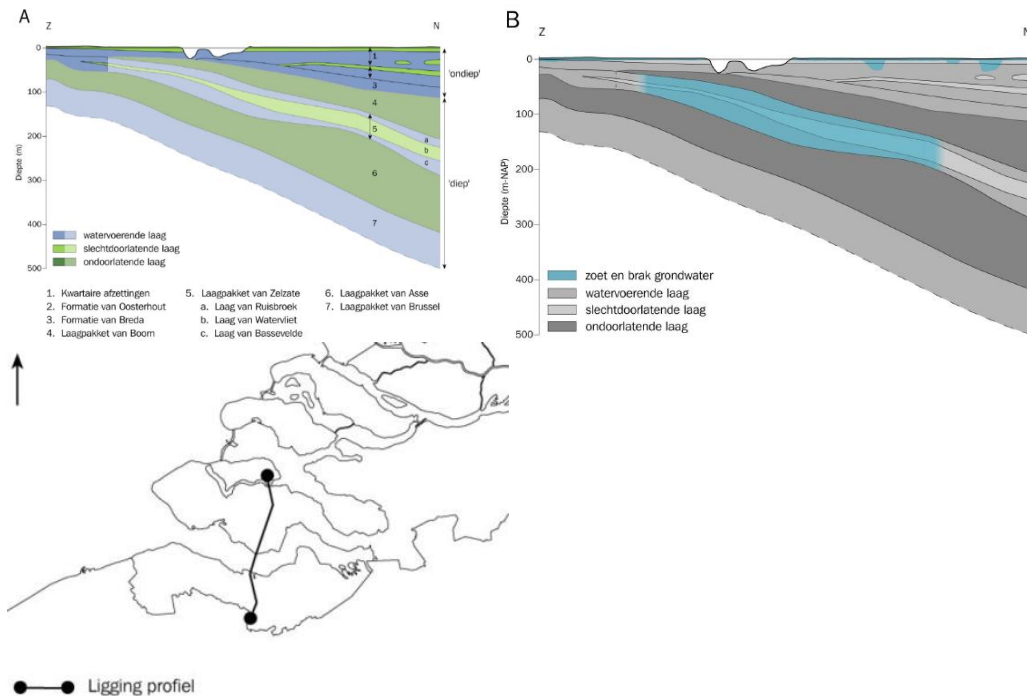


Figure 2.6: Regional cross section extending from Zeeuws-Vlaanderen (left) towards Zuid-Beveland (right). From: Goes en Vernes, 2000. REGIS Zeeland Deelrapport C: Zoet, brak en zout grondwater. In A, the green layers indicate the aquitards, whereas the blue layers indicate the aquifers. Names of the corresponding formations and member are also indicated. Below A the location of the transect can be seen. In B, blue denotes fresh and brackish water. The grey layers correspond to the aquifers and aquitards as indicated in A.

2.3.2 Freshening and salinisation processes

The Holocene genesis of Zeeland has determined the current salinity distribution in the shallow groundwater flow system to a large extent. During the last Ice Age (Weichselien, from 116.00 to 11700 B.P.) and in the beginning of the Holocene, Zeeland is not influenced by the sea and fresh groundwater infiltrates into the subsurface. Given the length of this period, it is likely that most of the shallow aquifers contained fresh groundwater. Upon a rise of the sea level during the Holocene, Zeeland is gradually influenced by the sea. Sediments are being deposited in a saline environment. In addition, saline groundwater intrudes into the subsurface. Driven by its higher density, the saline groundwater displaces and salinises the fresh groundwater. This process is called free convection. From previous studies (e.g., Gieske, 1991; Post, 2003, Delsman et al., 2014) we know that free convection can have salinised the Pleistocene and Holocene sediments within several decades. The salinisation of the (pre-)Pleistocene clay layers occurred at a much lower rate due to the low permeability. In the clay layers, solute transport mainly takes place by diffusion, whereas in aquifers this is mainly due to advection (solute transport along the bulk flow of the groundwater) and mechanical dispersion (difference in flow paths of water and solute in the subsurface). For this reason, some clay layers can still contain fresh groundwater while the surrounding aquifers are saline (Figure 2.7).

In case laterally-continuous clay layers are present, these layers can function as a barrier against rapid salinisation of the fresh groundwater by free convection from above. The

extensive pre-Holocene clay layers in Zeeuws Vlaanderen are a good example of such a situation. In this way, inversions can occur; saline groundwater above fresh groundwater.

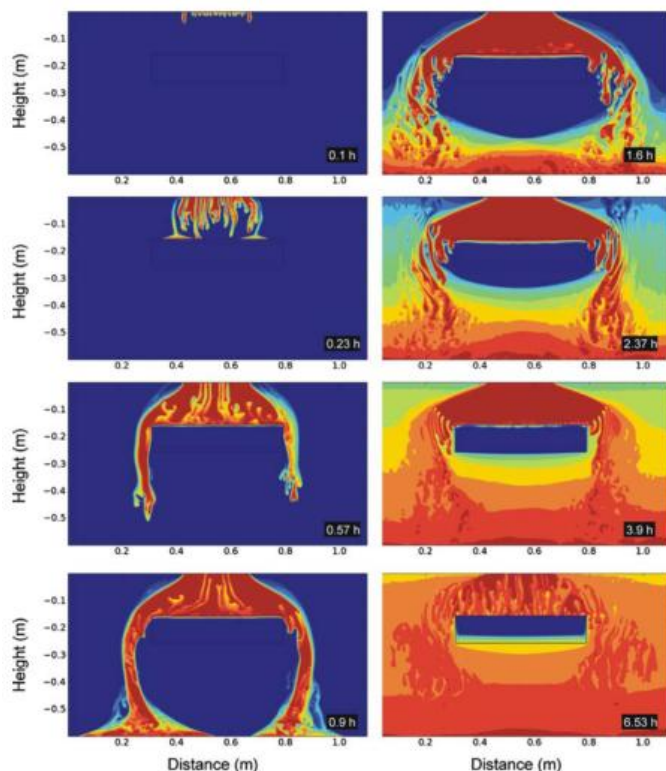


Figure 2.7: Numerical simulation of a laboratory experiment of free convection (from: Post en Simmons, 2009). In the middle of the model a low-permeable clay layer is present. The absolute speed of salinisation shown here is not representative for reality, however, the figures do illustrate the relative difference in speed of salinisation between the permeable section and the clay layer.

At the end of the Holocene, coastal defence structures developed by mankind prevent areas from inundation by the sea. The fresh groundwater recharge results in a freshening of the shallow groundwater system. Freshening occur(ed) primarily by vertical flow process driven by recharge processes (De Louw, 2013). Freshening in saline seepage areas is limited due to the constant upward flow, limiting the infiltration of rainwater and resulting in small size rainwater lenses (< 2-3 m thick). Unlike these thin rainwater lenses in seepage areas, the vertical downward flow of rainwater in the infiltration areas is not limited by upward flow but by the buoyancy force of the surrounding saline groundwater and if presence, low permeable layers. The density of the surrounding saline groundwater importantly determines lens thickness according to the Badon Ghyben Herzberg principle (Drabbe and Badon Ghijben, 1889; Herzberg, 1901). These systems build up much thicker lenses (BGH-lenses), varying from 5 to 15 m thick lenses in sandy creek ridges to 100 m thick lenses in the dunes. This difference in lens developing mechanisms explains the sudden increase in measured lens thickness (obtained by HEM) when moving from a seepage to an infiltration situation (De Louw, 2011) (see Figure 2.8).

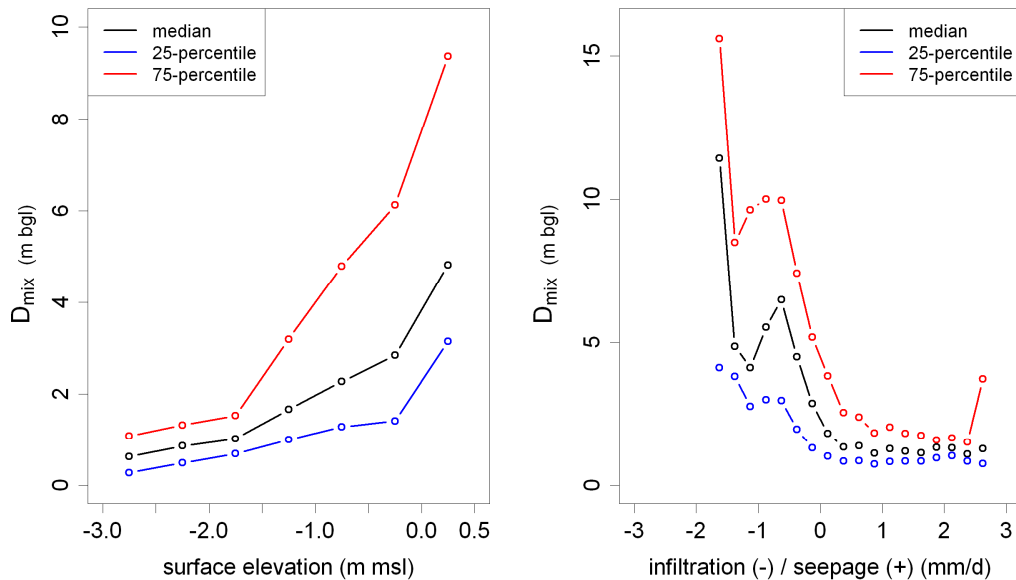


Figure 2.8 Relation of the middle of the fresh-saline interface (D_{mix}) derived from 84,300 HEM-measurements at Schouwen-Duivenland in 2009 with (a) Surface elevation (m MSL) and (b) Infiltration and seepage flux (mm/d). The 25-, 50- and 75-percentile of D_{mix} was determined and plotted for different classes of surface elevation and flux (dots represent middle of class) (De Louw, 2011).

Just like with free convection freshening takes place at a faster rate in aquifers than in aquitards. Below the creek ridges freshening takes place because the ground level and, hence, the drainage level, are higher than the surroundings (resulting in vertical downward flow). This type of freshening also takes place below the dune areas. For this reason, freshwater lenses are found below the dunes and below the creek ridges (Figure 2.9). Below the salt marsh deposits the groundwater is predominantly saline; continuous upward groundwater seepage hinders the infiltration of rainwater. Besides the Holocene freshening processes, there are also freshening processes that occur already for a longer time by regional groundwater flow from Noord-Brabant and Belgium.

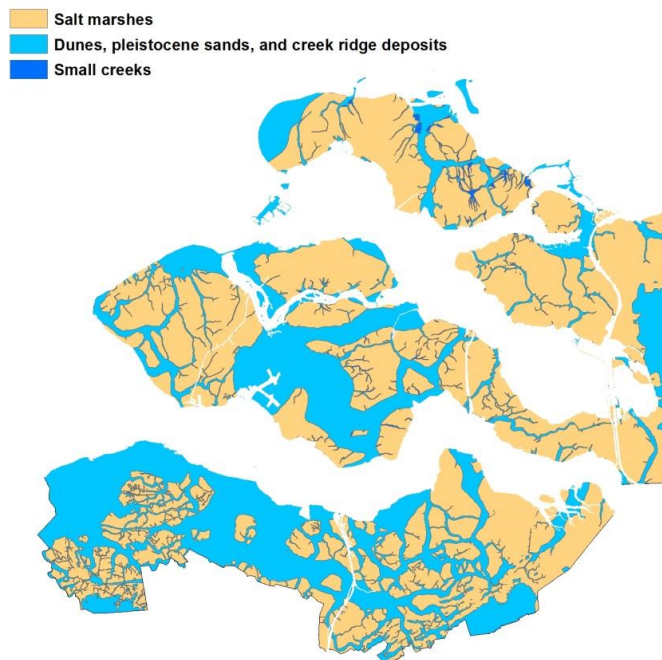


Figure 2.9: Types of deposits found at the surface: salt marshes, creek ridge deposits, small creeks, dunes, and Pleistocene sands. In general, fresh groundwater in the phreatic aquifer is found in the blue areas, whereas saline groundwater is found in the confining layer in the yellow areas.

3 Ground truth measurements

3.1 Theory and general procedure

The inversion results and the inferred chloride concentrations of the HEM data have been compared and validated with independent geophysical data and chloride analyses of the groundwater. This set of independent data is referred to as 'ground truth data'. In general, the geophysical ground truth data have a higher vertical resolution than the HEM data. The geophysical data can be expressed in two ways i.e., by the electric conductivity (symbol σ or EC, SI units Siemens / metre (S/m)) and by the electrical resistivity (symbol ρ , SI units Ωm). Electrical conductivity is the reciprocal of the electrical resistivity:

$$\sigma(\text{S/m}) = \frac{1}{\rho(\Omega\text{m})} \quad (3.1)$$

In this report, electrical conductivity is expressed using the unit mS/cm; 1 S/m = 10 mS/cm. Electrical resistivity is expressed using the unit Ωm .

The geophysical measurements are influenced by the electrical properties of the porous medium (sediment or rock) and the electrical properties of the groundwater (i.e., salinity). The chloride concentration of the groundwater can be inferred from geophysical measurements using petrophysical relationships. This is further discussed in chapter 8. The following sections describe the ground truth measurements that were used in this study.

3.1.1 TEC probe measurements

A TEC (Temperature - Electrical Conductivity) probe is an instrument to measure the temperature and the electrical conductivity of the subsurface in a one-dimensional (1D) profile. The TEC probe is pushed manually into the subsurface (Figure 3.1). The measurement interval is often 0.1 m. Usually, measurements are only carried out below the water table and in soft soils (clayey and peaty soils). The temperature / EC profile can be used to infer the salinity of the groundwater using petrophysical relationships. The end-depth is usually a few metres in soft sediments, like peat and clay. In coarser grained sediment, the cone resistance is usually too high for pushing the probe manually into the subsurface.



Figure 3.1: Field impression of the TEC probe.

3.1.2 Cone penetration tests

With a cone penetration test (CPT), a probe with a conical tip is pushed into an unconsolidated subsurface with a heavy track and the cone resistance, sleeve friction, water pressure, and electrical conductivity are measured simultaneously. The measurement interval is usually in the order of 1-2 cm. Like with the TEC-probe, the maximum depth of a CPT

measurement depends on the type of sediment; coarse sands result in a high cone resistance and therefore the end-depth is lower than in soft clay and peat. The water pressure, cone resistance, and sleeve friction can be used to determine the type of sediment. The electrical conductivity can be used to infer the salinity profile with depth.



Figure 3.2: A cone penetration test

3.1.3 Open hole geo-electrical borehole logging measurements

In a geo-electrical borehole logging measurement in an open borehole, a probe is used to measure the electrical resistivity of the subsurface with a vertical measurement interval of about 5 cm. Two electrode configurations are generally used for hydrogeological applications. The Short Normal electrical resistivity (SONO) is used to determine layer boundaries of lithology or water quality. The Long Normal electrical resistivity (LONO) is used to determine the electrical resistivity of the subsurface. Correct values of the electrical resistivity of the formation can be obtained if the effect of the borehole (e.g., diameter, borehole fluid) is corrected. Transition zones from fresh to brackish/saline groundwater can be determined with a vertical resolution of a few metres. Often, also the natural gamma-radiation is measured, from which the lithology can be estimated.

3.1.4 Vertical electrical sounding (VES)

A vertical electrical sounding is a geo-electrical method which is carried out at the surface. Using two electrodes, an electrical current is injected into the subsurface. Using two other electrodes, the electrical potential difference is measured in between. From these data the apparent resistivity of the subsurface can be determined. Upon a stepwise increase of both current and potential electrodes, a 'sounding' of the subsurface is obtained. From these data, an inverse model can be used to yield a layer model of the electrical resistivity of the subsurface. A common problem with the inversion of VES data is equivalence; often many combinations of layers and resistivities are possible to explain the observed apparent resistivities. The vertical resolution of estimating the depth of the fresh-saline transition zone of the groundwater depends on the depth, but is in the order of 5-10 metres.

3.1.5 Continuous Vertical Electrical Sounding (CVES)

A Continuous Vertical Electrical Sounding (CVES, also known as electrical resistivity tomography/ERT) is comparable to a VES measurement, but with many more electrodes and, hence, electrode combinations. The electrode combinations are coordinated by a computer. Inversion software is used to construct a model of the electrical resistivity, based on the apparent resistivity dataset. Equivalence problems are less than with the VES, because more

electrode combinations are used. The vertical resolution and depth of investigation depend on the electrode distance that is used.



Figuur 3.3: Impression of a CVES measurements

3.1.6 EM-Slimflex

The EM-Slimflex is a borehole logging tool developed by Deltares and the German company Anates. In the tool a primary electromagnetic (EM) field is generated by an alternating current in a 'transmitting' coil, which induces a secondary EM field in the subsurface. Both the primary and secondary fields are measured in a receiver coil. From the difference in phase and amplitude of the two EM fields the electrical conductivity of the subsurface can be determined. The tool is constructed such that the first few decimetres surrounding the open hole or piezometres don't influence the secondary EM-field. Hence, the salinity of the water in the open hole or piezometre doesn't significantly influence the measurement. The tool can be used to determine the electrical conductivity of the subsurface in uncased as well as cased boreholes (e.g., piezometres). The EM-Slimflex can be used in piezometres from 1.5 inch (3.8 cm) in diameter to determine the transition zone between fresh and saline groundwater. The measurement resolution is in the order of a few decimetres.



Figure 3.4: EM-Slimflex tool (left) and measurement (right)

3.1.7 Chloride analyses groundwater

Chloride analyses of the groundwater, retrieved from piezometres, were compared with the inferred chloride concentration of the HEM data. For higher salinity measurements, also the electrical conductivity of the groundwater was used, which was converted to chloride using empirical relationships. At higher salinities, the chloride concentration is linearly related to the electrical conductivity of the groundwater (at a constant temperature).



Figure 3.5: Chloride analyses of piezometres.

3.2 Measurements used for validation and calibration

The VES and CVES measurements were only used to compare different inversion methods of the HEM data. The EM-Slimflex, TEC probe, CPT, and chloride analyses of the groundwater were used more quantitatively for comparison with the HEM inversion results. This is explained in Chapter 12. In Figure 3.6 an overview is given of the different types of ground truth measurements.

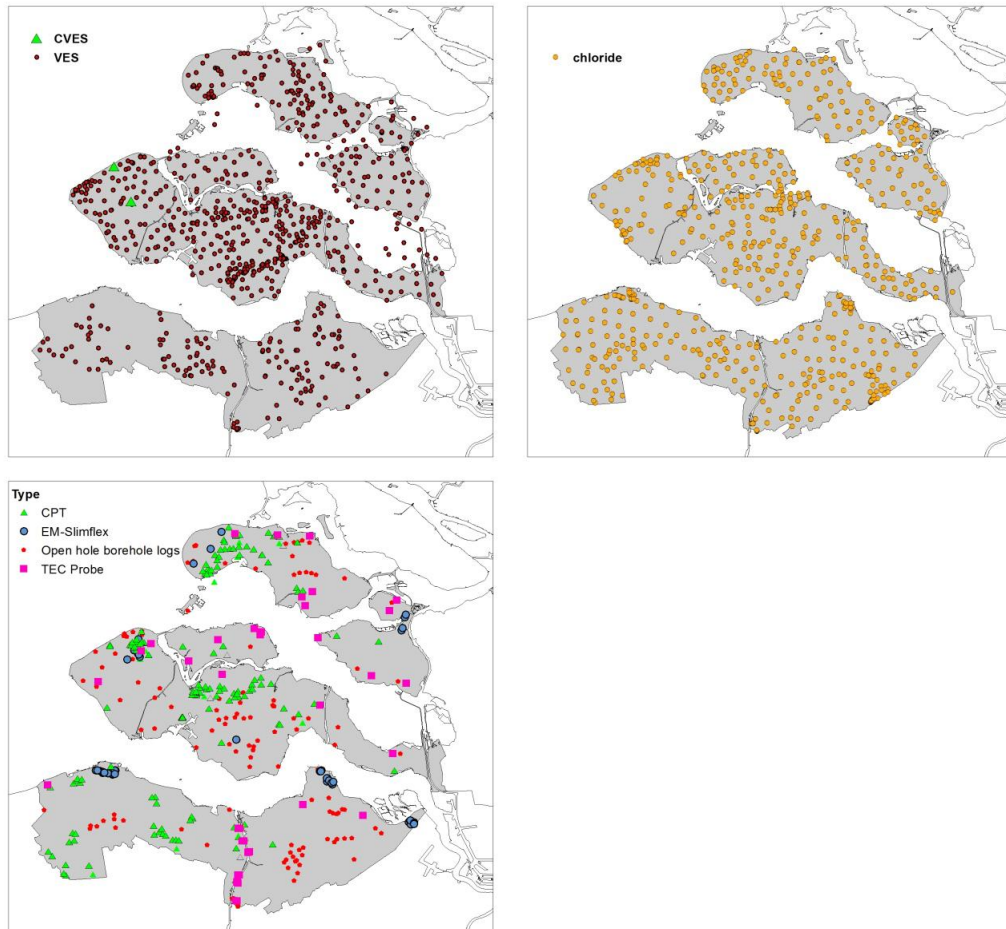


Figure 3.6: Overview of different types of ground truth measurements.

4 3D geological model GeoTOP

4.1 Introduction

The GeoTOP model is a 3D model of the shallow subsurface of the Netherlands. It is developed by the Geological Survey of the Netherlands (TNO – GSN), accessible free of charge at www.dinoloket.nl. The basics of the GeoTOP Zeeland modelling procedure is explained in this chapter, for a more thorough explanation please refer to Stafleu et al.(2011) and <https://www.dinoloket.nl/meer-weten>.

GeoTOP schematizes the subsurface in voxels (see Figure 4.1) each measuring 100x100x0.5 m, to a depth of 50 metres below NAP (Dutch Ordnance Level). Every voxel contains stratigraphical information, related to the age and dominant environment of deposition (fluvial, marine, aeolian etc.) and the lithological characteristics. Lithology is represented by 8 lithological classes:

- Organic material (peat)
- Clay
- Sandy clay and clayey sand
- Fine sand
- Medium sand
- Coarse sand
- Gravel
- Shells

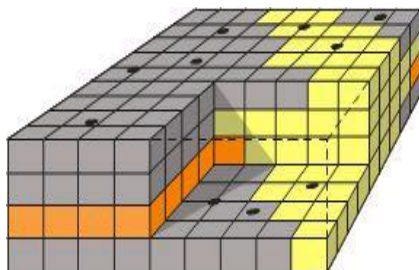


Figure 4.1: Concept of a voxel model

4.2 Data used

The GeoTOP Zeeland model is based on 23.000 borings that are stored in the DINO database. The time of drilling of these borings is variable as well is the quality. The depth reached shows strong variation, with many shallow borings while only a few percent reaches to the model base (Stafleu et al, 2011). The GeoTOP workflow combines this heterogeneous dataset with extensive knowledge of the geology of the Netherlands and the geological maps and models (e.g. Regis II) that are the result of mapping programs of the GSN and its predecessors (e.g. Hageman 1964, Van Rummelen 1965, 1972; Vernes et al. 2010). These data sources provide a wealth of information at a detailed level.

4.3 Method

As a first modelling step, all borings are assigned stratigraphical information and an interpretation is made of the depositional environment (facies). From the top and base of stratigraphical units in the boreholes, a detailed layer model is constructed of each

stratigraphical unit (see Figure 4.2). Facies interpretation (e.g. tidal channels and tidal flats) is unique to the GeoTOP modelling in Zeeland, as in Zeeland the facies type is an important clue to the dominant lithology. The cross section in Figure 2.3 shows a conceptual west-east profile of the Holocene units and lithofacies that are encountered in Zeeland. For every voxel the probability of belonging to a certain facies is calculated by interpolation with Sequential Indicator Simulation (SIS), with expert boundary conditions and guidance imposed on the simulation. By following a different random path through the modelling space, each iteration produces a (slightly) different realization with SIS. This procedure leads to 50 equally probable outcomes of facies distribution, from which the most probable facies of each voxel is determined. Following a similar procedure, 100 interpolations with SIS of the 8 lithology classes result in 100 equally probable realizations of the expected lithoclass of each voxel. From these 100 lithoclass realizations the most probable lithoclass is calculated, a property of the GeoTOP model that is often used. Figure 4.3 shows horizontal slices through the GeoTOP Zeeland model of the most probable lithoclass, where the sandy channel infill and the clayey deposits of the tidal flats of the Naaldwijk Walcheren are clearly visible. However, a better understanding of the lithological uncertainty that comes with GeoTOP is given by the probability of each lithoclass, resulting from the 100 lithoclass realizations. The availability of the lithological uncertainty has proven to be of great use for the calculation of chloride concentration as developed in this project.

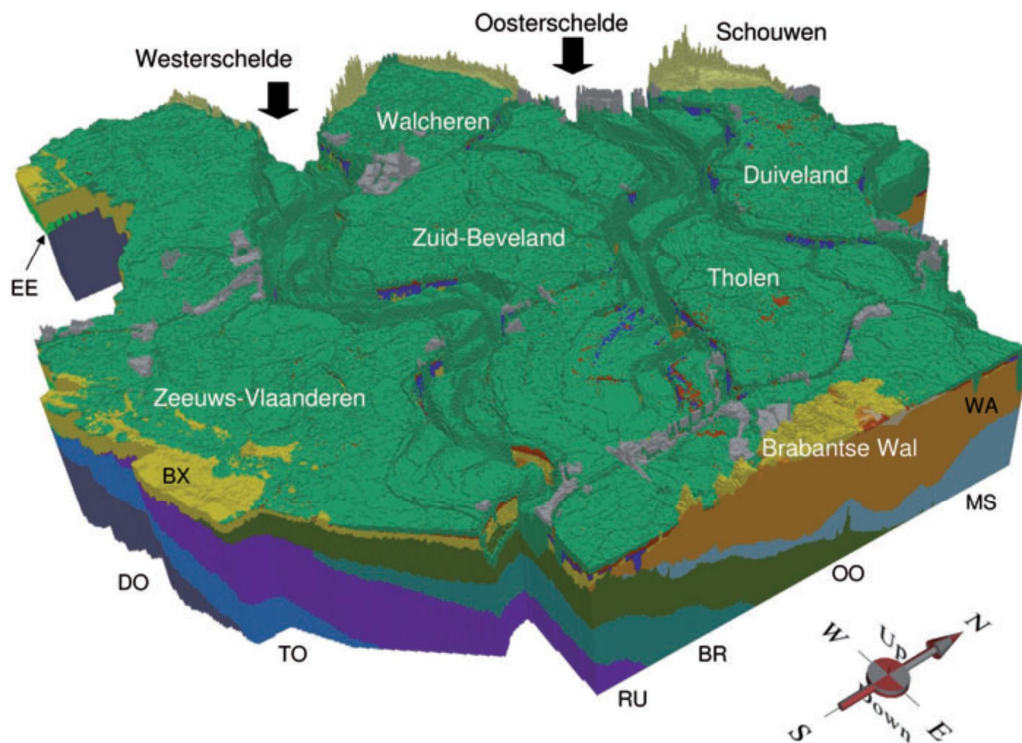


Figure 4.2: The modelled stratigraphical units (volumes). At the surface the Naaldwijk-Walcheren (tidal deposits, green), Naaldwijk Schoorl (coastal dunes, yellow) and anthropogenic deposits (gray) are dominant. The older Formations include: BX: Boxtel, EE: Eem, WA: Waalre, MS: Maassluis, OO: Oosterhout, BR: Breda, RU: Rupel, TO: Tongeren, DO: Dongen (Stafleu et al, 2011).

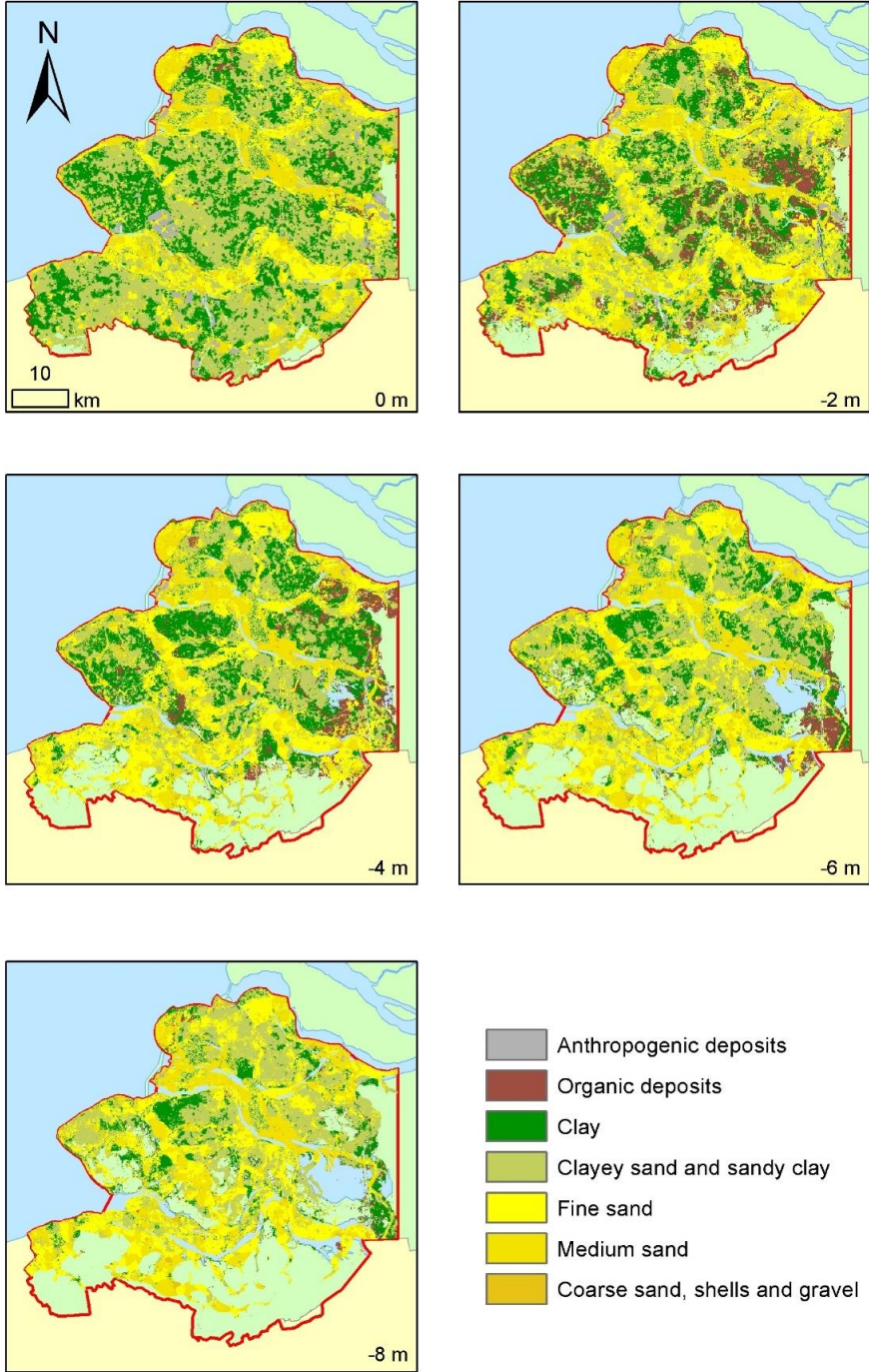


Figure 4.3: Horizontal slices through the lithofacies model at particular depths below Dutch Ordnance Datum revealing the position of tidal channels in the Walcheren Member (from Stafleu et al., 2011)

5 Data acquisition: Helicopter-borne electromagnetics

5.1 Introduction

Large-scale groundwater surveys increasingly apply airborne geophysical methods in order to investigate huge areas in reasonable time and at relatively low costs (Siemon et al. 2009b). From the most common airborne methods currently utilised airborne electromagnetics (AEM) contributes most to groundwater exploration purposes due to the dependency of the electrical conductivity (Figure 5.1) on a) the salinity of the groundwater, i.e., the groundwater quality, and b) the clay content of the subsurface (e.g. Kirsch 2006, Siemon et al. 2015). The separation between the contribution of the salinity and clay content is further described in chapter 8.

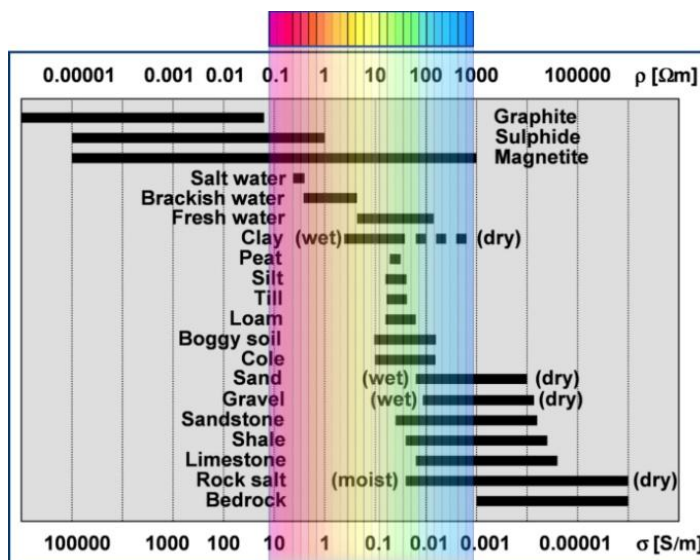


Figure 5.1: Typical electrical conductivities (resistivities) for diverse materials vs. with helicopter-borne electromagnetics detectable range (colours).

5.2 Airborne geophysical system

The Federal Institute for Geosciences and Natural Resources (BGR) operates a multi-functional helicopter (Sikorsky S-76B) for airborne geophysical measurements (Figure 5.2, Table 5.1). One of the systems is a modern frequency-domain helicopter-borne electromagnetic (HEM) system (RESOLVE, manufactured by Fugro Airborne Surveys, now CGG).

Each primary magnetic field (dipole) is generated by sinusoidal current flow through a transmitter coil at a discrete frequency. The eddy-current system induced in the subsurface by the primary magnetic field generates a secondary magnetic field that depends on the conductivity distribution in the subsurface. The secondary magnetic field is picked up by a receiver coil and related to the primary magnetic field expected at the receiver coil (cf. Figure 5.3, Figure 5.4). As the secondary field is very small with respect to the primary field, the primary field is generally bucked out (compensated for using so-called 'bucking coils') and the relative secondary field is measured in parts per million (ppm). Due to the induction process within the earth, there is a small phase shift between the primary and secondary field, i.e., the

relative secondary magnetic field is a complex quantity having in-phase I and quadrature Q components. The orientation of a transmitter coil is horizontal (VMD: vertical magnetic dipole) or vertical (HMD: horizontal magnetic dipole) and the corresponding receiver coil is oriented in a maximum coupled position, resulting in a horizontal coplanar (HCP) or vertical coaxial (VCX) coil system.

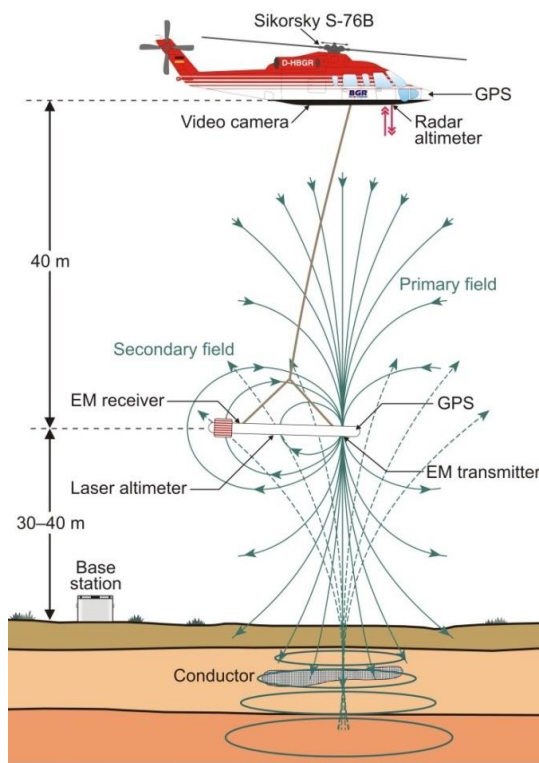


Figure 5.2: Sketch of BGR's airborne geophysical system.

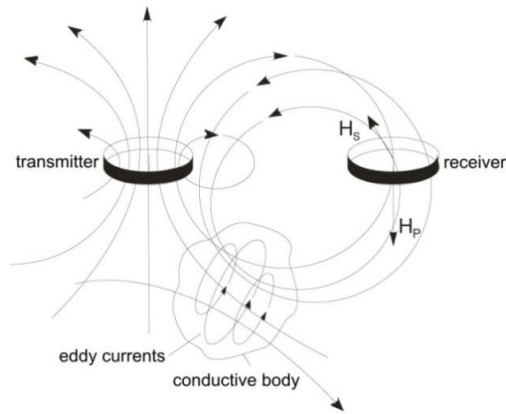


Figure 5.3: Transmitter and receiver EM concept (after Knödel et al. 2007).

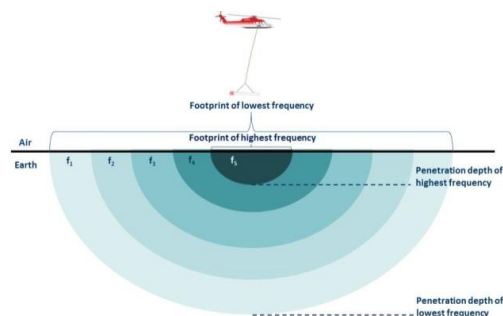


Figure 5.4: Footprint vs frequency of the HEM system.

The RESOLVE system consists of six pairs of small transmitter and receiver coils having a diameter of about half a metre and frequencies ranging from 380 Hz to 130 kHz. The coil separations of the five HCP and one VCX coils are about 8 and 9 m, respectively. BGR operates two RESOLVE systems which are similar, but not identical (Table 5.2).

The HEM system is dragged about 40 m below the helicopter and 30 – 60 m above ground level. The altitude must be increased when flying over trees, power lines and other man-made installations due to safety reasons. Unfortunately, the signals measured decrease with increasing sensor altitude and, thus, the signal-to-noise ratio is often too low when flying higher than 100 m so that the HEM data cannot be used there.

Table 5.1: BGR's airborne geophysical system.

Airborne geophysical survey system	
Helicopter:	Sikorsky S-76B
Helicopter equipment:	GPS-Navigation, GPS-Tracking, radar and barometric altimeters, video camera, instrument rack
Standard equipment:	Electromagnetic system, magnetometre, laser altimetre, gamma-ray spectrometre
Base station equipment:	Magnetic total field sensor, air pressure sensor, GPS
Survey speed:	130 – 160 km/h
Sampling distance:	about 4 and 40 m
Line separation:	variable, >50 m

Table 5.2: HEM systems.

Six-frequency HEM systems		
Type:	RESOLVE – digital HEM system BKS36a / BKS60 systems	
Length:	10 m	
Weight:	400 kg incl. cable (60 kg) and instrument rack (70 kg)	
Manufacturer:	Fugro Airborne Surveys, Canada	
Frequency [Hz]	Coil separation [m]	Coil geometry
387 / 380	7.94 / 7.92	horizontal coplanar
1820 / 1770	7.93 / 7.92	horizontal coplanar
5406 / 5410	9.06 / 9.04	vertical coaxial
8393 / 8300	7.93 / 7.96	horizontal coplanar
41430 / 41000	7.91 / 8.03	horizontal coplanar
133300 / 129500	7.92 / 7.91	horizontal coplanar

The BGR helicopter system used in Zeeland recorded not only electromagnetic and position data, but also magnetic and radiometric data (Table 5.2). These additional geophysical data sets may be used to identify man-made sources (magnetics) and to get information on the soil minerals (radiometrics). As more reliable information on both man-made sources and soil minerals were available through other sources, magnetic and radiometric data were not used in FRESHEM Zeeland.

The footprint in the shallow subsurface is about 50 m and at greater depth about 200 m (Figure 5.4). Hence, the 'point' measurement taken every 4 m is a measurement of a circular area with a diameter of approximately 50-200 m. Note, however, that the measured signals are mainly caused by conductivity structures directly beneath the system, i.e. narrow strongly conductive features will be detected.

The penetration of the EM fields into the subsurface strongly depends on the system parameter frequency and on the ground parameter electrical conductivity. Thus, the penetration depth is low at high frequencies and/or conductivities and high at low frequencies and/or conductivities. The exploration depth is thus also dependent on the conductivity structure and may reach maximum depths of up to about 160 m for fresh-water saturated sand above saline groundwater.

5.3 Airborne surveys

The FRESHEM airborne surveys were flown within three two-week periods in 2014 and 2015 in addition to the two surveys of the CLIWAT project flown in 2009 (one week) (De Louw, 2011). The airborne surveys covered the entire Province of Zeeland with a total area of more than 2000 km². The area of the province was split into 17 survey areas (Figure 5.5, Table 5.3) having flight-line separations of 100 m (six areas), 200 m (two areas) and 300 m (nine areas). Five of the six high-resolution areas were flown as part of the larger low-resolution areas making use of flightlines already flown before. The flight-line directions were chosen with respect to local conditions. The direction of the tie-lines was normally perpendicular to the line, but not always. In addition, a number of lines or tie-lines were flown freely (after sight). The length of all profiles totals to more than 9000 km. In addition, a large number of lines were flown over (or extended to) saline sea water for calibration purposes. All of the 51 survey flights commenced from the airport Midden Zeeland. The survey speed of the helicopter was about 140–150 km/h resulting in a sampling distance of about 4 m.



Figure 5.5: Sketch of the airborne survey areas in Zeeland. Areas in green, ochre and red were flown at 100 m, 200 m and 300 m line spacing, respectively. The area Dunes Schouwen was partially flown at 200 m line spacing and 200 m tie-line spacing. The area Oost Souburg was flown at 300 m line spacing.

Table 5.3: Details of the airborne survey areas in Zeeland.

Area no.	Area name	Area size [km ²]	Profile length [km]	Line spacing [m]	Line direction [°]	Lines #	Tie-lines #
135	Schouwen	58	313	200	98	42	16
136	Perkpolder	50	222	200	90	22	13
160	Terneuzen	31	357	100	0	36	22
161	Waterdunen	14	122	100	0	38	3
162	Zeeuws-Vlaanderen	516	1774	300	0	122	15
163	Zeeuws-Vlaanderen-East	278	965	300	0	67	10
164	Hedwigepolder	16	127	100	37	18	-
165	Dunes-Schouwen	76	460	300 (200)	50	38	24
166	Duiveland	163	609	300	98	46	17
167	Tholen	214	748	300	98	48	8
168	Eendracht	53	605	100	8	70	46
169	Walcheren	183	689	300	58	40	13
170	Beveland	453	1554	300	0	114	17
171	Beveland-East	108	342	300	122	36	5
172	Waterfarm	72	354	100	58	54	6
173	Oost-Souburg	27	75	300	57	14	-
174	Kreek-Terug	34	324	100	0	60	4
Total	17 areas	2346	9640			865	219

The realisation of this survey was challenging given the amount of infrastructure present. This infrastructure caused the pilot to regularly deviate from the planned flightlines in order to avoid buildings, power lines and radar devices (on land and on ships). Therefore, the true flight paths were often not straight and many turns were necessary causing rather strong movements of the HEM system (Figure 5.6). Particularly, areas where towns, industrial areas or larger villages exist could not be covered by the airborne surveys. Power lines, railway tracks and major roads were crossed at higher elevation.

Details of the individual airborne surveys are described in Siemon et al. 2014 (October 2014), Siemon et al. 2015b (March 2015), Siemon et al. 2015c (August/September 2015), Siemon et al. 2011a (August 2009), and Siemon et al. 2011b (August 2009).



Figure 5.6: Final flightlines (thin black lines and tie-lines) used for data processing.

6 Data processing

6.1 Introduction

As the reliability of the final inversion results strongly depends on the quality of the data used, not only the hardware capabilities are essential but also the software tools used for data processing. The goal of the data processing is to derive those field values from the data measured that correspond to the subsurface material parameters and to eliminate – or at least minimise – those portions in the data that are affected by influences not belonging to the subsurface. HEM data processing requires therefore a number of processing steps (Figure 6.1) such as conversion of measured voltages to relative secondary field values using calibration signals, standard and advanced drift corrections (zero-level drift correction / 2D levelling), and – if necessary – data corrections (Valleau, 2000; Siemon, 2006b; Siemon, 2009b).

Besides HEM data processing additional parameters like coordinates and altitudes have to be converted and/or corrected. Particularly the altitude data, the distance and the elevation of the system (or the helicopter) to the ground surface recorded by a laser altimetre and GPS receivers (or barometric altimetres), require thorough processing as they may be affected by system motion (attitude effects) and/or reflectors (buildings, trees) above ground level. Particularly, if the altitude is used as an input parameter for the inversion, the effects caused by the tree canopy have to be corrected in the altitude data beforehand by automatic inspection using a combination of appropriate filters and/or by time intensive manual inspection. In flat areas like Zeeland it is appropriate to use a digital elevation model and the GPS elevation of the HEM system to derive a synthetic laser altitude, which is not affected by system motion. Comparison with the measured laser altitude helps to identify portions in the HEM data, where the HEM data must be corrected for attitude effects.

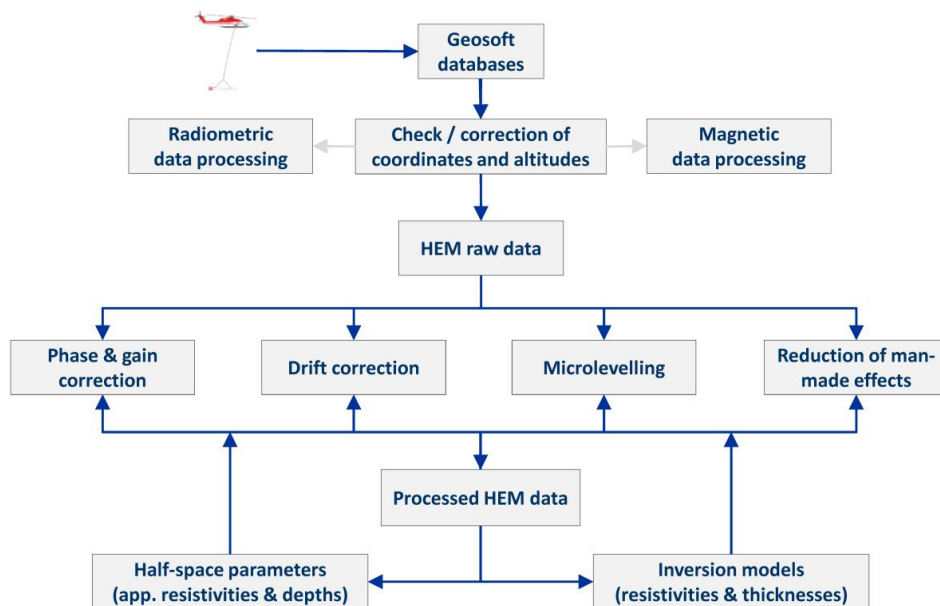


Figure 6.1: The advanced HEM data processing includes four principal steps: phase and gain correction, drift correction, microlevelling and reduction of man-made effects.

6.2 Calibration, phase & gain correction

Calibration is necessary to convert the induced voltages caused by the secondary magnetic fields measured at the receiver coils of a HEM system to relative values (in ppm) with respect to the primary fields at the receivers. This is done using calibration coils, which produce reference signals in the HEM data measured at each frequency.

The HEM system was calibrated on high-resistive ground by the manufacturer yielding a set of calibration factors valid for the internal calibration coils. At the beginning of each survey flight, the calibration coils were used to automatically adjust phase and gain at high flight altitude (e.g. 350 m) where the secondary fields are negligible, i.e. below the system noise level.

External sources and/or thermal effects may derange the calibration procedure. Therefore, flights over highly conductive water (Schelde, North Sea) were used during each survey flight to check and tune the calibration. This phase and gain correction, which is performed manually during data processing, is based on the assumption that the saltwater body is sufficiently homogeneous and thick (> 10 m), i.e. the results of the homogeneous half-space inversion (see section 7.3.1) are comparable for all frequencies.

6.3 Zero-level drift correction

Remaining signals due to insufficiently bucked-out primary fields, coupling effects with the aircraft, or (thermal) system drift are generally detected at high flight altitude several times during a survey flight. These basic values measured at reference points are used to shift the HEM data with respects to their base (zero) levels. This procedure enables the elimination of a long-term, quasi-linear drift; short-term variations caused by e.g. varying air temperatures due to alternating sensor elevations, however, cannot be determined successfully by this procedure.

Therefore, additional reference points – also along the profiles at normal survey flight altitude – may be determined where the secondary fields are small but not negligible. At these locations, the estimated half-space parameters (see SECTION C.2) are used to calculate or to check the expected secondary field values which then serve as local reference levels (Siemon 2009).

6.4 Microlevelling

Standard airborne surveys consist of a number of parallel profile lines covering the entire survey area. Level errors appear on the maps as stripes (or blocs) which differ from their surroundings. In addition, tie lines, which are flown more or less perpendicular to the lines, may help to identify wrong line levels. Thus, statistical methods and/or 2D filter techniques called statistical levelling (tie-line levelling) and empirical levelling (microlevelling), respectively, are applicable to correct stripe patterns in airborne geophysical data sets (e.g. Huang 2008). Standard levelling procedures developed for e.g. airborne magnetic data are, in general, not directly applicable to HEM data, because the dependency of the secondary fields on both the resistivity of the subsurface and the sensor altitude is strongly non-linear. Therefore, the half-space parameters apparent resistivity and apparent depth, followed by a recalculation of the secondary magnetic field components based on the half-space parameters levelled, should be used for HEM data levelling (Siemon 2009).

The microlevelling procedure consists of two major steps. First, the half-space parameters apparent resistivity and apparent depth (see section 7.3.1) are independently calculated for all frequencies. Tools provided by Geosoft's Oasis montaj software are used to conduct the microlevelling (combination of Butterworth and directional cosine filters) of the (parallel) lines. The tie-lines (and all lines not parallel to the principal line direction) are levelled using the grids of the already microlevelled lines. Second, synthetic HEM data values are derived from the resulting levelled half-space parameters along all lines and tie-lines. These (levelled but

often too smooth) values are compared with the unlevelled HEM data and drift corrections are derived. After applying these smooth drift corrections to the HEM data, the final HEM data sets are derived which are levelled without losing (lateral) resolution (Figure 6.2).

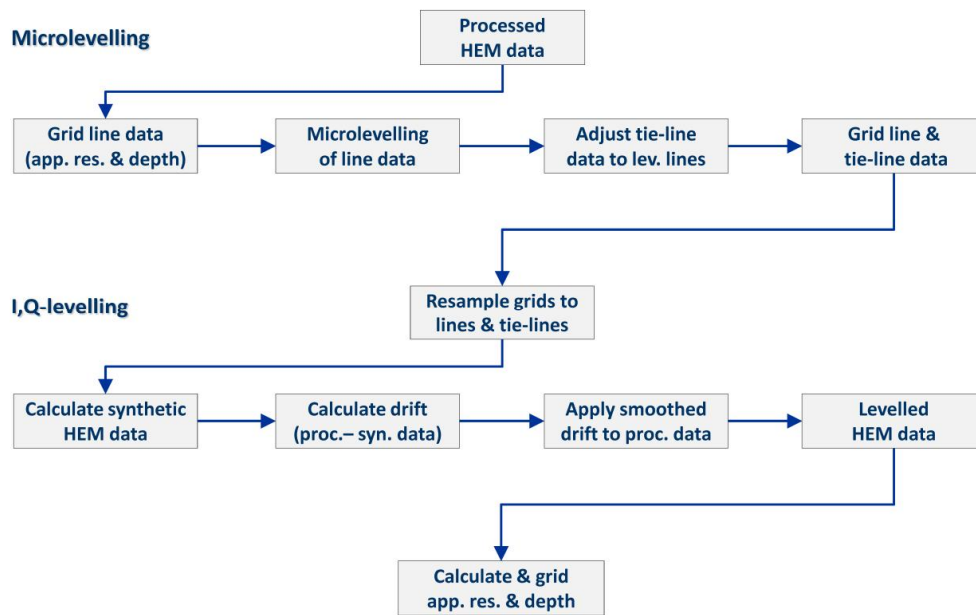


Figure 6.2: Levelling procedure.

6.5 Data corrections, reduction of man-made effects

Effects caused by man-made infrastructure such as power lines, radar stations, railway tracks, roads, buildings, metallic fences and cables affect the HEM measurements. Particularly those cables having an AC current flow (power lines) strongly affect the HEM measurements, because they act as external transmitters. In addition, the altitude of the HEM system must be increased crossing the power lines (due to safety reasons). Both effects reduce the signal-to-noise ratio so that the HEM data close to power lines must be erased and the subsurface cannot be investigated sufficiently. Similarly, the HEM data close to roads and buildings must be erased, but the resulting gaps are smaller. All these data gaps are preliminarily filled-up with interpolated data as long as the gaps are not too large. Such an interpolation is reasonable if the resistivity variations within the gaps are sufficiently small (Siemon, 2011). In the next step, data of inadequate quality was flagged and removed from subsequent processing.

6.6 Data quality assessment

A data error based on a statistical variation of repeated measurements is not available for HEM data, because all the measurements consist of single values. In order to derive a kind of error value, the standard error is calculated of 30 consecutive values data values, which are recorded along line segments of about 120 m. The standard errors are referred to the corresponding smoothed HEM amplitudes to get relative standard error values (rel. STE). HEM data of low quality occur if man-made effects (particularly external transmitters) bias the measurements or the sensor altitude is high, and thus, the data values are small. These low quality data segments are automatically and/or manually marked and erased from the data. After the levelling procedure, these gaps are interpolated, e.g. using the synthetic HEM data. If the interpolation fails due to too large gaps, the flightlines have to be split on both sides of the gaps and the entire data processing has to be repeated.

A novel quality control parameter (QCP), which takes care not only of the erased data segments but also of the relative standard error and the sensor altitude, is defined as:

$$QCP = 1 - CHECK - STD - ALT \geq 0,$$

where: CHECK marks the erased (and interpolated) data segments, STD represents the standard error, and ALT indicates high altitude data.

These three quantities should be balanced reasonably. Therefore they are defined as:

CHECK = 0.04 per frequency (without VCX data, max. = 0.2),
STD = total rel. STE of all I,Q components (in ‰, without VCX data, max. = 0.8),
ALT = ((altitude – 50)/150 \geq 0), i.e. 0 at 50 m, 0.2 at 80 m, 0.4, at 110 m, etc.

Thus, the erasure (and interpolation) of data has the same effect as a STD of 0.2 or a sensor altitude of 80 m. In case of high or bad data quality, QCP is close to 1 or 0, respectively.

In addition to this dynamic quality parameter, a discrete marker (QCPM) is defined, which only has a value (= 1), where the data quality is too low for a reliable data interpretation. The calculation of this marker consists of two steps. First, all segments are selected with rather low data quality, i.e. $QCP \leq 0.5$. Second, these segments only remain if they dominate within an interval of 100 values in order to avoid small gaps (<200 m), which can be reasonably interpolated, or very short data segments. Data with a QCPM of 1 was removed for further processing.

7 Data processing: Inversion

7.1 Introduction

Inversion is used to calculate vertical resistivity profiles from the (levelled) raw measurements. The process of inversion starts from a conceptualised model of the subsurface, defined by a certain layering and properties for each layer. The electromagnetic response of this conceptualised model of the subsurface can then be calculated, and compared to the levelled measurements. A large number of conceptualised models are thus evaluated; the model that best fits the measurements best represents the real subsurface properties.

In FRESHEM, inversion is performed both with BGR software (Siemon, 2012), and Aarhus workbench (Auken, Viezzoli and Christensen, 2009). Both apply somewhat different inversion methods. This chapter outlines the inversion methods that were applied, and how uncertainty in the inversion was accounted for.

7.2 Forward calculation

The synthetic secondary magnetic field for a stratified subsurface caused by an oscillating magnetic dipole source in the air can be calculated using well-known formulae (e.g. Wait 1982, Ward and Hohmann 1988). For a HCP coil pair with a coil separation r [m] and at an altitude h [m] above the surface, the relative secondary magnetic field Z [ppm] at a frequency f [Hz] is given by

$$Z = r^3 \int_0^{\infty} R_1(f, \lambda, \rho, \mu, \varepsilon) \frac{\lambda^3 e^{-2\alpha_0 h}}{\alpha_0} J_0(\lambda r) d\lambda \quad (7.1)$$

where $\alpha_0^2 = \lambda^2 - \omega^2 \mu_0 \varepsilon_0 + i\omega \mu_0 / \rho_0$ with λ = wave number, $\omega = 2\pi f$, $\mu_0 = 4\pi \times 10^{-7}$ Vs/Am, $\varepsilon_0 = 8.854 \times 10^{-12}$ As/Vm and $\rho_0 > 10^8 \Omega\text{m}$, J_0 is Bessel functions of first kind and zero order, and R_1 is the complex reflection factor containing the material parameters isotropic resistivity ρ [Ωm] (reciprocal of the electrical conductivity), dielectric permittivity ε [As/Vm] and magnetic permeability μ [Vs/Am] of a layered subsurface. This complex integral as well as similar formula valid for the VCX configuration are evaluated numerically using fast Hankel transforms (e.g. Anderson, 1989; Johansen and Sørensen, 1979; Auken, 2002; Siemon, 2012).

This type of inverse Hankel transform integral can be evaluated very efficiently using digital filter methods as described by (Johansen and Sørensen, 1979) and (Christensen, 1990). Given the ability to efficiently solve inverse Hankel transform type integrals allows for fast calculation of any EM field component, by simple means of differentiation of the vector potential equations. In the calculation of the type of integral in Equation 7.1 the most time consuming part becomes the evaluation of the integrand function f . This function includes a frequency dependent reflection coefficient, essentially accounting for the amplitudes of up- and down-going damped waves within the layered half-space. Recent developments in the integration of equation 7.1 (Siemon 2012) allowed for more accurate modelling of data from higher altitudes. Higher altitudes occur when manmade installation dictates higher flying altitudes. It is worth mentioning that BGR and Aarhus code use different integration methods that might produce slightly different results, especially in higher altitudes.

7.3 Inversion

Inversion tries to find a model that explains the data sufficiently, i.e. synthetic data belonging to a specific model are compared with field data and from the differences corrections are derived. Generally, the (measured) secondary field data (in-phase and quadrature) are inverted into

resistivity using two principal models: the homogeneous half-space and the layered half-space (Figure 7.1). While the homogeneous half-space inversion uses single frequency data, multi-layer (or one-dimensional, 1D) inversion is able to take the data of all frequencies available into account.

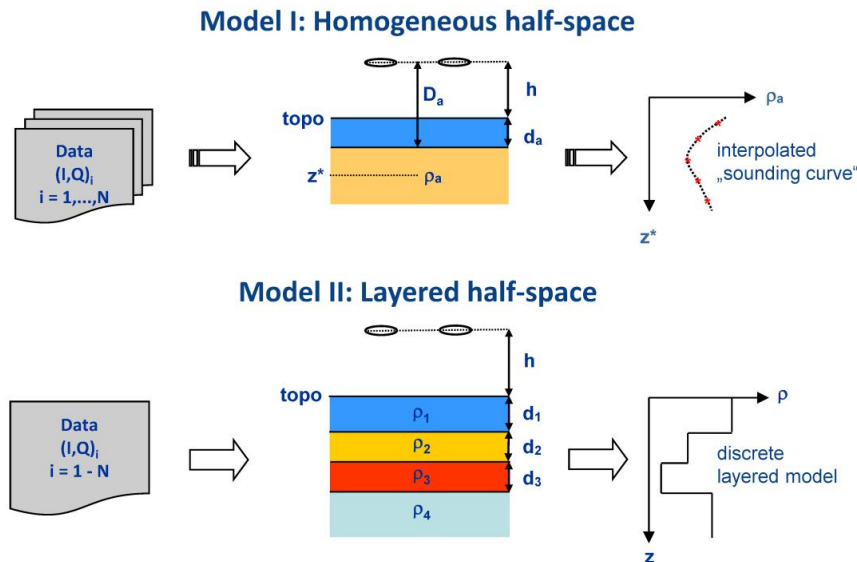


Figure 7.1: HEM data inversion based on homogenous and layered half-space models.

7.3.1 Homogeneous half-space

The resulting parameter of the half-space inversion is the apparent resistivity (or half-space resistivity) ρ_a [Ωm], which is the inverse of the apparent conductivity. Due to the skin-effect (high frequency currents are flowing on top of a perfect conductor) the plane-wave apparent skin depth p_a [m],

$$p_a = \sqrt{\frac{2\rho_a}{\omega\mu_0}} \approx 503.3 \sqrt{\frac{\rho_a}{f}}, \quad (7.2)$$

increases with decreasing frequency f and increasing half-space resistivity ρ_a . Depth resolution is achieved using several frequencies: the lower the frequency the greater the depth of investigation (DOI). The DOI depends also on the resistivity of the subsurface: the higher the resistivity the greater the DOI. Therefore, high frequencies are used to investigate the shallow subsurface and low frequencies are used to get information from greater depth. Typical depth ranges which can be investigated with the HEM system are: 0.5 – 15 m (sea water), 1 – 30 m (salt-water saturated sands), 2 – 60 m (fresh-water saturated clays), 5 – 150 m (fresh-water saturated sands). The HEM system is suitable for shallow groundwater exploration as the VMD transmitters induce currents which are predominantly flowing horizontally and thus resolve layered structures best.

The calculation of the apparent resistivity ρ_a and the apparent distance D_a [m] of the HEM system to the top of the conducting half-space requires two data values (in-phase and quadrature or amplitude and phase). The apparent distance D_a can differ from the measured sensor altitude h . The difference of both, the apparent depth $d_a = D_a - h$ is positive in case of a resistive cover (including air); otherwise a conductive cover exists above a more resistive substratum. From the apparent resistivity and the apparent depth the centroid depth z^* [m] is derived: $z^* = d_a + \rho_a/2$ (Siemon, 2001), which is a measure of the mean penetration of the induced currents.

Half-space parameters obtained for a number of frequencies enable the presentation of FRESHEM results as apparent resistivity maps (Fraser, 1978) or apparent resistivity/depth sections (Sengpiel, 1983; Sengpiel, 1990).

7.3.2 Layered half-space

There are several procedures for the layered half-space inversion of HEM data available which are often adapted from algorithms developed for ground EM data. The goal of the 1D nonlinear inversion least-squares algorithm is to recover the distribution of electrical conductivity (reciprocal to resistivity) with depth beneath each sounding. Inversion of AEM data is ill-posed and non-unique; that is, many resistivity models are consistent with the measured data, and some kind of regularization is needed to stabilize the inverse problem. Regularization is introduced through the model norm, which favours specific properties in the inverted model such as proximity to a reference model or smoothness. The relative importance of fitting the data compared to controlling the model through regularization is controlled by a trade-off parameter. Set too low, the algorithm will tend to fit noise in the data and result in models with too much structure. Set too high, the algorithm can easily fit the data with many models, and the resulting models are strongly controlled by the regularization term.

A comparison is presented by (Hodges and Siemon, 2008). Here, a Marquardt-Levenberg inversion procedure (Sengpiel & Siemon, 2000) is used which requires a starting model that can be derived from a resistivity/depth sounding curve (Siemon 2006a) or from external data.

As the lateral variability of the resistivity is often not very strong in groundwater surveys, particularly for sedimentary aquifers, the model parameters can be tied together by constraints to increase the number of data variables per model and, thus, to enhance both, resolution and stability (Auken et al. 2005). Siemon et al. (2009a), Viezzoli et al. (2008) and Steuer et al. (2008) presented laterally or spatially constrained inversion (LCI/SCI) results for HEM data. Applying LCI or SCI also enables using external data as a priori information during the inversion of HEM data (Gunnink et al. 2012). These a priori data can be derived from lithology (boreholes or geological models) and/or salinity (groundwater models). The use of a priori data was tested and discarded in the FRESHEM Canal zone Gent-Terneuzen pilot study, given encountered problems with large spatial variability (and thus the relatively small 'footprint' of measurements), and difficulties assigning proper weight to available a priori spatial information in the inversion (Van Baaren et al., 2015).

The inversion is performed iteratively, by following the established practice of linearized approximation of the non-linear forward mapping of the model to the data space, by the first term of the Taylor expansion (Menke 1989; Auken et al. 2005). The (n+1)th update of the model vector m_{n+1} is obtained by:

$$m_{n+1} = m_n + [G_n^T C^{-1} G_n + \lambda_n I]^{-1} [G_n^T C^{-1} \delta d_n'], \quad (7.3)$$

where G_n' is the Jacobian matrix, $\delta d_n'$ is the data vector update, and C' is the covariance matrix.

The SSI approach used at BGR ($G_n' = G_n$) applies the general matrix inversion based on singular value decomposition (e.g. Menke, 1989). The included regularisation weights the singular values v_i ($i = 1, \dots, N$, sorted by size, $N = 2N_L - 1$, $N_L =$ number of layers) so that the largest singular values dominate and the small ones are suppressed. The weights are defined as $(v_i^2 + (cw)^2)^{-1}$, where w is automatically determined by minimising the misfit and c is a pre-set (selectable) scaling factor (normally = 1.0). This regularisation enables usage of an arbitrary number of model layers, i.e. it is allowed to use more model parameters than data values available. Model smoothness is achieved by an increase of the scaling factor.

Model constraints are applied between any two parameters of the same type by specifying the variance of the difference between the two and the uncertainty of prior information is similarly specified by the variance of the given prior value. Typically, we apply constraints in the form of 1D laterally constrained inversion (LCI; Auken et al. 2005) and 1D spatially constrained inversion (SCI; Viezzoli et al. 2008) for producing quasi 2D and quasi 3D models, respectively. The constraining formulation is flexible and allows for constraints and prior information on both primary and secondary model parameters.

For 1D LCI/SCI solutions in the Aarhus software the Jacobian matrix is expressed as:

$$G_n^i = \begin{bmatrix} G_n \\ P \\ R \end{bmatrix}, \quad (7.4)$$

where P is the matrix necessary to impose the constraints on the a-priori values, R is the roughness matrix in which each row represents one roughness constraints, i.e. lateral constraints. More information can be found at Auken et al. (2014). 1D LCI of continuous HEM data has proven to be a robust tool to obtain reliable inversion results in quasi-layered environments. The layered model parameterization allows easy identification of formation boundaries improves the resolution of poorly resolved parameters (Auken, 2005).

SCI provides smooth models in every direction. It was tested but not used for the final maps since it requires resampling the data along flights in order to set a grid. That would make the direct use of all three methods to produce uncertainty maps problematic. Additionally, the different flightline separation between the areas would require different parameters per area. The vertical smoothness of the obtained models stems from the application of Occam-type regularization constraints, which are meant to address the ill-posedness of the problem. An important side effect of such regularization, however, is that horizontal layer boundaries can no longer be accurately reproduced as the model is required to be smooth. This issue can be overcome by inverting for fewer layers with variable thicknesses; nevertheless, to decide on a particular and constant number of layers for the parameterization of a large survey inversion can be equally problematic (Viezzoli et al. 2015). Thus we utilized a sharp inversion scheme which is a focusing regularization technique to obtain the best of both methodologies. The new focusing approach allows for more accurate reconstruction of resistivity distributions using a fixed vertical discretization while preserving the capability to reproduce horizontal boundaries. The combined use of all inversion schemes increases the confidence of the final resistivity maps, since every scenario is covered and analysed.

For the inversion of airborne data we allowed for including the instrument altitude as a model parameter. In the case of helicopter data the pilot attempts to follow the terrain topography and maintains a relatively constant altitude range. While correction are applied during the pre-processing of the data, there may still be small errors in the helicopter altitude. In our approach using the Aarhus code, we inverted for altitude after the 7th iteration of the algorithm. Thus after 7 iterations, if the algorithm has high residual error, we adjusted the altitude of the bird. This resulted in minor elevation changes in the order of a few centimetres.

We finalise the inverse modelling procedure by calculating the DOI for the resulting output models, an operation which relies on a reweighting of the Jacobian matrix. The computations employ a global and absolute sensitivity threshold value, which has been tuned for operating in logarithmic model/data space (Christiansen and Auken, 2012). For a given model, the DOI calculations consider only the parts of the Jacobian related to observed data, implying that the

effect of lateral, spatial or vertical model parameter constraints and a priori information is not included. With this type of DOI estimate it is possible to judge when the information in a model is driven by data or heavily dependent on the starting model or specifics of the regularisation.

7.4 Selection of inversion approaches

7.4.1 Conclusions from pilot study Canal zone Gent-Terneuzen

The HEM data of the high-resolution pilot survey area Canal zone Gent-Terneuzen (van Baaren et al. 2015) were used to evaluate the best inversion approaches. The inversion strategies used were single-site Marquardt-Levenberg inversion (SSI) as well as laterally and spatially constrained inversions (LCI, SCI).

The SSI and LCI inversions were tested using diverse starting models with and without a-priori data derived from ground-truth and/or 3D (hydro-)geological model data. They were conducted based on both few (≤ 6) model layers, i.e. inverting for resistivity and thickness, and many (20) models layers with fixed thicknesses (Siemon et al. 2009). The fixed layer thicknesses were adopted from a) an internal starting model derived from half-space inversion results or b) an external starting model based on (hydro-)geological data. In case a), N_L-2 layer thicknesses increase with depth between upper and lower bounds given by the centroid depth values z^* of the highest and lowest frequency, respectively. In addition, the top layer is split into two using the apparent depth value d_a of the highest frequency. This is meaningful, because d_a often represents the depth to a prominent conductor, e.g. the (shallow) groundwater table. If $d_a \leq 0$, i.e. there is no resistor on top covering a conductor, a minimum value of 0.5 m is used. All N_L-2 layer thicknesses are fixed in the smooth inversion (with 20 layers), but the thickness of the top layer remains variable during the inversion. In case b) the layer thicknesses are given by the multiples of the vertical cell size (0.5 m) of the (hydro-)geological models used and increase with depth.

The most reasonable results within this pilot study were achieved using SSI and LCI (both standard and sharp) with no external starting models. This enables reproduction of small-scale up-coning effects along ditches and avoids misleading inversion results due to weak starting models derived from existing groundwater and geological models based on 100 m x 100 m x 0.5 m grids.

7.5 Assessment of HEM inversion options using groundtruth data

In the FRESHEM project different options for the inversion of the HEM data were evaluated by comparing the results with independent geophysical measurements (ERT and slimflex measurements). The inversion options that were tested are the following: (1) The lateral constrain look ahead, i.e. what is the radius of influence between nearby soundings, (2) The strength of the LCI regularization, (3) smooth, LCI and sharp inversion results.

ERT (Electrical Resistivity Tomography) is a land-based geophysical method used to investigate the resistivity subsurface distribution along profiles. Two profiles were conducted in April 2016 (FRES01 and FRES02; Figure 1) for comparison with HEM inversion results. FRES01 was taken south of the village Grijpskerke, on a creek ridge. This line is within a few metres parallel to hem line 23.1. FRES02 was taken ~150 m parallel to HEM line 7.9, in the dune area north of Oostkapelle. The electrode spacing used is 2m and the array used gradient. It is important to note that no leveling or calibration is required to process the ERT data, in contrast of HEM data. Data from both profiles were of good quality.

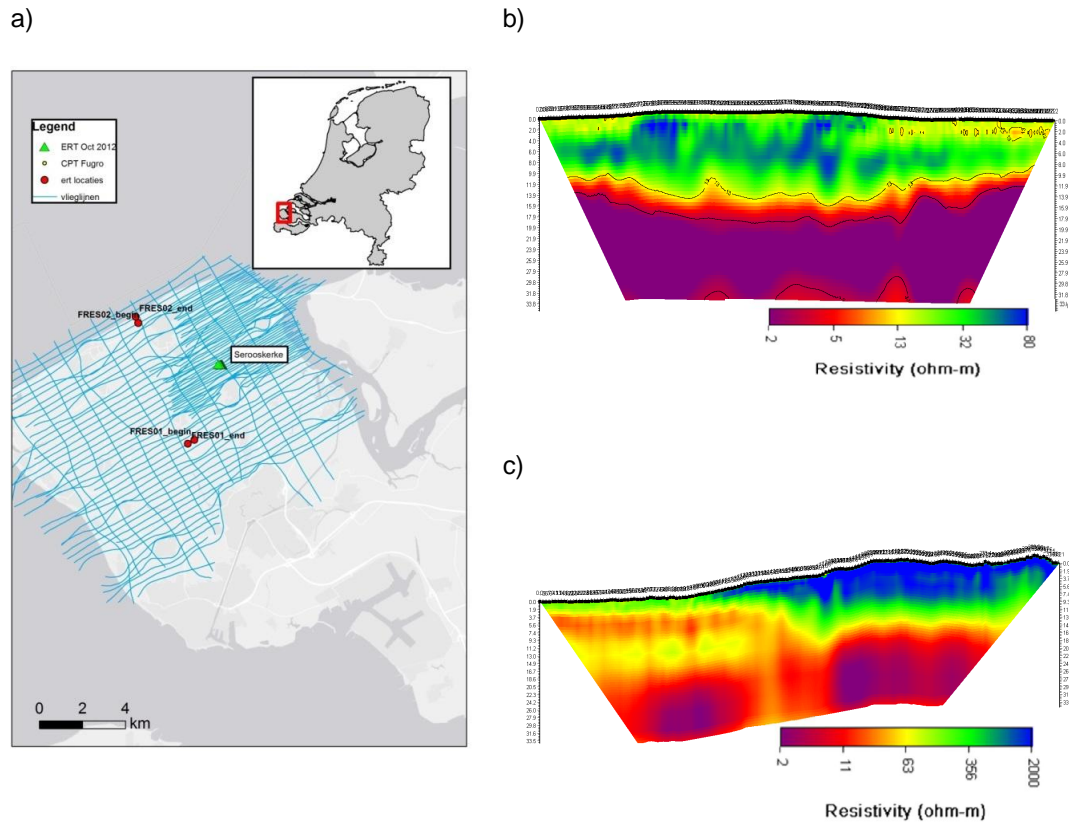


Figure 7.2: a) Map showing the locations of the two ERT profiles FRES01 and FRES02 and the flightlines. The additions ‘_begin’ and ‘_end’ indicate respectively the beginning and end of the two ERT profiles. b) ERT result for FRES01, c) ERT result for FRES02. Note the difference in color scale between b) and c).

ERT results for the two profiles were quantitatively (RMS error) compared to results of a large number of different inversion parameters for the corresponding HEM flightlines. Resulting differences in RMS error between the different parameter sets were, however, either small, or inconclusive between the two ERT profiles.

7.5.1 Final selection of inversion methods

Based on the analysis there is no definitive best choice on which HEM inversion to use. We therefore opted to invert all flightlines using three different inversion methods, with fixed parameter sets, and include all three results in the Monte Carlo uncertainty procedure.

- ‘Aarhus workbench’, smooth LCI, 20 layers
- ‘Aarhus workbench’, sharp LCI, 20 layers, medium strength constraints
- ‘BGR’, SSI, smooth, 20 layers

8 Transformation of bulk resistivity to groundwater chloride concentration

8.1 Theory

Helicopter-borne electromagnetics, as most geo-electromagnetic measurements, measures the total (bulk) conductivity of the soil-pore water-matrix. Both the pore water and the surface of the soil particles contribute to some extent to the bulk conductivity. Pore water conducts current by ions dissolved in the pore water, its conductive properties are hence a function of the salinity of the water. In brackish to saline water, this contribution is generally largest (see also Figure 5.1). Clay and organic particles in the soil conduct currents by means of the exchange of cations on the so-called electrical double layer surrounding the grains. These two contributions to the bulk conductivity must be separated to obtain the conductivity of the pore water (groundwater), the parameter of interest. Note that we only address saturated soils in the following, in unsaturated soils one must also account for pore space occupied by (non-conductive) air.

The contributions of both pore water and surface conductivity to the bulk conductivity may be regarded as a simple parallel electrical circuit. The contribution of the conductivity of the pore water to the bulk conductivity is dependent on the pore space and the 'connectedness' of the pores, both accounted for in the intrinsic formation factor F . The surface conductivity is likewise dependent on the pore space and hence on F , but this is implicitly accounted for in the value of the surface conductivity. In formula (Waxman and Smits, 1968):

$$EC_b = \frac{1}{F} EC_w + EC_s, \text{ with} \quad (8.1)$$

$$F = \frac{1}{\phi^m}, \quad (8.2)$$

with EC the bulk (b), pore water (w) or surface (s) conductivity, F the intrinsic formation factor, ϕ porosity and m the 'cementation factor'. The cementation factor was thus named by (Archie, 1942), who observed the parameter m to increase with increasing cementation of rocks. However, more in general, the cementation factor m describes how coupled or not the inverse of the formation factor and the connected porosity are. The inverse of the formation factor is a representation of the "dynamic porosity" or "effective porosity" connected by the electrical current lines. Simply put, the formation factor can be regarded as a correction for the fact that only part of the measured volume (i.e. the pore space) contributes to the bulk electrical conductivity, the formation factor would decrease to one when regarding a volume of only conducting fluid.

The surface conductivity depends on intrinsic properties of the soil (the amount of exchange sites available, properties of the electrical double layer, amount of clay particles). The current is, however, still transmitted by the pore water. At lower pore water salinities, the conductivity of the soil therefore becomes limited by the conductivity of the pore water. At higher pore water salinities (for clayey soils in Zeeland higher than around 2 mS/cm), the surface conductivity reaches a maximum value and remains constant at higher pore water salinities (Figure 8.1).

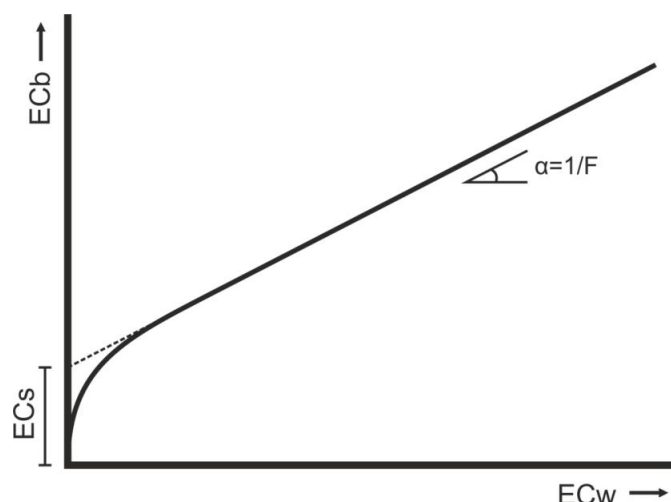


Figure 8.1 Relationship of bulk conductivity (EC_b) and pore water conductivity (EC_w). The tangent of the linear part is the reciprocal of the formation factor. The linear part crosses the y-axis at maximum surface conductivity (EC_s)

In FRESHEM, we assume surface conductivity to be constant over the entire pore water conductivity range. The contribution of surface conductivity is thus overestimated at lower pore water salinities, and this assumption results in an underestimation of pore water salinity in the lower range. This assumption was deemed justifiable given that: (1) differences occur in the freshwater range, at salinities that are all regarded as freshwater by water users, (2) differences are small compared to other uncertainties in the procedure.

Box 1: Apparent formation factor

The use of an 'apparent' formation factor for translation of bulk resistivity to pore water conductivity is still commonplace in geophysical surveys. The apparent formation factor (often just called formation factor) is the ratio between bulk conductivity and pore water conductivity:

$$F_{app} = \frac{EC_w}{EC_b}, \quad (8.3)$$

with F_{app} the apparent formation factor.

The apparent formation factor is then used to directly derive pore water conductivities from the bulk resistivity, assuming F_{app} to be independent of the pore water conductivity. For instance (De Louw et al., 2011) derived and used apparent formation factors in Schouwen-Duiveland, Zeeland:

Lithology	Apparent Formation Factor (-)	Stdev. (n)
Peat	2.1	0.7 (41)
Clay	2.5	0.6 (192)
Sandy clay, clayey sand	2.8	0.8 (52)
Fine sand	3.2	0.4 (299)
Medium coarse sand	4*	
Coarse sand	5*	
Gravel	6-7*	

* formation factors from (Goes et al., 2009)

However, as is clear from Equation 9.1, the apparent formation factor is dependent on the pore water conductivity, especially in the freshwater range and in clayey soils with a significant surface conductivity. The surface conductivity must therefore be explicitly accounted for (Revil and Glover, 1998; Revil et al., 2012).

8.2 Determination of formation factors

8.2.1 Introduction

Transformation of bulk conductivity in pore water conductivity requires both a formation factor and surface conductivity, for the different lithologies present in the study area. (De Louw et al., 2011) present values of the formation factor for different soil types in Zeeland. Their values, however, are values of the 'apparent formation factor' (see box 1). Separating the influence of pore water and surface conductivity in the apparent formation requires a number of assumptions, including estimates for the surface conductivity (Baaren et al., 2016). No other estimates for formation factor and surface conductivity are available for lithologies present in Zeeland. It was therefore decided to derive estimates for formation factors and surface conductivities based on laboratory measurements of soil samples from a sampling campaign in Zeeland.

8.2.2 Methods

In a sampling campaign carried out in May 2016, 71 sediment samples were obtained at 8 different locations on Walcheren. These samples were obtained by using a hand auger above the water table, and a piston sampler and gouge auger below the water table. The drilling depth ranged from 3 to 8.5 m below ground level and the drilling diameter was about 7 cm. At each location a lithological description of the sediment in the field was made using the GEOTOP classification system (Staffeu et al., 2011). This method was preferred over laboratory grain size analyses to ensure maximum compatibility when attributing formation factors and soil conductivities to GEOTOP lithological units. Many drillings showed lithological heterogeneity (layering) on a very small scale (cm to dm). We selected homogenous sections selected as much as possible to sample about 300 cm³ of sediment. We classified the samples into peat (4), clay (16), sandy clay (28), fine sand (22), and medium coarse sand (1) and conserved them in glass containers for laboratory analyses. Sample locations were chosen to maximise the distribution of samples over the most common stratigraphical units in the Zeeland area.

Table 8.1 Distribution of samples over GEOTOP lithological classes and stratigraphical units

Lithological description	n samples	Stratigraphical description	n samples	Combination litho, stratigraphy	n samples
Peat	4	Naaldwijk, Walcheren member (NAWA)	20	NAWA, clay	1
Clay	16	Nieuwkoop, Hollandveen (NIHO)	3	NAWA, sandy clay	9
Sandy clay	28	Naaldwijk, Wormer member (NAWO)	40	NAWA, fine sand	10
Fine sand	22	Nieuwkoop, Basisveen (NIBA)	1	NIHO, peat	3
Medium sand	1	Boxtel (BX)	3	NAWO, clay	15
		Naaldwijk, Schoorl member (NASC)	4	NAWO, sandy clay	19
				NAWO, fine sand	6
				NIBA, peat	1
				NASC, fine sand	4
				BX, fine sand	2
				BX, medium sand	1

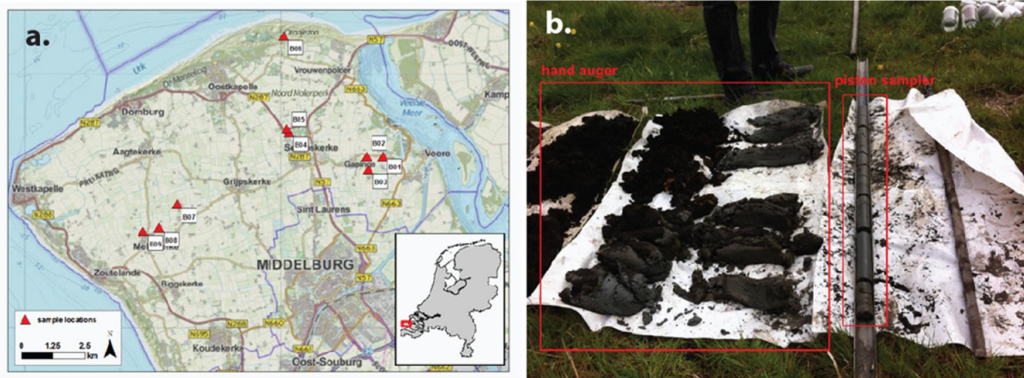


Figure 8.2 Sampling campaign: a) sample locations, and b) example of soil collection using hand auger and piston sampler.

The collected samples were analysed by the Université Savoie Mont Blanc, CNRS, in Chambéry, France. The analysis involved saturating the samples with brines of different conductivities and measuring the bulk conductivity using the four-terminal method with a high-precision impedance analyser (Figure 8.3). The samples were saturated with NaCl brine solutions of 0.31, 5.26, 11.5, 57, 147, and 220 mS/cm (at 25°C). The first brine saturation (5.26 mS/cm) occurred under vacuum (Figure 8.4), other saturations were performed by diffusion in a regularly refreshed large tank filled with a solution of the appropriate concentration. The diffusion process took several weeks to complete per brine.

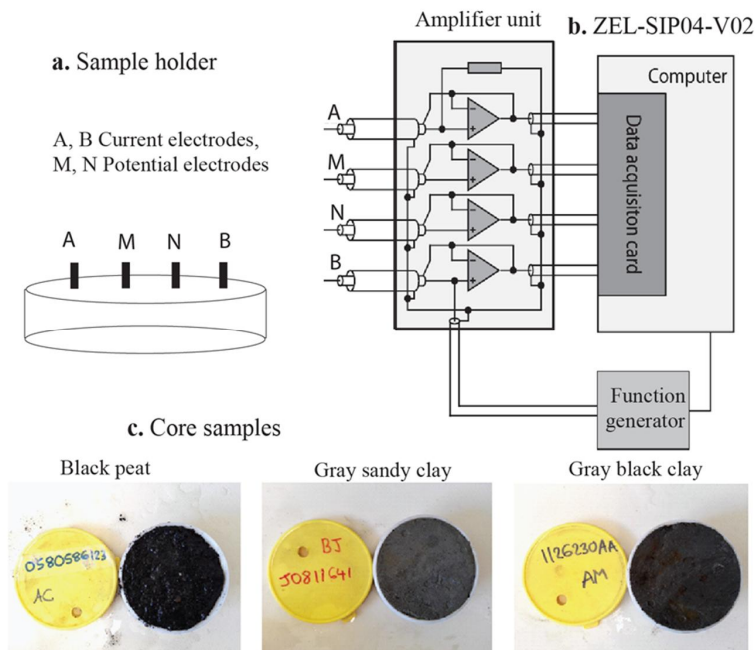


Figure 8.3 Measurement setup for conductivity measurements

The measurement of different bulk conductivities at different pore water conductivities allowed for plots akin to Figure 8.1, and thus allowed for the derivation of a formation factor and surface conductivity for each sample (Revil et al., 2017).

To obtain a single formation factor and surface conductivity per GEOTOP lithoclass, EC_w – EC_b data of all samples of a given lithoclass were combined, before fitting Equation 9.1 to the combined data. The uncertainty of the fitted relation was calculated from the spread in the data. In the fitting process, data from the first saturation (5.26 mS/cm) was excluded. This was due to the fact that, likely due the vacuum extraction employed for this saturation, these measurements plotted consistently out of the relation shown by the other saturations.

Within one lithoclass the formation and surface conductivity will show differences between stratigraphical units, due to differences in e.g. depositional environment and subsequent processes (soil genesis, loading). However, the number of samples for combined lithology-stratigraphy classes are not sufficient for statistically correct quantification per class. Also, not all relevant stratigraphy / lithoclass combinations are represented in the dataset.



Figure 8.4 Saturation of samples under vacuum

8.2.3 Results

Measurement of the samples resulted in 71 times 6 EC_w – EC_b pairs. The different conductivity pairs yielded good fits with Equation 8.1 (Figure 8.5). These fits resulted in 71 values of the formation factor and surface conductivity (Revil et al., 2017). Surface conductivities are significant for almost all samples (mean value 3 mS/cm, σ 1.2 mS/cm). Even for, for instance, the clay-poor aeolian dune sands of the Naaldwijk – Schoorl member, surface conductivities are around 2 mS/cm. Generally though, surface conductivities are highest for clay samples, and lowest for sand samples.

Figure 8.6 shows the fits of Equation 8.1 combining all samples per GEOTOP lithoclass. The obtained values for formation factor and surface conductivity with their standard deviations are shown in the legend of Figure 8.6, as well as in Table 8.3. The Clay and Sandy clay lithoclasses have very similar values, with a formation factor of 4.1 and 4.5 (standard deviation 0.15 and 0.12) and a surface conductivity of 3.0 and 2.6 mS/cm (standard deviation 0.7 and 0.5 mS/cm). Fine sand has very different properties, with a formation factor of almost 6 (standard deviation 0.21) and a lower surface conductivity of 1.6 mS/cm (standard deviation of 0.5 mS/cm). Peat has again different properties and especially a remarkably large spread in the data (resulting in high standard deviation). The formation factor is 2.66 (standard deviation of 0.33) and a surface conductivity of 2.9 mS/cm (standard deviation 3.7 mS/cm). The high standard deviations for the peat sample are possibly due to the presence of two distinct types of peat (from two stratigraphical members, the Basal Peat member and Holland Peat member).

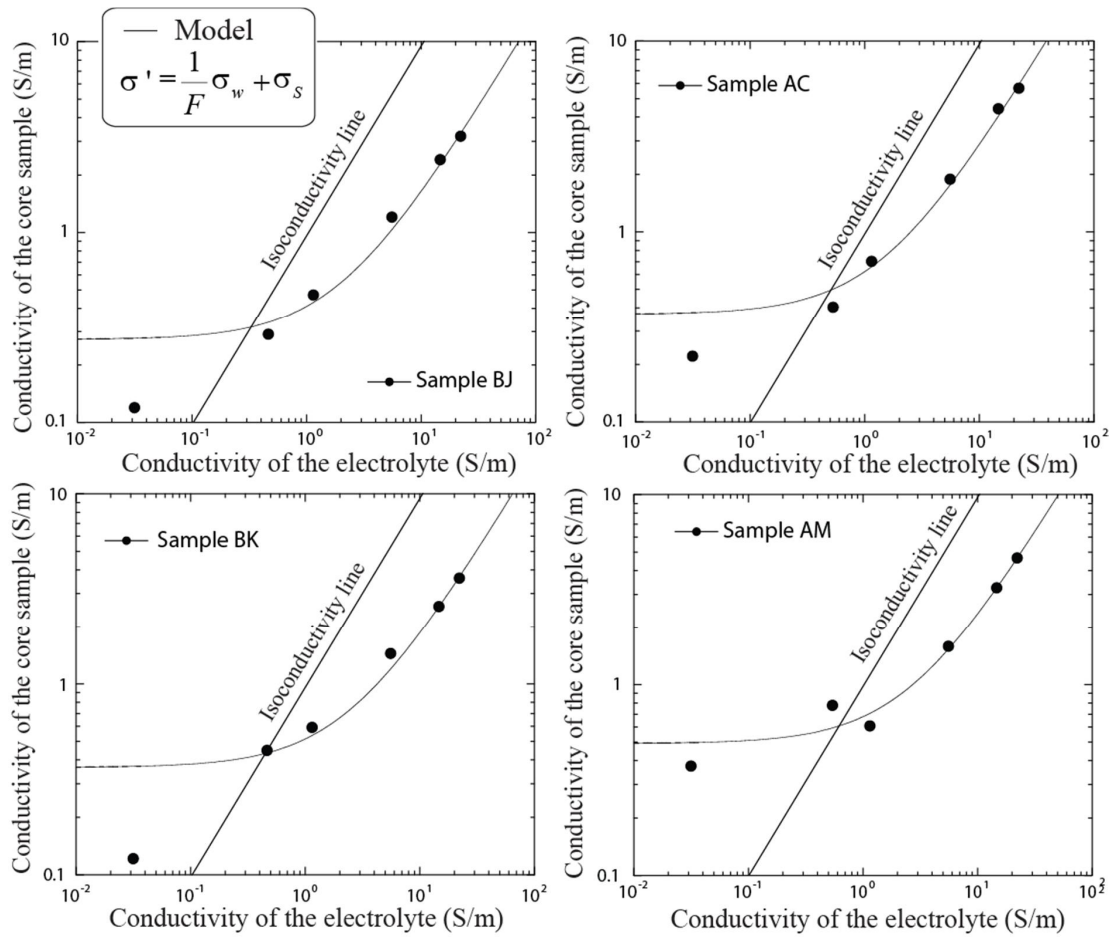
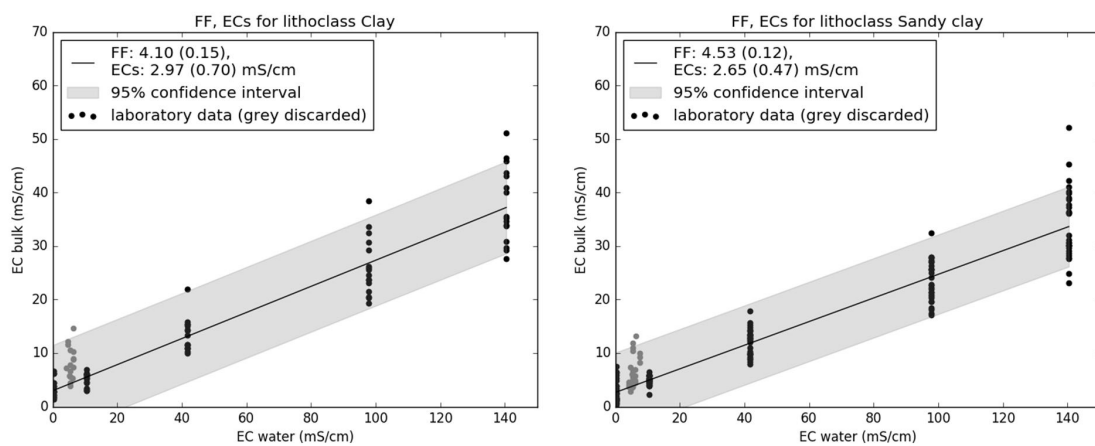


Figure 8.5 Fits of Equation 9.1 to bulk conductivity measurements of different samples saturated with known pore water conductivities. Note that axes are on log-scale, so the linear line of Figure 8.1 is curved in these plots.



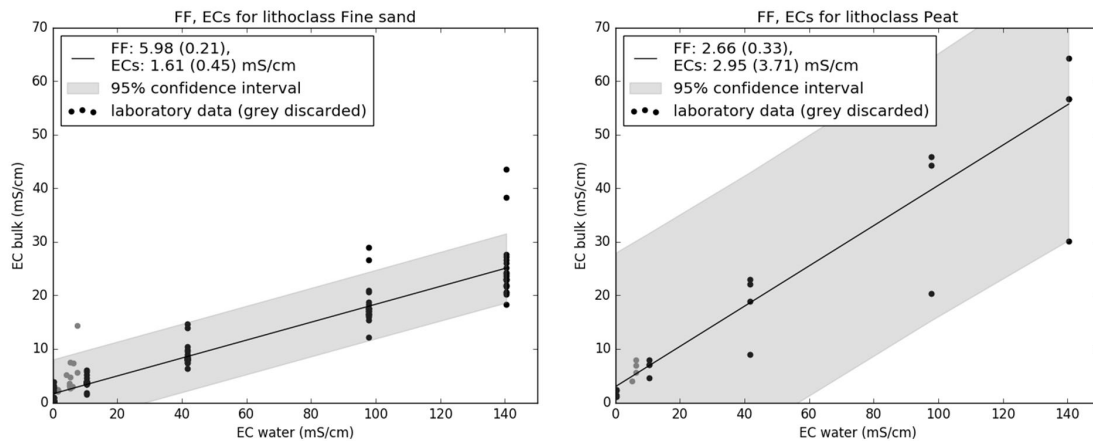


Figure 8.6 Results of derivation of formation factor FF and surface conductivity ECs per lithoclass.

8.2.4 Discussion

The applied laboratory analyses to derive formation factors and surface conductivities from several EC_b – EC_w pairs per sample have not previously been applied to soft sediments (Revil et al., 2017). The approach has been validated by thorough calibration of the measurement equipment, and the plausible relations between surface conductivity, quadrature conductivity, and comparison to previously investigated hard rock formations (Revil et al., 2017).

When compared to values for the formation factor and surface conductivity applied in the FRESHEM Kanaalzone pilot, values for both the formation factor and surface conductivity are notably higher (Table 8.3). Values in the Kanaalzone pilot were obtained by correcting apparent formation factors as given by (De Louw et al., 2011), with literature-based values for the surface conductivity.

Table 8.2 Formation factor and surface conductivity used in Kanaalzone pilot

Lithology	Formation factor (-)	Surface conductivity (mS/cm)
Clay	2.9	1.24
Sandy clay	3.2	1.
Fine sand	3.4	0.35
Peat	2.6	2.5

Both formation factors and surface conductivities for fine sand, clay and sandy clay are notably higher than the values used in the Canal Zone Gent-Terneuzen pilot study. Reasons for these differences could include: (1) a systematic difference in lithological properties between the sampled lithologies and the lithologies sampled by (De Louw et al., 2011), (2) scaling issues between laboratory samples and the TEC probe measurements of (De Louw et al., 2011), exhibiting a footprint of decimetres, (3) sampled locations not being a valid representation of the different lithologies, (4) laboratory EM measurements deviating in an absolute sense from field EM measurements, or (5) laboratory samples not well representing field conditions. Discussions with Université Savoie Mont Blanc pointed in the direction of the latter: a systematic difference between field and laboratory conditions, caused by the packing of the material, resulting in a probable overestimation of intrinsic formation factors. This difference in packing influences only the measured intrinsic formation factor, and not the measured surface conductivity.

Differences between the values used here, and the values used in the Canal Zone Gent-Terneuzen pilot study result in: (1) lower groundwater salinity in the fresh water range, due to the higher surface conductivity, and (2) higher groundwater salinity in the brackish to saline range,

due to the higher formation factor, as compared to the pilot results for the Canal Zone. The used formation factors have been shown to result in chloride concentrations exceeding seawater concentration in the saline parts. These values have been truncated to the class > 15000 mg/L, and therefore have no adverse effect on the end-result.

8.3 Calculation of groundwater chloride concentration within a Monte Carlo uncertainty approach

In FRESHEM the following basic calculation procedure is used to calculate groundwater chloride concentration from the inverted FRESHEM results (bulk conductivity):

1. Get bulk conductivity for given location and depth (HEM inversion result)
 - Uncertainty by including 3 different inversion schemes and standard deviation around two of the three inversion schemes (not available for third inversion scheme)
2. Obtain lithoclass for location and depth from GEOTOP
 - Uncertainty using the probability of lithoclasses provided by GEOTOP
3. Obtain formation factor and surface conductivity for lithoclass
 - Uncertainty using the standard deviation in Table 8.3
4. Calculate pore water conductivity using Equation 8.1
5. Calculate chloride concentration from conductivity
 - Uncertainty using the standard deviation of α and β (section 8.3.5)

All these steps, however, include to some extent uncertainties. The inversion of HEM measurements contains uncertainties, in the lithoclass prediction by GEOTOP uncertainties are involved, et cetera. The basic procedure is therefore executed within a Monte Carlo uncertainty approach. This Monte Carlo approach basically entails performing the calculations a large number of times, each time drawing a parameter from a parameter distribution, instead of applying a fixed value. Uncertain parameters are thus treated as stochastic, instead of deterministic. Below, each of the basic steps is further elaborated, including the specifics of the uncertainty approach. The number of calculations performed in the Monte Carlo analyses is 600. The number of draws is a compromise between accuracy of the resulting probability distribution and calculation time; preliminary analyses showed 600 draws to suffice to obtain a consistent, and hence accurate, probability distribution of groundwater chloride concentration.

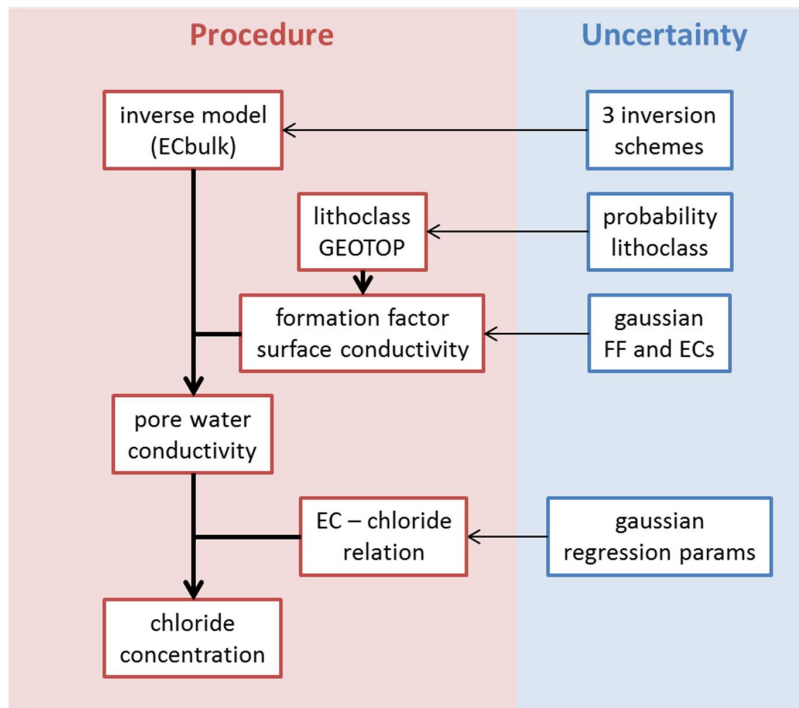


Figure 8.7: Overview of procedure and uncertainty approach

8.3.1 Inversion result: bulk conductivity

For each flightline, FRESHEM results are inverted using three inversion schemes (Chapter 7). The three resulting bulk conductivity results are mapped to the same vertical layering. The layering is based on the 'BGR' result; the two 'Aarhus' inversion results are linearly interpolated to the BGR vertical layering. The 'depth-of-investigation' of the 'BGR' result (bottom of the (n-1)th layer) is taken to apply to all three inversion results.

In the Monte Carlo procedure, the three inversion schemes are given equal weight: each is equally likely to be drawn. For the two Aarhus inversions also a standard deviation for each HEM layer is taken into account, assuming a normal distribution. The BGR inversion did not provide a standard deviation.

8.3.2 Obtain lithoclass from GEOTOP

For each vertical layer for each spatial location, the corresponding lithoclass probabilities are obtained from the GEOTOP lithological model. These probabilities are used straightforwardly in the Monte Carlo procedure: the probability of a lithoclass being drawn is equal to the GEOTOP probability of occurrence of that particular lithoclass. Note that the HEM layers are not exactly coinciding with and are often thicker than the GEOTOP vertical layering (0.5m). For HEM layers extending deeper than GEOTOP model boundary (50 m below Dutch Ordnance Level, NAP) the fine sand lithoclass was used. All GEOTOP layers within the HEM-vertical layer are selected, vertical mismatches are accounted for in the vertical upscaling procedure (9.3.4).

8.3.3 Obtain formation factor and surface conductivity for lithoclass

For a drawn lithoclass, a formation factor and surface conductivity is obtained from TABLE XX. The formation factor and surface conductivity are regarded as normally distributed, with a mean and a standard deviation derived from the regression result (9.2.3). No information was available on uncertainty in formation factor and surface conductivity of lithoclasses medium-coarse sand, coarse sand and gravel. Uncertainty for these lithoclasses was therefore set to zero.

Table 8.3 Values used for formation factor and surface conductivity

Lithology (GeoTop classes)	Formation Factor (-)	Stdev. (-)	ECs (mS/cm)	Stdev. (mS/cm)
Peat*	2.66	0.33	2.95	3.71
Clay*	4.1	0.15	2.97	0.70
Sandy clay*	4.53	0.12	2.65	0.47
Fine sand*	5.98	0.21	1.61	0.45
Medium coarse sand**	6.6	0	1.1	0
Coarse sand**	5.0	0	0	0
Gravel**	6.5	0	0	0
Shells**	5.0	0	0	0

* values from laboratory procedure, ** values from (Baaren et al., 2016, adapted from De Louw et al., 2011)

8.3.4 Calculate pore water conductivity

For each location, for each vertical HEM layer, for each Monte Carlo draw, pore water conductivity is calculated using Eq. XX. However, as different lithoclasses may be present within a single HEM layer (vertical resolution of GeoTOP is generally higher than HEM), Eq 8.1 has to be upscaled over the various GEOTOP layers within a HEM layer:

$$EC_w = \frac{n \cdot EC_b - \sum_{i=1}^n EC_{s_i}}{\sum_{i=1}^n \frac{1}{F_i}}, \quad (8.4)$$

with i denoting the layer index, and n the number of GEOTOP layers within the considered HEM layer.

Again note that application of the linear Equation 8.1 over the full domain of pore water conductivities is not valid for low conductivities (paragraph 8.1). Applying Equation 8.1 for low bulk conductivities then often yields negative pore water conductivities. Such negative values are corrected to zero.

8.3.5 Calculate chloride concentration

First, obtained pore water conductivity is converted to conductivity at a reference temperature of 25 °C (EC_{25_w}), by assuming a constant groundwater temperature of 11 °C and correcting for temperature. Groundwater chloride concentration is then calculated from the temperature-referenced pore water conductivity by applying the linear relation established by (De Louw et al., 2011):

$$Cl \text{ (mg/l)} = \alpha \cdot EC_{25_w} \text{ (mS/cm)} - \beta \quad (8.5)$$

Where $\alpha = 360$ with a standard deviation of 6 and $\beta = 450$ with a standard deviation of 190. This linear relation is based on regression analysis ($R^2=0.98$) on 79 groundwater samples obtained from two sites in Schouwen-Duiveland (De Louw et al., 2011).

This relation is only valid when Chloride and Sodium ions dominate the electrical conductivity. This is the case from an EC_{25_w} of about 2 mS/cm (Cl 270 mg/l). Below this threshold, other ions (bicarbonate, sulphate) also significantly contribute to the overall conductivity. The contribution of these ions is much more variable, no clear relation therefore exists for lower conductivity values. Because the above pertains chloride values that predominantly fall in a single (lowest) chloride-

class, this does not significantly influence the FRESHEM results. The above relation has therefore been applied over the entire conductivity range.

Chloride results are finally classified in 10 discrete intervals, to both simplify the 3D interpolation effort, and to match the precision of the results to the uncertainty around the data, to avoid overly precise use of the final data.

8.4 Results

Results of this procedure are probability density functions for chloride concentrations per vertical HEM layer, per HEM measurement point along a flightline. An example probability distribution is shown in Figure 8.8. In this (somewhat exaggerated) example, 25% of the calculations of chloride concentration would be below 500 mg/L, 50% below 1660 mg/L and 75 % below 2785 mg/L.

The concentrations for these three percentiles are shown for each flightline in a graph to give insight in the distribution of saline and fresh water along a flightline and the uncertainty between these percentiles (examples in Figure 8.9, Figure 8.10). The largest differences are visible around the brackish zone, while the fresh water lenses and saline areas have a smaller difference between the percentiles. The figures clearly display the decrease of amount of fresh water with higher percentiles and the shallower depth of the interface between fresh and saline water (Figure 8.9).

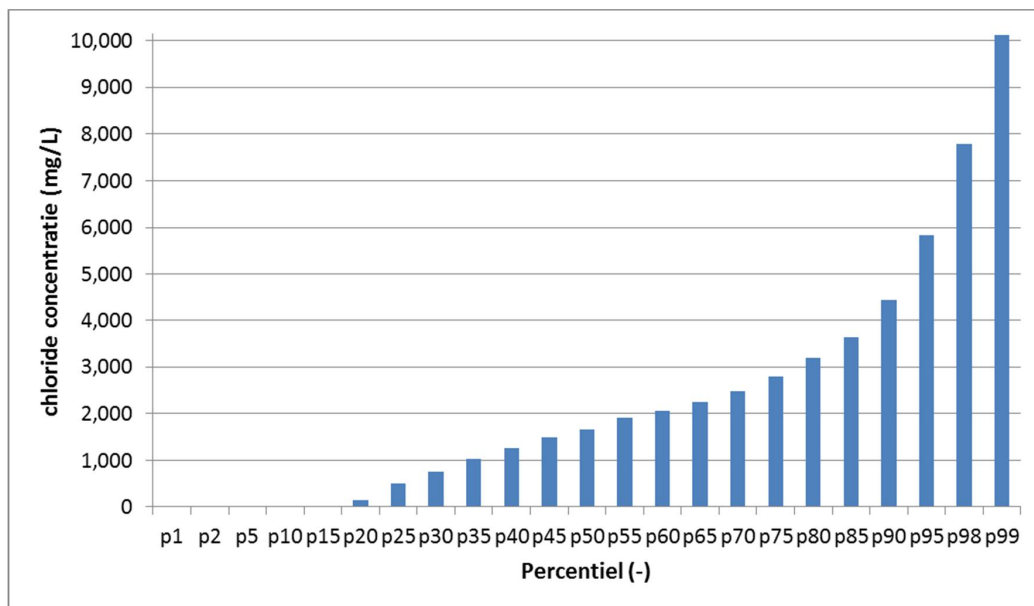


Figure 8.8: Example probability distribution of chloride concentration

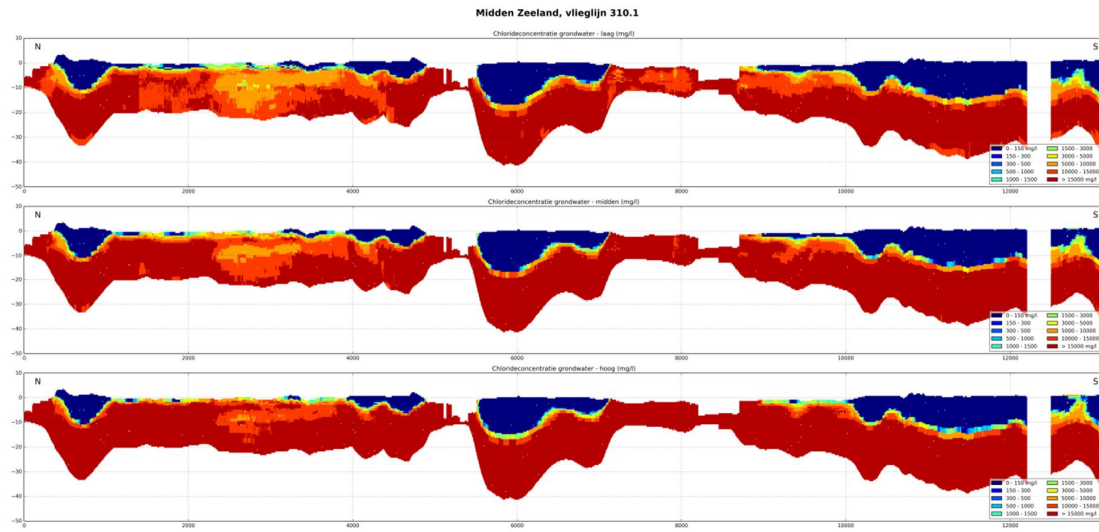


Figure 8.9: 25th, 50th and 75th percentile chloride concentration (top, middle, bottom) for flightline 310.1 (Midden Zeeland)

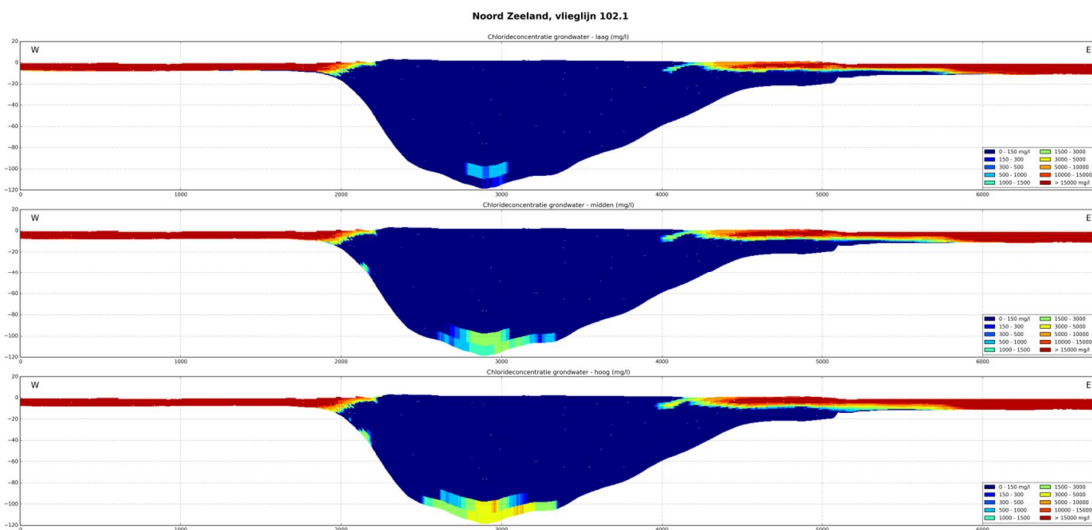


Figure 8.10: 25th, 50th and 75th percentile chloride concentration (top, middle, bottom) for flightline 102.1 (Noord Zeeland)

9 3D interpolation

9.1 Introduction

Interpolation is used to estimate a chloride concentration at locations where no data is available. Constructing a reliable 3D model of chloride concentration based on HEM data, has its challenges because of the very high data density on the flightlines (approx. 4m between datapoint on the flightline), while the individual flightlines are separated 100 – 300m. The 3D model schematises the subsurface in voxels (3D pixels), each measuring 50 by 50 metres in the horizontal directions and 0.5 metre in the vertical direction. After interpolation the entire model will be filled with voxels containing an estimation of chloride concentration. Due to the voxel size being much greater than the data separation on the flightlines, averaging of data is inevitable and there will be some loss in detail compared to the 2D result at the flightline locations.

9.2 Resampling the 2D dataset

The 2D dataset contains stochastic estimates of chloride concentration for 1084 flightlines. On every flightline 20 layers are defined with a thickness of 0.5m to several metres. For each layer a stochastic chloride concentration is calculated at a horizontal spacing of approx. 4 metres between measuring points. This results in a large dataset of data locations containing a Probability Density Function (PDF) of chloride concentration. To balance the importance of thick layers compared to thin layers for the interpolation, this data is resampled vertically to a sample every 0.5 metre instead of one for each layer. This amounts to a dataset of over 151 million points, each containing a full PDF of chloride concentration. Unfortunately, interpolation calculation times are strongly correlated with the size of the input dataset. This dataset therefore has been stripped of some redundancies. Data at a smaller scale resolution than the voxel size has little added value and is resampled to the average PDF of chloride concentration in each voxel. The dataset that has been used for interpolation then adds to 12.8 million data locations.

9.3 Model boundaries

Lateral extent

The 3D model has been calculated to a maximum distance of 300 metres from the HEM measurements. This means there will be a 'hole' inside the 3D model where data is separated by more than 600 m. This can occur at locations of villages and some power lines. The outer boundaries of the model are determined by the maximum extrapolation of 300 m from data coverage.

Model bottom

The 2D dataset has a lower boundary where chloride concentration could be calculated. This lower boundary is depending on the penetration depth of the airborne EM signal. The base of the 3D model has been determined by Inverse Distance Weighted (IDW) interpolation of the depth of the deepest measurements of the 2D result.

Model top

The vertical location of the uppermost measurements of the 2D result is largely dependent on groundwater level. The upper boundary of the 3D model should therefore follow the groundwater level. A simple IDW interpolation cannot represent these structures at, for example, the locally elevated groundwater level along creek ridges. For every measurement location the difference between the vertical location of the uppermost measurement and the average summer groundwater level from the Zeeland model (Van Baaren et al, 2016) is determined. This difference is interpolated by IDW and added to the groundwater reference level. This makes for an upper boundary of the 3D model that is equal to the uppermost measurements of the 2D result, at the same time honouring the shape of the groundwater level in between the flightlines.

9.4 3D interpolation of chloride probability distribution

9.4.1 Interpolation method

There is a wide range of different interpolation techniques, where some can provide a measure of uncertainty of the interpolation result. The choice of the interpolation method depends on the statistical and spatial characteristics of the data, as well as the format of the desired result. For interpolation of spatial data Kriging is often used. One of the advantages of Kriging is its ability to correct for data clustering. Clustered data tend to unduly influence the interpolation results because the amount of data in a cluster is overwhelming other data that is not clustered. Kriging corrects for data clustering by assigning low interpolation weights to clustered data points compared to more solitary data points. Kriging interpolation predicts the value of a location by assigning specific weights to all data samples in the neighbourhood. The size and shape of the neighbourhood define the number and spatial distribution of the data samples that are used for the estimation, (see 9.4.2). The weight that is assigned to each data point is (a.o.) determined by the semivariogram (see 9.4.3). Definition of the neighbourhood and semivariogram are parameters that should be carefully set, as they can influence the 3D interpolation result significantly. This chapter deals with the particular problems and solution that we have experienced in this project. The background of kriging can be found in many standard geostatistical textbooks, e.g. (Isaaks and Srivastava, 1989; Goovaerts, 2006).

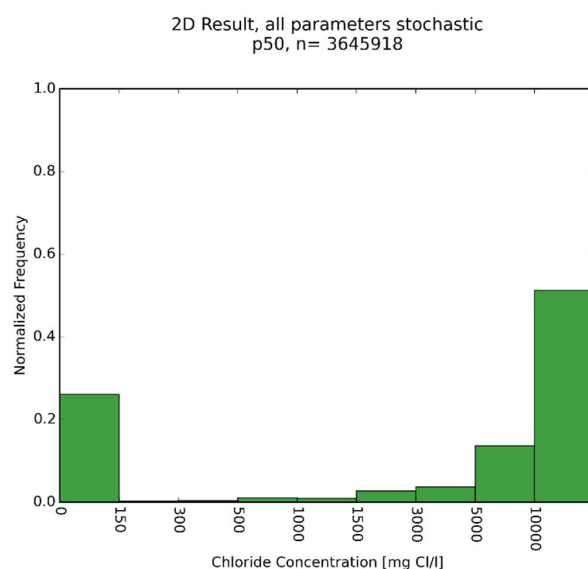


Figure 9.1: Histogram of the median value (p50) of chloride concentrations of the 2D result, for the area indicated in Figure 10.1.

The 2D result (data on the flightline) shows chloride concentrations with a strong bimodal distribution. Figure 9.1 shows a histogram of the median of the PDF of the chloride concentrations from the 2D result, for the eastern half of Walcheren (for location, see Figure 9.5). In this area 26% of the data falls in the lowest class of 0-150 mg Cl/l. All classes between 150 and 5000 mg Cl/l only make up 10% of the data, while 64% of the data has a chloride concentration above 5000 mg Cl/l. Although the balance between fresh and salt groundwater changes for different areas in Zeeland, the strong bimodal distribution of chloride concentration is consistent. Interpolation always causes a certain amount of averaging of data, which will cause an increase in predicted 'brackish' values. To minimize this smoothing effect the Kriging variety Indicator Kriging is used. The indicator method is often used for interpolation of datasets with a non-Gaussian distribution. With Indicator interpolation the data values themselves are divided into threshold values, the indicator values. Thresholds are chosen at critical values, with most

thresholds at the part of the distribution with most interest. A separate Kriging interpolation is then performed for every indicator. After interpolation for each location the chance of exceeding each threshold value will be defined.

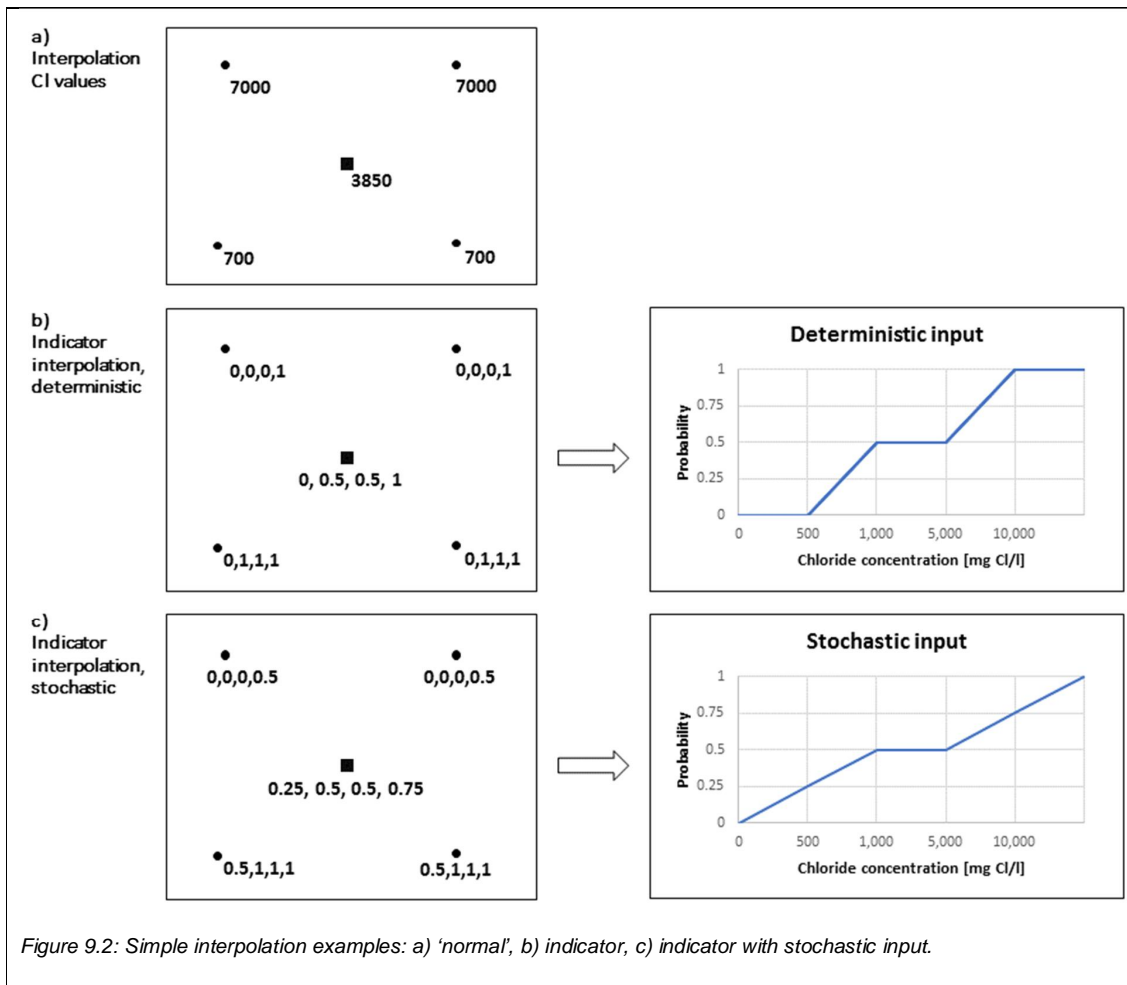
Indicator interpolation has some advantages for this dataset. First, by using indicator interpolation, no assumptions about (near) normality of the data needs to be honoured, which is the case by “normal” kriging. By using Indicator interpolation, the PDF of chloride for the voxel will be determined from the discretised PDF of the data points in the neighbourhood. This results in an estimated PDF that resembles the PDF of the input values. The histogram of the 3D model will therefore be more similar to the histogram of the 2D result, compared to direct interpolation of chloride concentration values. This means the increase of the brackish zone from 2D to 3D is limited. Second, Indicator Kriging produces a model uncertainty depending on the spatial distribution *and* values of the input data. Direct Kriging of the input data would result in an estimation of uncertainty only dependent on spatial configuration of the input data and the variogram, independent of input data values. Third, the use of stochastic input data that comes from the 2D result is straightforward. The PDF of the 2D result can be directly transformed into indicator values. Indicator interpolation does have some disadvantages, including a linear increase in calculation time when more indicators are used (as every indicator needs a separate interpolation) while the use of more indicators increases the accuracy of the 3D model. Threshold values should therefore be carefully chosen and at least include the indicators of the class boundaries.

Box 2: Example Indicator Interpolation of chloride probability

A simple configuration of 4 sample locations is given in Figure 9.2a, with four sample locations (round dots) at an equal distance to the location we want to interpolate (square in the middle). Most interpolation methods will give an expected value equal to the mean of the four observations: $(7000 + 7000 + 700 + 700) / 4 = 3850$. This can be an undesired result, as a value around 3850 is not present in the data at all. Indicator interpolation can correct for this, by interpolation of the indicator values at specific thresholds instead of the data values themselves. First data is transformed to a binary indicator value of 0 (value is above threshold value) or 1 (value is below threshold value).

The same data as used in Figure 9.1a, with threshold values of 500, 1000, 5.000 and 10.000, will translate to indicator values of $ind_{500}=0$, $ind_{1000}=0$, $ind_{5.000}=0$ and $ind_{10.000}=1$ for the sample locations with a value of 7000, and to $ind_{500}=0$, $ind_{1000}=1$, $ind_{5.000}=1$ and $ind_{10.000}=1$ for the locations with a value of 700. Interpolation of each indicator separately will result in the average values $ind_{500}=0$, $ind_{1000}=0.5$, $ind_{5.000}=0.5$ and $ind_{10.000}=1$ (see Figure 9.2b). This result gives a probability of 50% being between the boundaries 500 and 1000, and 50 percent between 5000 and 10000. Note that the predicted probability of being between 1000 and 5000 is 0%, while direct interpolation resulted in an estimation of 3850.

Another advantage of Indicator interpolation is the possibility to handle stochastic input data. The data values in this example can be given an associated uncertainty, e.g. take an $ind_{10.000}$ value for the two upper locations is 0.5 instead of 1 (corresponding to a chance of being below the 10.000 threshold of 50%) and the ind_{500} value for the two lower locations of 0.5. The interpolation procedure is then the same, only with continuous data between 0 and 1 instead of binary data. The uncertainty of the input now translates to an estimation with 25% chance being in the classes 0-500, 500-1000, 5.000-10.000 or above 10.000. There is still a 0% probability of our estimation being in the 1.000-5.000 class.



9.4.2 Neighbourhood

The neighbourhood defines the area where data can be selected. Increasing the size of the neighbourhood will increase the estimation accuracy, but also increase calculation times. The maximum number of samples used for estimation of a single location is set to 16. Simply selecting the 16 closest samples will result in sudden jumps of chloride concentration estimations in between flightlines, as the selected samples would always be taken from one flightline. Better interpolation results are achieved by selecting data from the two nearest flightlines. This is achieved by splitting the neighborhood horizontally in four sectors, with the four nearest samples selected in each sector separately. This procedure ensures a more gradual transition of chloride concentration in between two flightlines. The size and shape of the neighbourhood is taken from the local anisotropic behaviour of the data, and is adjusted locally based on the data characteristics. This is explained in section 9.5.

9.4.3 The semivariogram

The semivariogram model represents the spatial correlation that is expected in a dataset. The characteristics of this spatial correlation defines the weight that samples in the neighborhood are assigned, based on distance from the estimation location. An experimental semivariogram can be constructed based on data, where semivariogram values are calculated as the average difference of samples separated by a specific distance:

$$\hat{\gamma}(\bar{d}_j) = \frac{1}{2N_j} \sum_{i=1}^{N_j} ((s_i - (s_i + d))^2), \forall (s_i, s_i + d): h \in [d, d_j + \delta] \quad (9.1)$$

With d the distance between two data points, d_j the minimum distance between two points in class j , δ the class size, N_j the number of data points in class j . The experimental semivariogram of the p50 of the 2D result from Walcheren is given in Figure 9.3a. Because interpolation is performed on indicator values, the spatial correlation of the indicators will define the semivariogram that is used for interpolation. Luckily, the experimental variogram shows similar characteristics as does the p50, see Figure 9.3b.

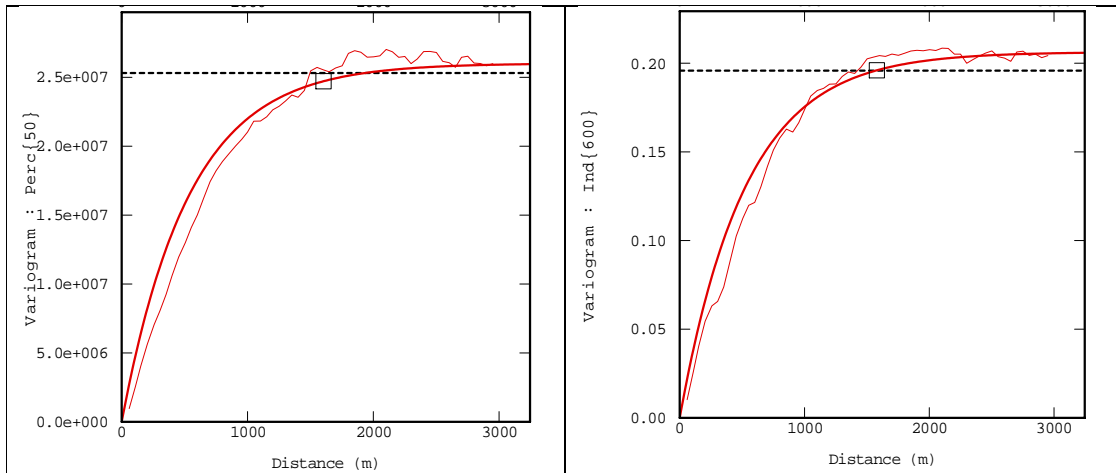


Figure 9.3: Omnidirectional experimental variograms (wiggly line) and a fitted exponential variogram model (stable line) for the 2D result from the area indicated in Figure 9.5, for a) the p50 , and b) the 600 mg C/I indicator

From the experimental semivariogram, the variogram model can be determined. This is a somewhat arbitrary step, as there is some freedom in choosing the variogram shape. An exponential model with a nugget gives an acceptable fit to our data, with the variogram model defined as:

$$\gamma(d) = C_0 + C \left(1 - e^{\left(\frac{-d}{r}\right)}\right) \quad (9.2)$$

With nugget C_0 , a sill C and range r (see Figure 9.4). For indicator interpolation the chosen value for nugget and sill is not essential for the estimation result, as we are only interested in the most likely estimation for each indicator and the estimation uncertainty for each indicator is ignored. This leaves the definition of the range parameter, the distance after which no spatial correlation is expected. As will be made clear in the next section, an approach is used where the range shows anisotropic behaviour and is adjusted locally, based on the data characteristics.

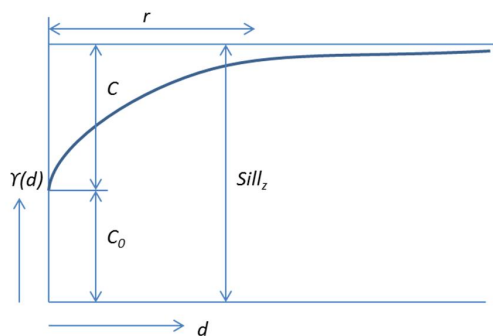


Figure 9.4: Meaning of the nugget (C_0), sill (C) and range (r) in an variogram model.

9.5 Anisotropy

9.5.1 Necessity

Interpolation predicts a value based on multiple data points and will always result a certain degree of averaging with respect to the original data. This can result in small scale structures, like a small fresh water body under a creek ridge, having limited expression in the 3D model. In Zeeland creek ridges are an important factor controlling the distribution of fresh groundwater. Figure 9.5 shows the surface elevation of Walcheren, dominated in the central part by the creek ridge morphology. A depth slice of the 2D result at 6 m below NAP is shown in Figure 9.6a) to c). Under the creek ridges more or less north-south orientated elongated fresh water bodies are present at this depth. Kriging interpolation assigns weights to data points depending on their distance (and clustering). As there is a mix of data expressing high as well as low chloride concentrations around the narrow creek ridges, interpolation will result in a large uncertainty regarding the size of these fresh water bodies. The p10, p50 and p90 of the interpolation result of the same area is shown in Figure 9.6d) to f). The fresh water body at the top displays a very high uncertainty, being 300 to 400 metres wide at the p10 but virtually non-existent in between the flightlines at the p90. This differs considerably from the 2D result, where the width of the fresh water lens is about 150m at smallest.

Using intuition it is easy to improve the above interpolation result, as the north-south direction of the fresh water body is easily visible. Samples oriented within the same direction as the creek ridge system have a high chance being similar, while samples oriented perpendicular to the creek ridge will more likely be dissimilar. But as long as we don't tell our interpolation method what the direction highest correlation is, interpolation is blind with respect to the expected structures and treats every direction equal.

Anisotropy is the concept that properties are more continuous in one direction than another. Although anisotropy is often imposed on kriging interpolation to improve modelling results, mostly a global anisotropy is used where everywhere in the model area the same direction and magnitude of anisotropy is assumed. As our creek ridge systems change direction rapidly, global anisotropy will do no justification to the observed variability. The expected spatial variability of anisotropy should be defined locally and give anisotropy parameters for each voxel. Although the implementation of such a Locally Varying Anisotropy (LVA) field in kriging interpolation is available in specialized interpolation software, determination of the local anisotropy is not straightforward and no generally applicable methods are available.

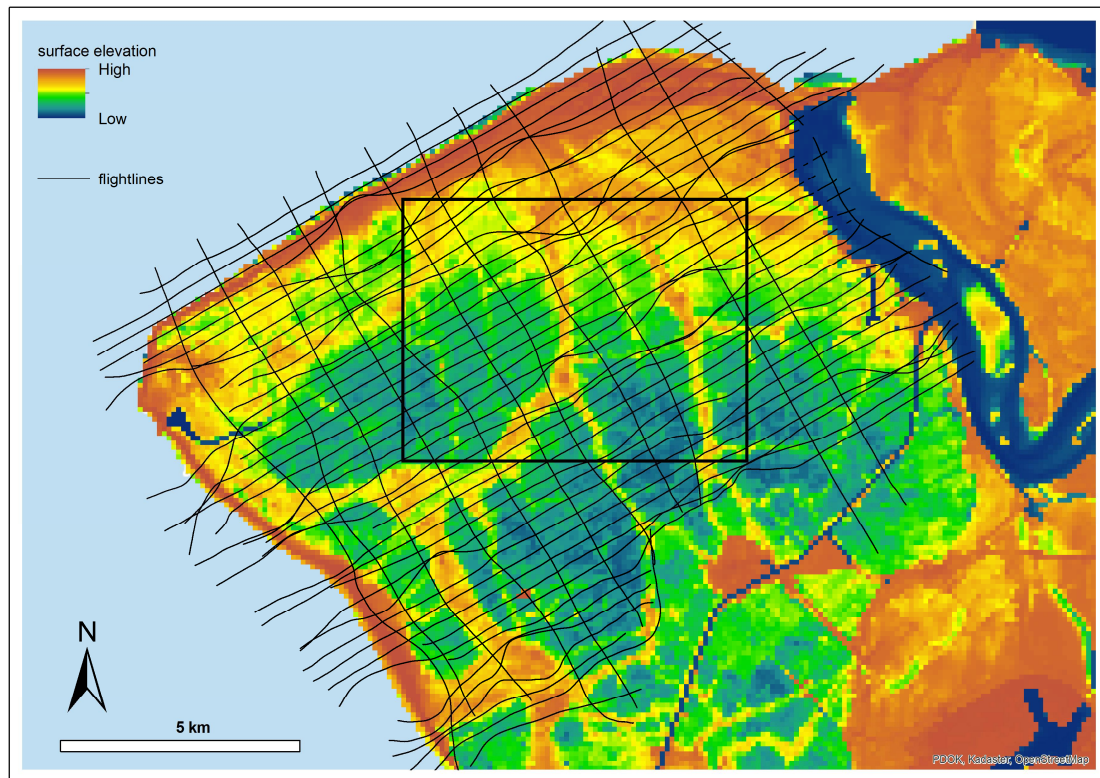


Figure 9.5: The surface elevation on Walcheren shows the elevated creek ridge morphology where elongated fresh water bodies are present. Flightlines are of set 169, that have been used for the anisotropy analysis in this section. The black box indicates the area of interest in this section.

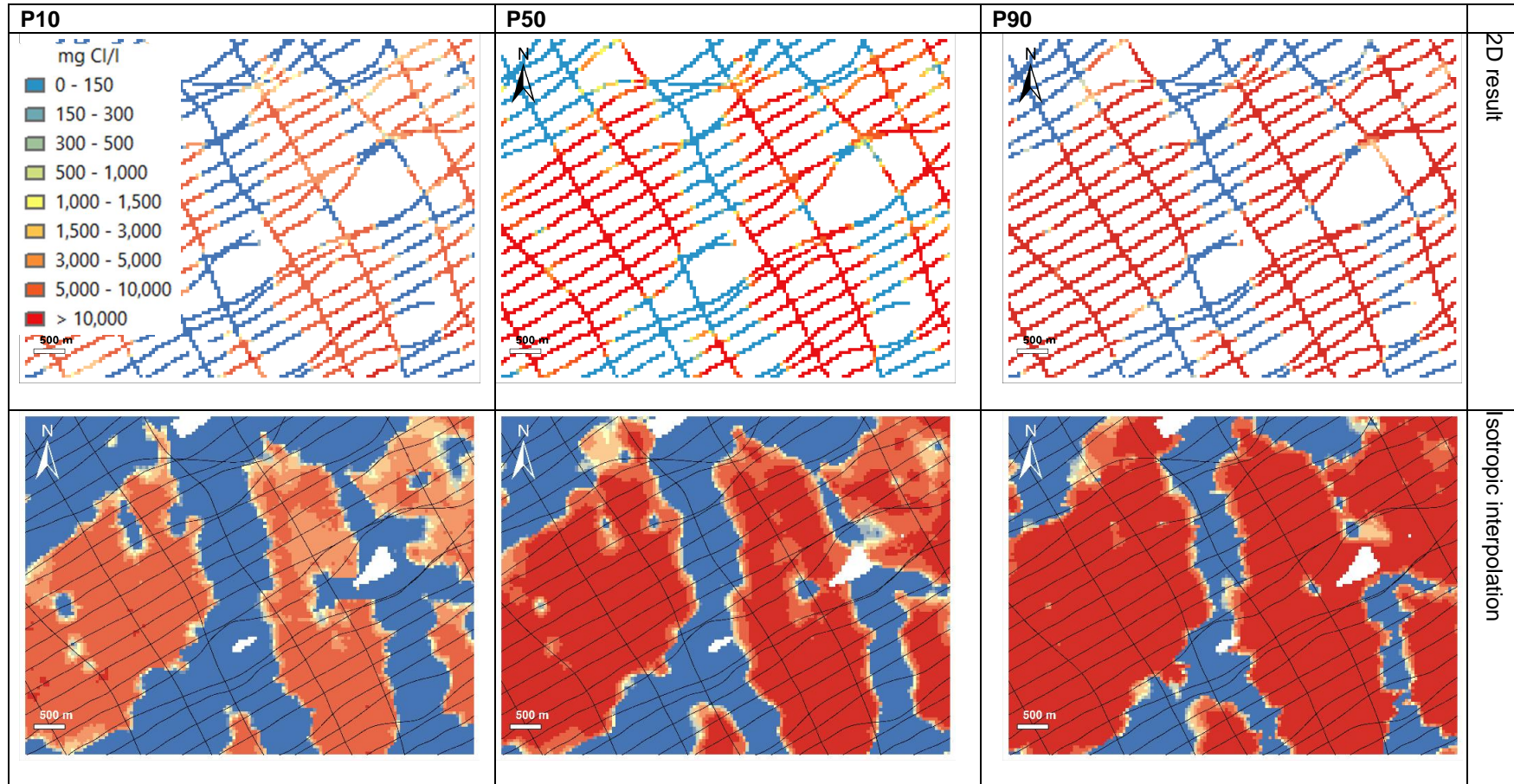


Figure 9.6: Depth slices at 6 metres below NAP. P10, P50 and P90 are shown for the 2D result and a 3D model using isotropic indicator kriging. The area of interest is indicated in Figure 9.5, black lines indicate flightlines.

9.5.2 Quantifying anisotropy

Previous work

Anisotropy is often easily detected visually in the 2D result, but the 3D model of Zeeland is too large to manually construct the LVA field. A number of different methods to quantify the LVA field automatically can be found in literature, mostly making use of prior information. Object-based simulation algorithms (e.g. Deutsch and Wang, 1996) simulate many instances of specific geometries in the model space. Another approach is conditional simulation using multiple-point statistics read from training images (e.g. Strebelle 2002). Both methods rely heavily on the quality and suitability of the prior information, and are often used for modelling when data is sparse and extra input from geological knowledge is needed. The data density of the FRESHEM project justifies a method for construction of the LVA field that is purely based on chloride concentration data from the 2D result. Te Stroet and Snepvangers (2005) introduce the local anisotropy kriging method that does not need any prior information about the structures in the data. Following an initial kriging interpolation, a gradient algorithm is used to calculate an LVA field. Kriging is then performed with the LVA field imposed, and from this new interpolation result a new LVA field is determined. This step is repeated until an iteration criterion is reached. Although fit for our data, this method relies on many interpolation iterations. A single kriging interpolation run with the FRESHEM dataset for the entire Zeeland modelling area already takes multiple days, which prevents a run with many iterations to be practical. Another way to determine anisotropy directly from input data is by automated calculation of the variogram model. If directional variograms are calculated based on local data, the range of each of the directional variograms contains the expected correlation distance in that direction. This is a promising method that is applied in some geostatistical software packages, e.g. the gstat module in R (Pebesma, 2004) and the Isatis modelling software package (www.geovariances.com). However, automated variogram estimation can be very time consuming on the FRESHEM modelling scale and the experimental character can result in unexpected results.

The FRESHEM method, determine anisotropy parameters

All methods to estimate the LVA field that are mentioned above might be applicable in the usual situation where data is scarce. This limits their use for the FRESHEM project. This is why a new approach has been developed where the LVA field is calculated purely from data. It is simpler than previously mentioned methods, which enables the use for the current project and gives more robust results given large continuous datasets. The general workflow to construct the LVA field is based on:

1. Identification of the anisotropy parameters for all 'fresh' voxels that are located on flightlines.
2. Interpolation of the anisotropy parameters to the 3D model area.

Anisotropy can be described by an ellipse with three parameters, see visualization in Figure 9.7:

- Angle of the long axis relative to a fixed reference (α in Figure 9.7)
- Length of the long axis (a in Figure 9.7)
- Length of the short axis (b in Figure 9.7)

These parameters are determined for every voxel where the 2D result yields a p50 value that is considered 'fresh'. Although the determination of anisotropy can be done on the salt water bodies as well, there is little added benefit doing both.

In a horizontal plane, starting at a 'fresh' voxel, chloride concentrations of the 2D result are considered that occur at a certain angle. In the direction specified by this angle, the distance from the starting voxel to first occurrence of a chloride concentration above a cut-off value (this is: the distance to the brackish zone) is determined. This then is an indication of the degree of spatial correlation in that direction. As the anisotropy ellipse is symmetrical, the distances in two

opposite directions are added (0° and 180° , 5° and 185° , etc). Following this procedure the 'distance-to-salt' can be determined for many different angles. The angle α , the direction of highest correlation, is then given by the angle where the 'distance-to-salt' is greatest. The length of the short axis b is given by the smallest 'distance-to-salt' found. Considering the increase in both accuracy and calculation times with finer intervals between the angles, the 'distance-to-salt' has been determined for angles with a 5° interval (5° , 10° , ..., 175° , 180° , each with their corresponding opposite angle).

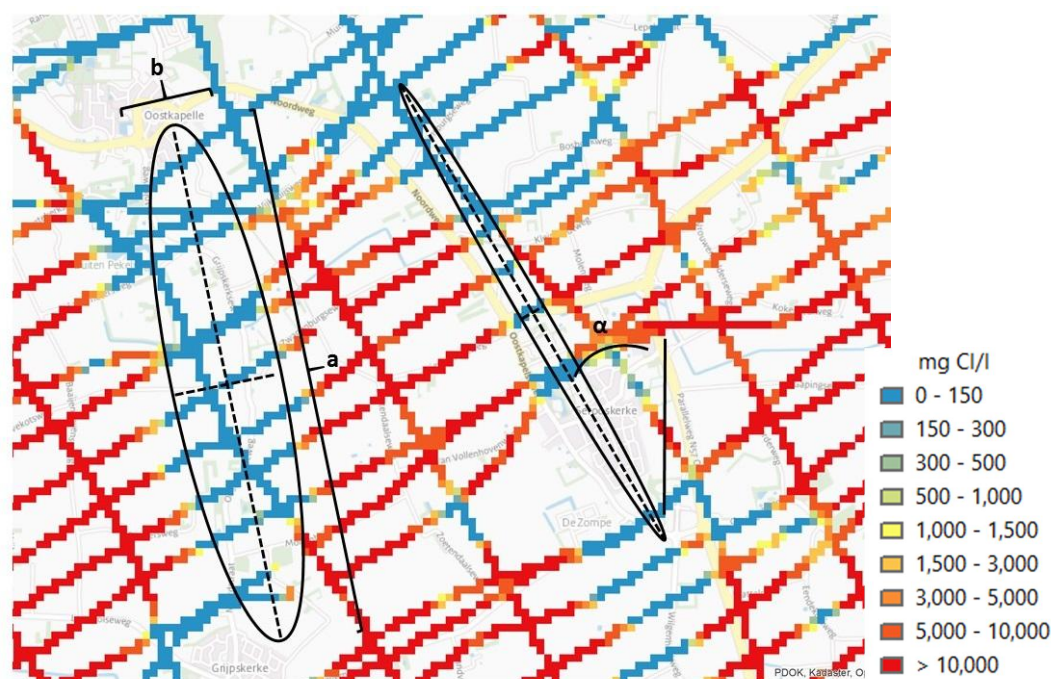


Figure 9.7: Visualisation of the parameters of the anisotropy ellipse, with p50 of 2D result at 6 m below NAP: α angle of long axis, a length of long axis, b length of short axis.

Trial and error has led to the following rules:

- The length of the long axis a is fixed at 1000 metres, also at locations where spatial correlation in all directions is smaller. There should always be enough samples in the search neighbourhood to allow for a decent interpolation.
- For the same practical reason, the **minimum** length of the short axis b is taken as 100 metres.
- If more than one angle has a correlation length > 1000 metres, the average of these angles is taken as the final angle α .
- An apparent high correlation length can be obtained at angles that are almost parallel to flightlines, as it will often take a long distance to reach the next data point. To avoid this unrealistic effect of the flightline configuration, the direction of highest correlation should cross at least 2 flightlines before reaching the chloride concentration cut-off value.
- The 'distance-to-salt' should at least be 500 metres.
- The angle of smallest 'distance-to-salt' often depends on the flightline configuration and has no meaning for the orientation of the anisotropy ellipse. Only where the angle of minimum and maximum correlation is too similar (a difference $< 30^\circ$), the result is conspicuous and neglected.
- The whole procedure is repeated for two different chloride cut-off values: 1000 and 3000 mg/l. α is taken from the 3000 mg/l result, as correlation lengths tend to be slightly longer and

sometimes more accurate. **b** is taken from the 1000 mg/l result, as this is a shorter distance to the brackish zone.

Application of these rules limit the number of 'fresh' data points where anisotropy parameters are successfully calculated. Only the locations where anisotropy has successfully been determined will be used to construct the complete 3D LVA field. The result of anisotropy determination for our area of interest is shown in *Figure 9.8*. With only few exceptions, the direction of anisotropy nicely matches the expected direction as indicated by de creek ridge morphology. The amount of flattening of the anisotropy ellipse now depends on the distance to the brackish zone. Inside a larger fresh water body the chloride concentration will have more isotropic characteristics, which translates in a more circular shape of the anisotropy ellipse. Towards the fresh-salt interface the anisotropy becomes larger and the anisotropy ellipse more flattened.

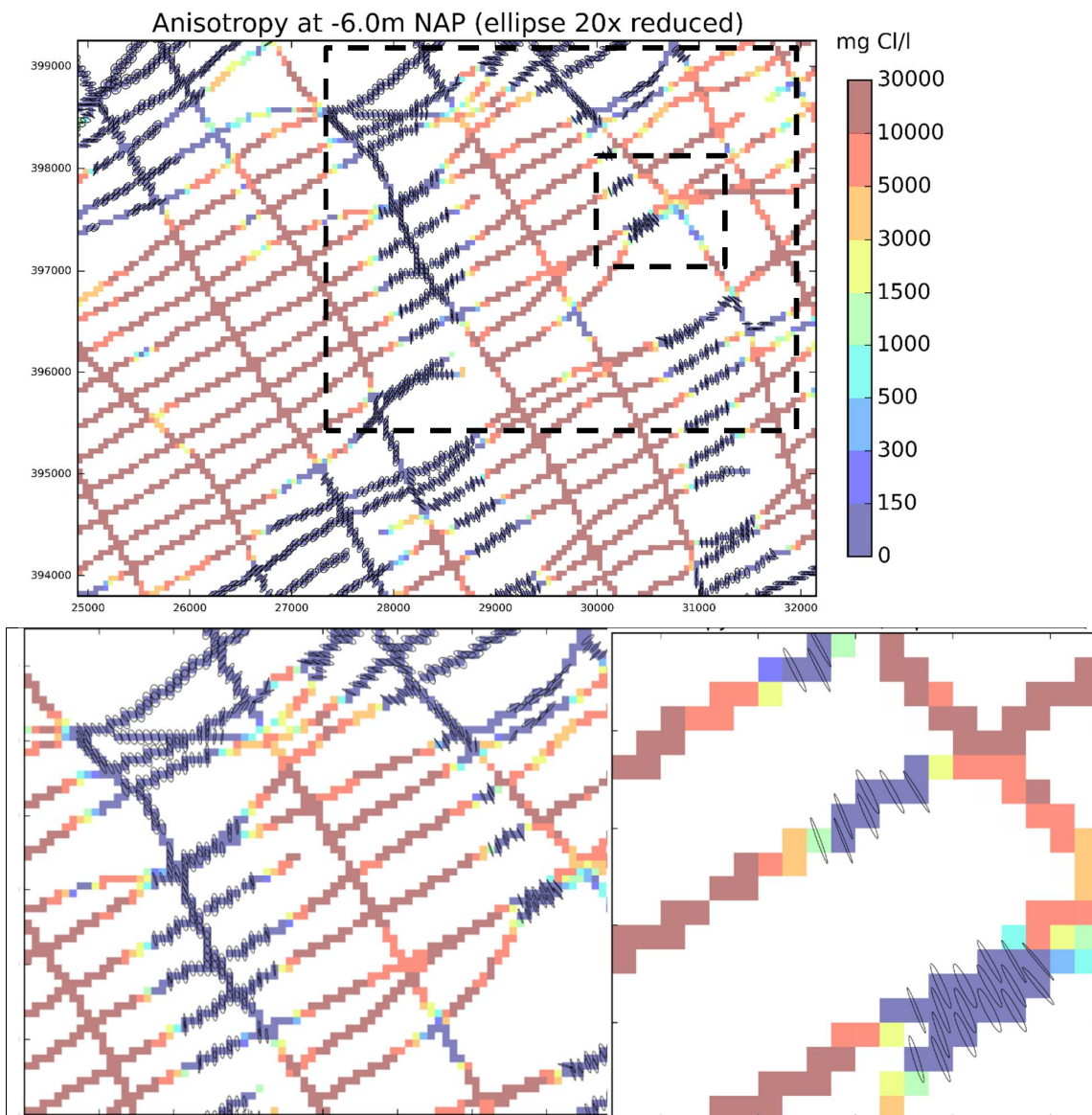


Figure 9.8: a) Anisotropy ellipses as determined directly from the 2D result, visualized at 6 m below NAP with p50 of 2D result, size of the ellipses is reduced 20 times. b) enlargement of area indicated in a), c) enlargement of smallest area indicated in a).

The FRESHEM method, interpolation of anisotropy parameters

The use of anisotropy for kriging interpolation requires an LVA field where anisotropy is defined for every voxel. As the long axis of the anisotropy axis is taken as a constant, we are left with interpolation of the length of the short axis **b** and the angle of the anisotropy ellipse **α**. Anisotropy is directly determined for the fresh water voxels at flightline locations. By interpolation all remaining locations on and in between the flightlines will be filled with anisotropy values.

A stepwise IDW interpolation for the short axis **b** is chosen where with each iteration 25 metres is added to the 'new' **b** values. This ensures a gradual decrease of anisotropy with increasing distance from the fresh-salt interface, to circular (isotropic) values.

Interpolation of the angle **α** is hindered by the fact that the geometric average of two angles is not simply their numerical average. For example, the geometrical average of an angle of anisotropy of 20° and 170° is 5° (while their numerical average 95° is in fact perpendicular to the geometric average). This is solved by first decomposing the angles into their x- and y-vectors:

$$x = \sin(2\alpha) \tag{9.3}$$

$$y = \cos(2\alpha) \tag{9.4}$$

The x- and y-component are separately interpolated by IDW. With the 3D model now filled with values for the components, the anisotropy angle **α** can be calculated as:

$$\alpha = (\arctan(y/x))/2 \tag{9.5}$$

The resultant LVA field for our area of interest at 6 m below NAP is shown in *Figure 9.9*. Note the smooth transition of anisotropy angles in between creek ridges with a different orientation. The calculated LVA field is in accordance to the anisotropy that would intuitively be given to this area.

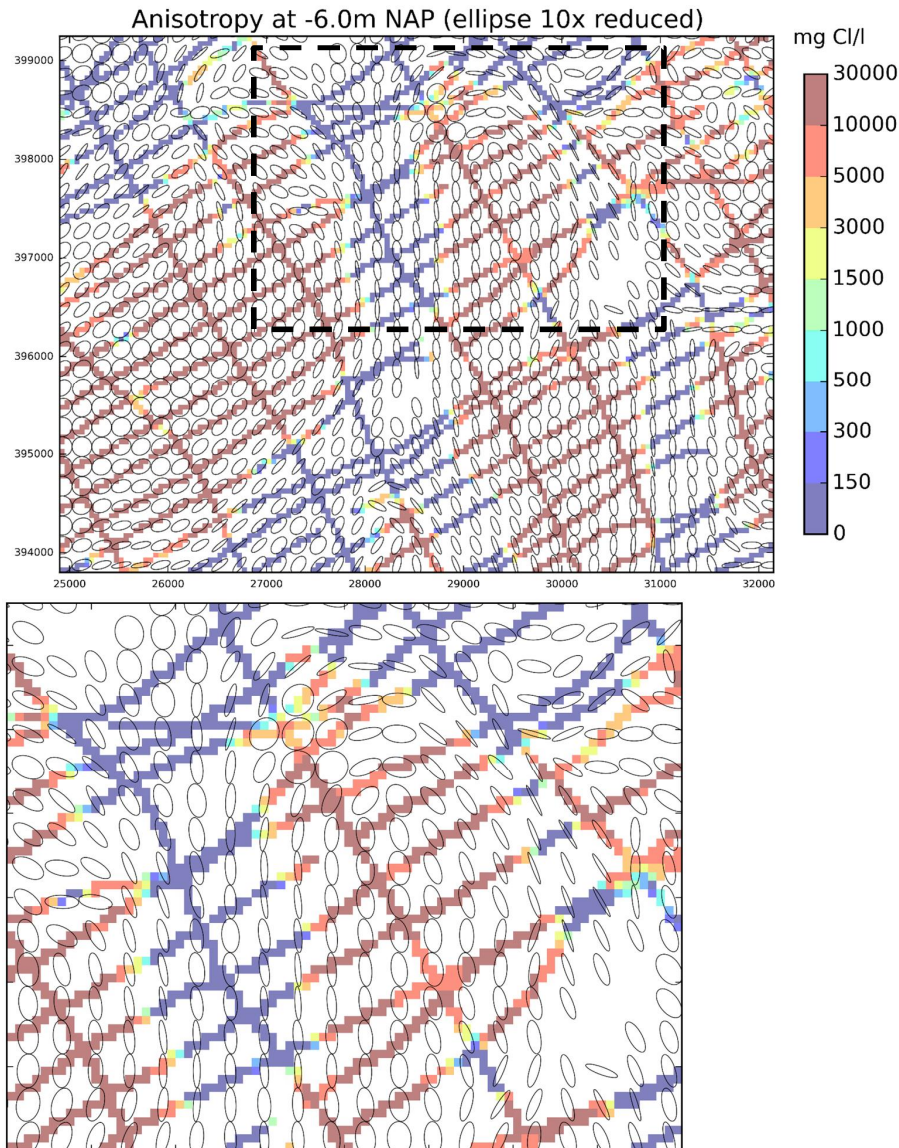


Figure 9.9: a) The LVA field, visualized at 6 m below NAP with p50 of 2D result, size of the ellipses is reduced 10x. b) enlargement of area indicated in a)

9.5.3 Interpolation with anisotropy: a qualitative analysis

Kriging weights

The LVA field is imposed to the kriging algorithm for both the neighbourhood and the variogram. Figure 9.10 shows the change in data selection and the weights that are assigned to individual points when anisotropy is taken into account. The narrow creek ridge system in the northwest of the area shows strong anisotropy. Estimation of a voxel that intuitively is located in the fresh water body dramatically changes. In the isotropic case about 40% of the weight is assigned to 'fresh' data points (Figure 9.10a). With anisotropy about 90% if the weight is assigned to 'fresh' data points (Figure 9.10b). As we will see, this has a large effect on the interpolation estimation.

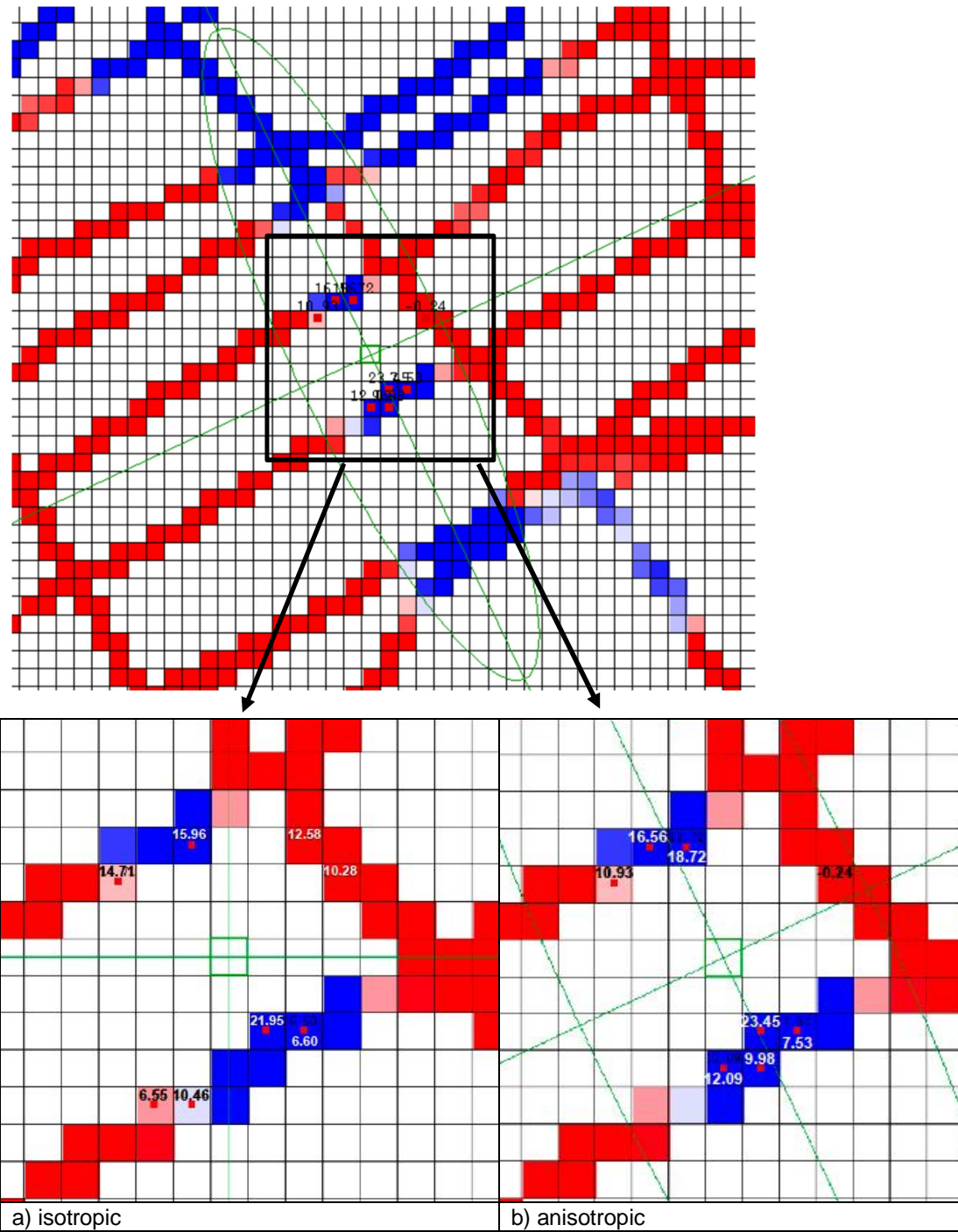


Figure 9.10: Effects of isotropic vs. anisotropic neighborhood and variogram on data selection and Kriging weights. a) isotropic, b) anisotropic.

Effects anisotropy on interpolation result

The effect of imposing anisotropy to kriging interpolation is shown in Figure 9.11. The interpolation result of the 1500 mg Cl/l indicator is shown for the narrow creek ridge in the northwest of the area. In between the flightlines uncertainty is reduced dramatically and our sought-after connectivity of the narrow fresh water lens now seems to be established.

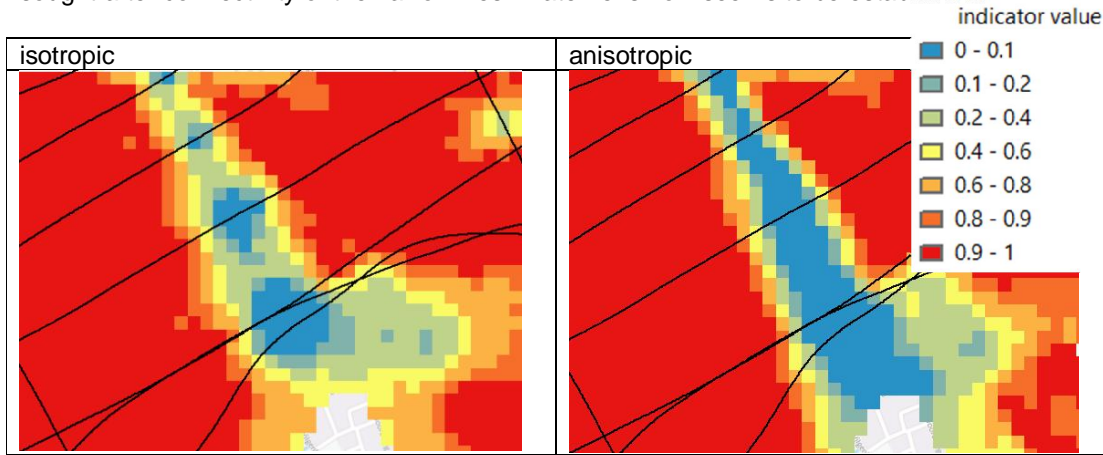


Figure 9.11: Interpolation result for the 1500 mg Cl/l indicator for interpolation with isotropic (left) and anisotropic neighbourhood and variogram (right). Black lines indicate flightlines.

Figure 9.12 shows a depth slice at 6m below NAP of the p10, p50 and p90 of the 3D model. The interpolation result is shown for both the isotropic and anisotropic Indicator Kriging case. Depending on the magnitude of the local anisotropy, some parts of the model have undergone dramatic improvements. Largest gain is seen in the 'extremes' of the model solution. The fresh water 'islands' that are seen on some flightlines in the p90 of the isotropic model result, are connected when anisotropy is imposed. The difference between p10 and p90 is decreased considerably in between the flightlines around the brackish zone.

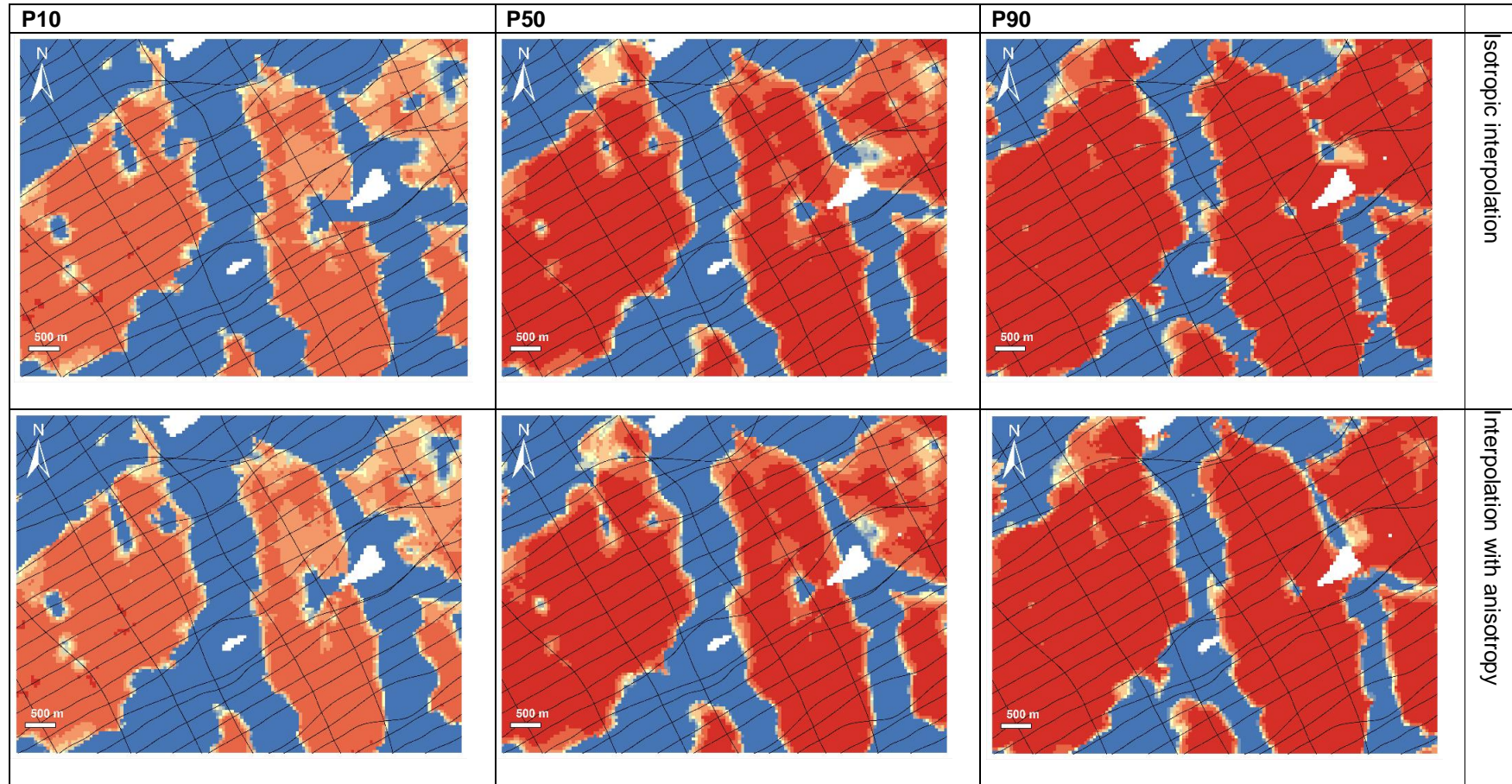
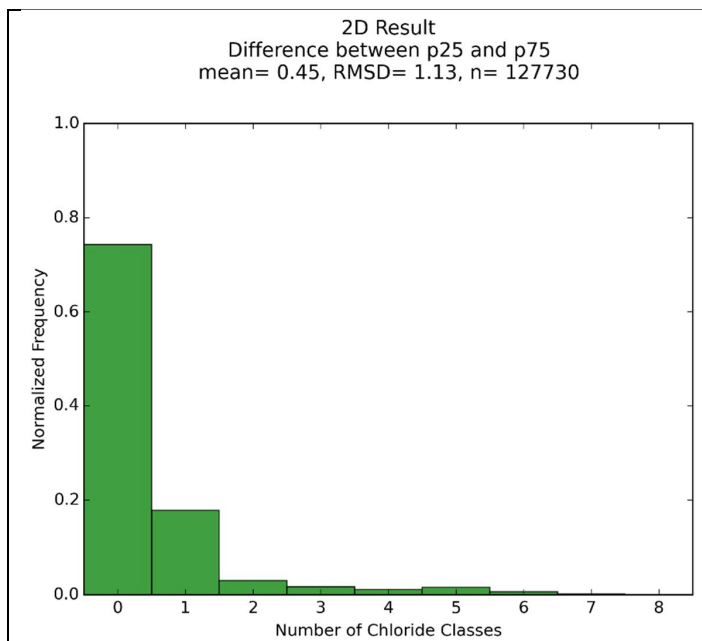


Figure 9.12: Depth slices at 6 metres below NAP. A comparison between the P10, P50 and P90 of the 3D model using isotropic and anisotropic indicator kriging. The area of interest is indicated in Figure 9.5

9.5.4 Interpolation with anisotropy: quantitative analysis

Uncertainty of the 2D result and the 3D model can be expressed as the difference between a low probability estimate, e.g. the p25, and a high probability estimate, e.g. the p75, of the chloride concentration. Improvements in the interpolation method are aimed to reduce the uncertainty of the estimation of chloride concentration. In case of a perfect estimation, the uncertainty of the 3D model would be equal to the uncertainty of the input data. Figure 9.13a shows the uncertainty of the 2D result of the area indicated in Figure 9.5. The uncertainty is expressed as the number of chloride classes difference between the p25 and the p75 for each voxel, with data classified in nine classes (class boundaries at 150, 300, 500, 1000, 1500, 3000, 5000 and 10000 mg Cl/l). More than 70% of the 2D result shows an uncertainty of 0 classes. These are mainly locations deep inside a fresh or salt water body. An uncertainty of 3 classes or more is found in almost 5% of the 2D result. These are locations near the fresh-salt interface, where estimations of chloride concentration become more uncertain. The average uncertainty of the 2D result in this area is 0.45 classes. Interpolation adds spatial uncertainty to the data and will increase the overall uncertainty. After interpolation with anisotropy (Figure 9.13b) an uncertainty of 0 classes difference between p25 and p75 is present at about 65% of the 3D model. For 10% of the model the uncertainty is 3 classes or more. The average uncertainty from the 2D result to the 3D model increases with 0.3 classes to 0.75. For this area a 3D interpolation has been performed with 'normal' isotropic interpolation as well. The histogram of associated uncertainty is shown in Figure 9.13c. The average uncertainty increases with 0.39 classes with respect to the 2D result to 0.84. Visual comparison of the histograms between interpolation with and without anisotropy does not yield spectacular difference. This is caused by the vast majority of the voxels being located away from the fresh-salt interface, where anisotropy is no important factor. Still, considering the bulk statistics of this model area, the increase in uncertainty by interpolation is reduced from 0.39 to 0.3 classes. This means that the uncertainty of the 3D model would be 30% higher if interpolation had been performed without anisotropy.



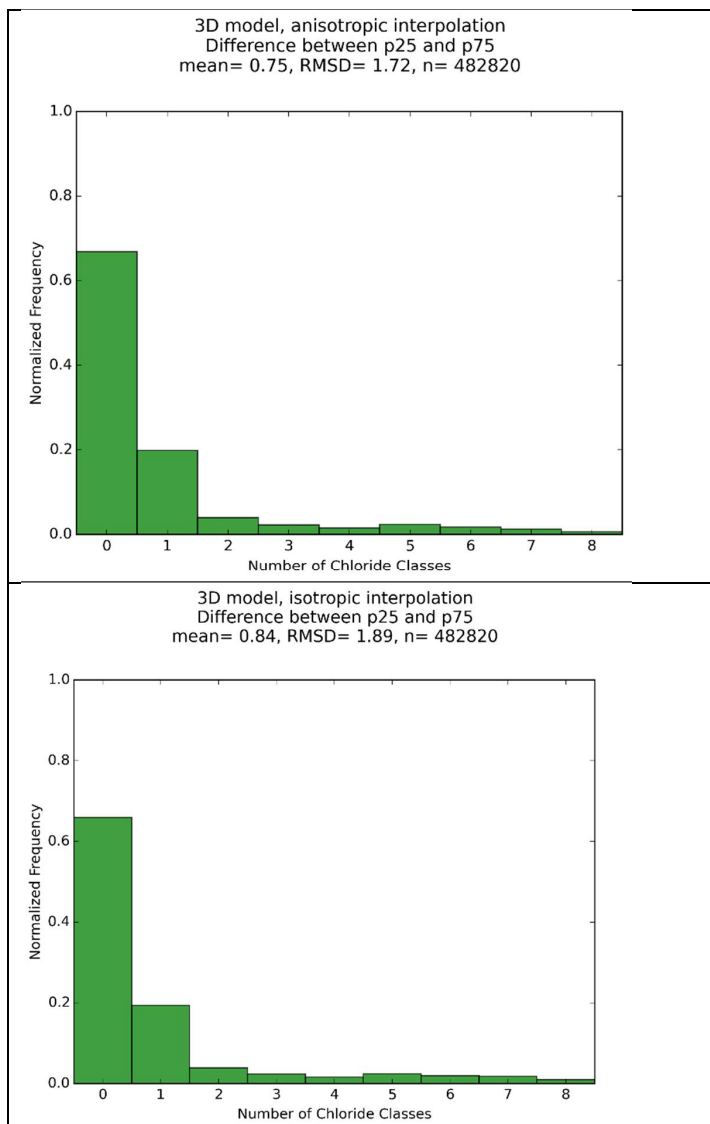


Figure 9.13: Uncertainty of the FRESHEM dataset expressed as the difference between the p25 and the p75 of the chloride concentration, for a) the 2D result, b) the 3D model as calculated with anisotropic interpolation, c) the 3D model as calculated with 'normal' isotropic interpolation

10 Parameter and interpolation uncertainty

10.1 Parameter contributions to uncertainty

The Monte Carlo approach of FRESHEM to calculate chloride concentration from the HEM measurements takes into account the uncertainty stemming from the mathematical inversion, lithology (GeoTOP), formation factor and surface conductivity and the salinity – chloride concentration relation. See Table 10.1 for uncertainty ranges. Each of these variables has its contribution to the overall uncertainty of the calculated chloride concentration of the 2D result. Interpolation of the 2D result to a 3D model additionally introduces spatial uncertainty. All the mentioned uncertainties are incorporated in the uncertainty of the end results of FRESHEM. Knowledge of the contribution of each source of uncertainty to the final chloride concentration can potentially be of great help to future studies that use similar methods, as it will give guidance which parameters or steps could be improved to decrease the final uncertainty.

Table 10.1: uncertainty range for each methodological step.

Methodological step	Uncertainty range
Mathematical inversion	3 different inversion schemes included; 2 of the 3 schemes inclusion of (varying) standard deviation around the estimate
Lithology	Probability distribution GEOTOP
Intrinsic formation factor (FF)	Normal distribution with mean and standard deviation Peat: mean: 2.66, sd: 0.33 Clay: mean: 4.1, sd: 0.15 Sandy clay: mean: 4.53, sd: 0.12 Fine sand: mean: 5.98, sd: 0.21
Surface conductivity (ECs)	Normal distribution with mean and standard deviation Peat: mean: 2.95, sd: 3.71 Clay: mean: 2.97, sd: 0.70 Sandy clay: mean: 2.65, sd: 0.47 Fine sand: mean: 1.61, sd: 0.45
EC25 to chloride	Normal distribution with mean and sd Parameter α : mean: 360, sd: 6 Parameter β : mean: 450, sd: 190

10.1.1 Approach

The uncertainty analysis is performed on a subset of all available data. Figure 10.1 shows the area that is considered, including the location of flightlines. This area is selected, based on the occurrence of creek ridges and associated high uncertainty of the fresh-salt transition zone. Also it avoids the high resolution 172 Waterhouderij/Waterfarm area in the northern part of Walcheren where flightlines are flown with a higher density. A resampled version of the 2D result is used, where every layer is resampled to a value every 0.5 metre in vertical. If no resampling would have been done, thicker layers would be underrepresented with respect to thin layers. In this uncertainty analysis the chloride concentration calculations are performed following the procedure as developed for this project (Section 8.3), only differing with respect to the treatment of stochastic variables. At each run only a single variable is considered stochastic, while all other variables are considered deterministic input. The calculated chloride concentration will then show an uncertainty range that is only attributed to the stochastic properties of this single variable. This step is then repeated for every stochastic variable, leading to the relative contribution to uncertainty of each variable. From a comparison of the 2D result with the 3D model the added spatial uncertainty by interpolation is quantified.

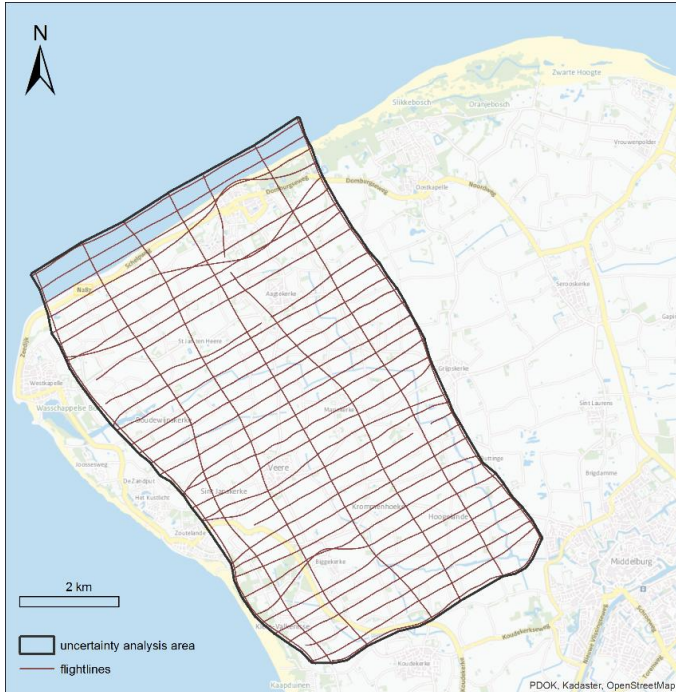


Figure 10.1: Area considered for the uncertainty analysis (black line), with the flightlines in this area (brown lines).

10.1.2 Result

The uncertainty of chloride concentration can be expressed as the difference between a low and a high estimate (low and high percentiles of the chloride distribution). In general, this can be the difference between the p25 and p75, or the difference between p10 and p90. The same absolute difference in chloride concentration is more important when comparing low chloride concentrations than high concentration. To avoid overrepresentation of the difference between high chloride concentrations, differences are expressed in number of chloride classes. 9 classes are defined, with class boundaries at 150, 300, 500, 1000, 1500, 3000, 5000 and 10000 mg Cl/l. The overall difference can be expressed by the mean of all class differences, or the Root Mean Squared Difference (RMSD, a measure with emphasis on large differences):

$$\text{RMSD}_{\Delta(p(\text{low}),p(\text{high}))} = \sqrt{\frac{\sum_{i=1}^n (Cl_{i,p(\text{low})} - Cl_{i,p(\text{high})})^2}{n}} \quad (10.1)$$

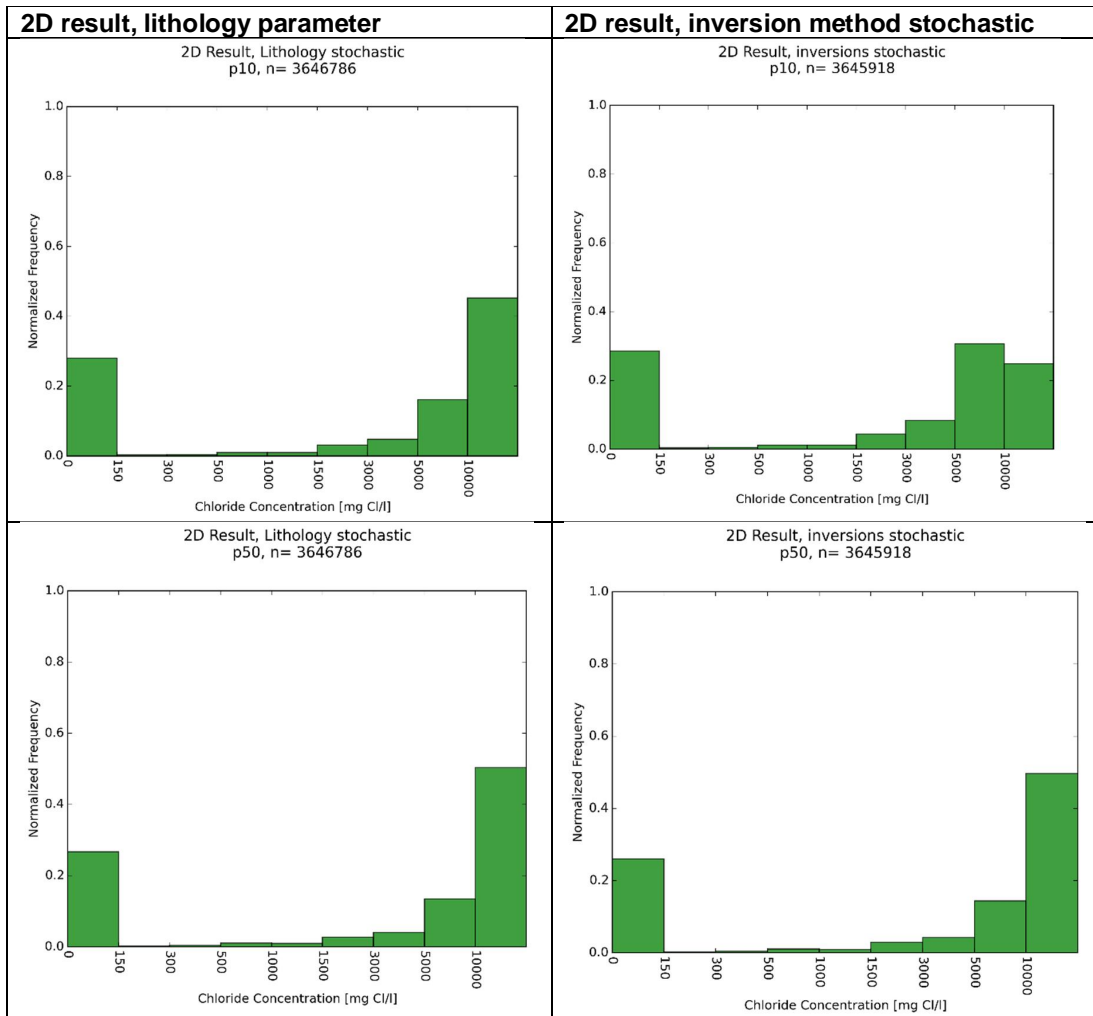
For the 2D result the difference in number of chloride classes between the p25 and p75, and the p10 and p90, is given in Table 10.2. By subsequently isolating stochastic variables the relative contribution of each variable in relation to the total uncertainty becomes apparent. Figure 10.2 shows the histograms of p10, p50, p90 and the difference between p10 and p90 for two stochastic variables, 1) the use of all realizations of GeoTOP lithology and 2) the use of different inversion methods.

The use of different inversion methods gives the largest contribution to the overall uncertainty, with an average of 0.38 classes difference between the p25 and p75. The uncertainty from the inversion attributes 77% to the overall uncertainty. The lithology (all realizations of GeoTOP) and surface conductivity (ECs) also have a significant uncertainty, both with an average of 0.17 classes difference between the p25 and p75. The other parameters have a

smaller contribution to the uncertainty. Please note that uncertainties cannot be summed to obtain the overall uncertainty of 0.49 classes.

Table 10.2: Mean and RMSD of class differences for the different stochastic variables.

		# classes difference between p25 and p75		# classes difference between p10 and p90	
		mean	RMSD	mean	RMSD
2D result, stochastic variable is:	Inversion	0.38	0.93	0.88	1.52
	ECs	0.17	0.65	0.33	1.04
	FF	0.01	0.12	0.03	0.17
	ECw to CI	0.05	0.24	0.09	0.36
	Lithology	0.17	0.53	0.30	0.80
2D result, all variables stochastic		0.49	1.13	1.06	1.85



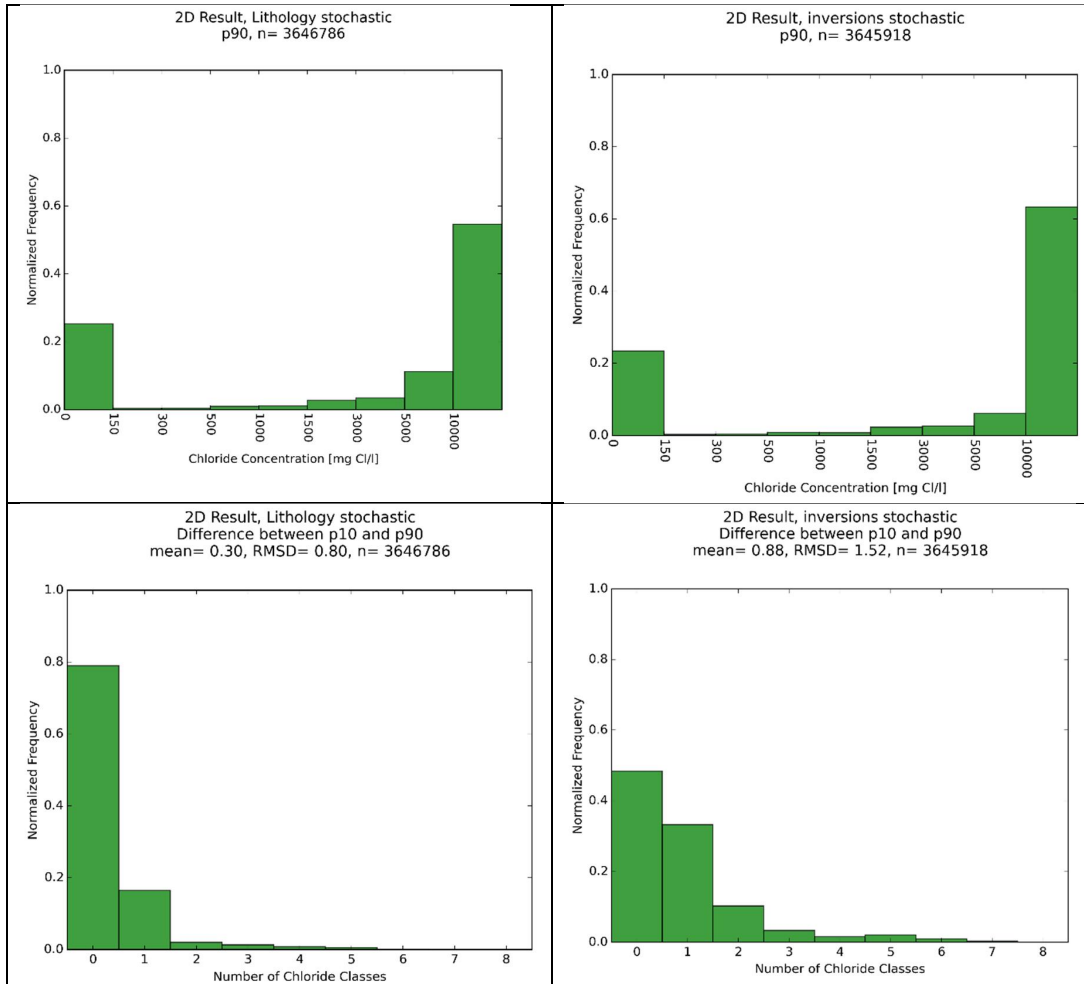


Figure 10.2: Histograms of p10, p50, p90 and number of classes difference between p10 and p90, for the 2D result with the stochastic variable lithology and different inversion methods respectively.

The relative importance of the different stochastic variables is given graphically in Figure 10.3 for the difference between p10 and p90. The largest contribution to uncertainty comes from the inversion method, followed by surface conductivity and lithology. The RMSD shows a smaller contribution to uncertainty from the inversion methods than does the mean, indicating that the use of different inversion methods causes consistent small differences, but is somewhat less important when the large uncertainties are considered.

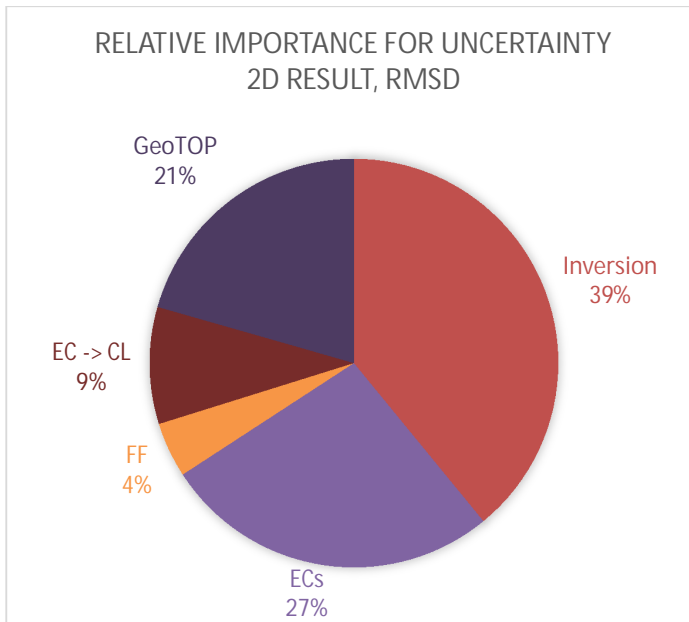
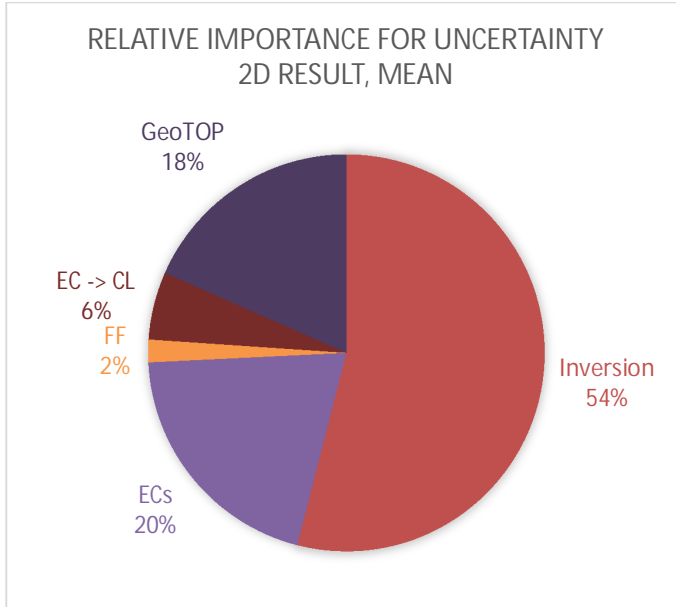
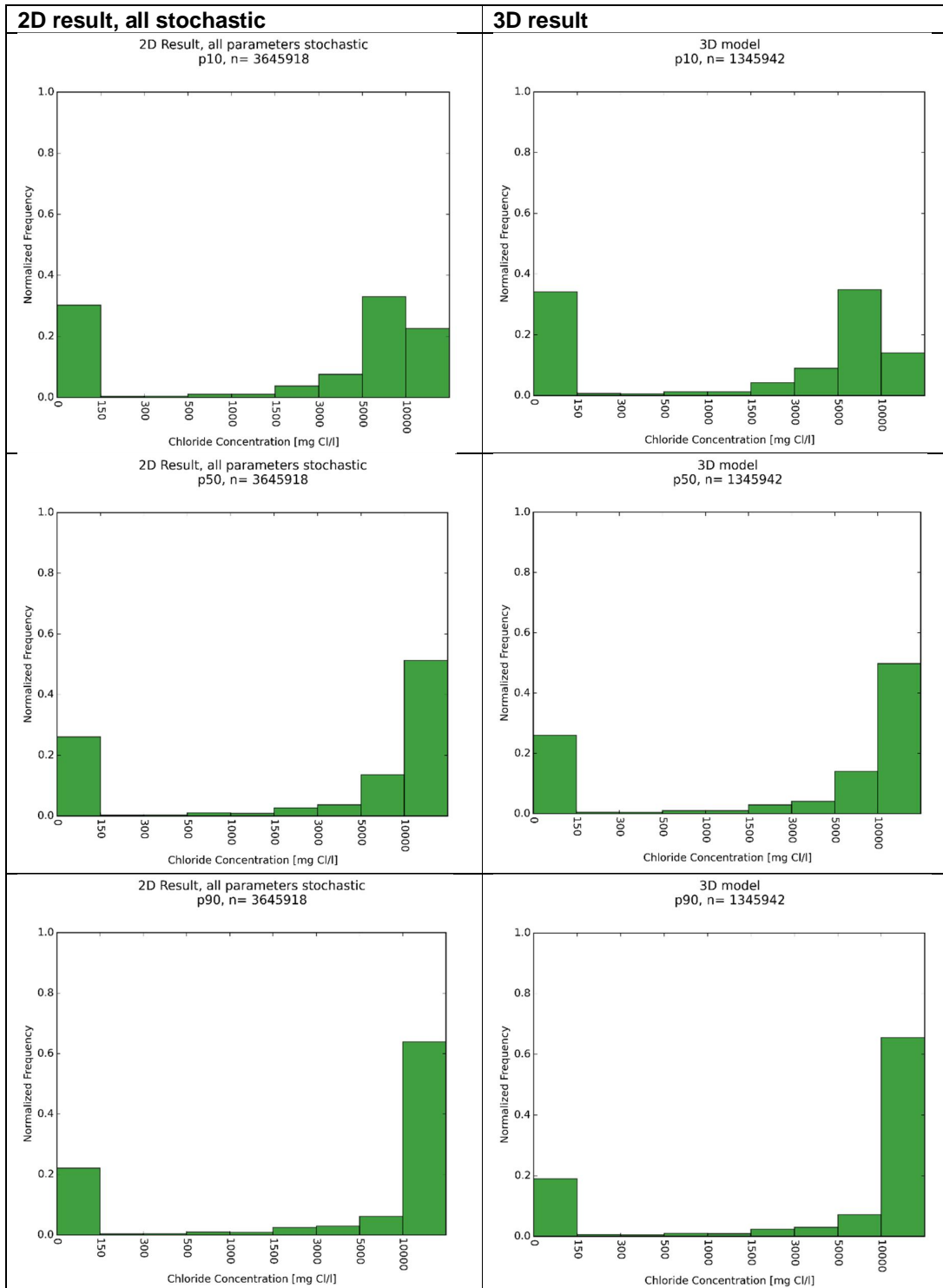


Figure 10.3: Pie charts of: a) the mean and b) the RMSD, of the difference between p10 and p90 for the different stochastic variables that are used to calculate the 2D result.

10.1.3 Relative contribution spatial uncertainty to complete uncertainty of the 3D model

For the 2D result and the 3D model the histograms of the p10, p50, p90 and the difference between p10 and p90 are given in Figure 10.4. The shape of the p10, p50 and p90 is very similar for both the 2D result and 3D model, which can be interpreted that no spatial bias is present and a comparison of the bulk statistics can be made with confidence. The mean shows a difference between p10 and p90 of 1.7 classes for the 3D model, and 1.06 classes for the 2D result. The added uncertainty by interpolation, the spatial uncertainty, therefore

accounts for 33% of the total uncertainty of the 3D model (mean). For the RMSD this is 38%, indicating that spatial uncertainty is somewhat more important when considering larger uncertainties. These numbers are represented graphically in Figure 10.5.



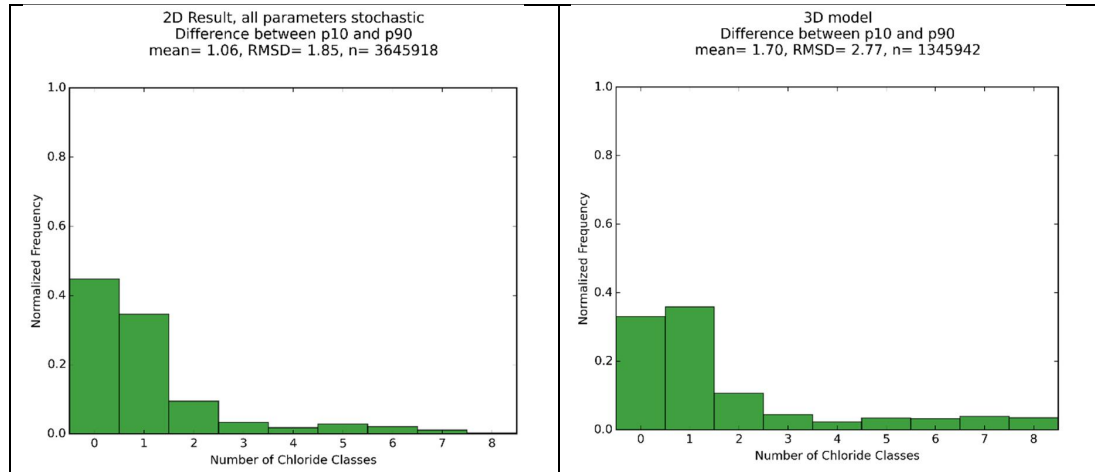


Figure 10.4: Histograms of p_{10} , p_{50} , p_{90} and number of classes difference between p_{10} and p_{90} , for 2D result and 3D model.

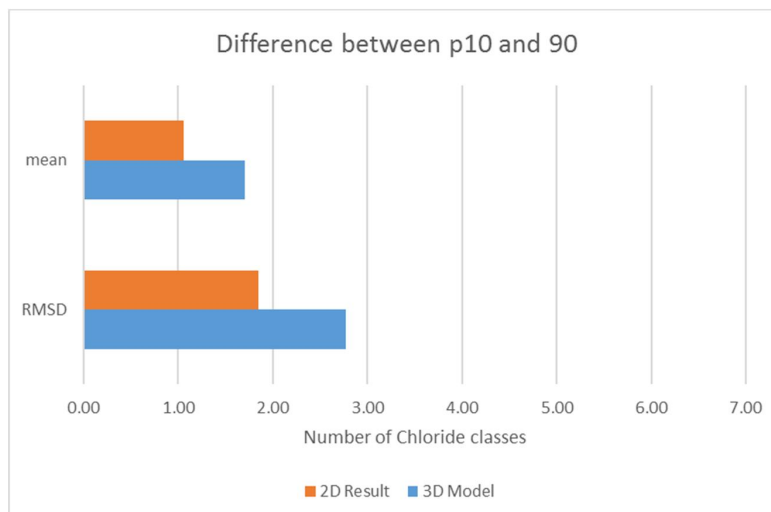


Figure 10.5: Mean and RMSD of the difference between p_{10} and p_{90} for the 2D result and the 3D model. 33% (mean) or 38% (RMSD) of the total uncertainty of the 3D model can be attributed to the spatial uncertainty added by interpolation.

10.2 Flightline resolution

During the FRESHEM Zeeland survey different resolutions between the flightlines were applied. In general 300 metre between the flightlines was chosen and 2000 metre between the tie-lines. For several high resolution areas a distance of 100 metre between the flightlines was chosen. This raises questions about the added value of 100 metre instead of 300 metre between the flightlines. As a test area, the high resolution area Waterhouderij Walcheren was chosen. This area of approximately 50 km² has a distance of 100 metre between the flightlines and a distance of 1000 metre between the tie-lines. The 3D interpolation (Chapter 9) was additionally carried out for only every third line and every second tie-line. Here, the influence of the distance between the flight lines on the chloride distribution is investigated for the test area.

The results of the depth of the 1500 mg Cl/l boundary ('middle') are shown in Figure 10.6; Figure 10.6a shows the 100 m resolution result and Figure 10.6b the 300 metre resolution result. In Figure 10.7b the differences in depth are visualised. The differences occur at locations where the 300 m resolution results have a lack of data, hence where the result is interpolated (Figure 10.7b); at the borders of the 300 m resolution result and in between the flightlines.

In between flightlines the uncertainty of the chloride concentration and hence the depth of the 1500 mg Cl/l boundary increases. In general, the 'low' result (Figure 10.7a) is more saline for the 100 metre resolution result and the 'high' result (Figure 10.7c) is less saline for the 100 metre resolution result (less difference between p25 and p75 chloride concentration). This occurs mainly in areas with a relatively large difference in thickness of the freshwater lens: borders of dune areas and sandy creek ridges.

The 300 metre resolution result is not able to map small fresh or saline groundwater features. One example is located near the dunes: the saline seepage area next to the dunes was missed in the 300 metre resolution result (Figure 10.8). Another example is shown in Figure 10.9: the southeast – northwest oriented boundary of the freshwater lens was not well located for the 300 metre resolution result.

Note that the differences in location of freshwater lenses are less than 300 metre (distance between the lines). Since line kilometres are expensive it is recommended to carefully design the flight plan with the flightlines. In areas where no small freshwater lenses are expected, it is recommended to choose a bigger distance between the flightlines. In areas where differences are expected (for example large groundwater extractions, sandy creek ridges) it is recommended to fly across and perpendicular to the fresh or saline feature. In areas where differences between fresh and saline groundwater are expected but the exact location is unknown (but important), 100 metre between the flightlines is recommended.

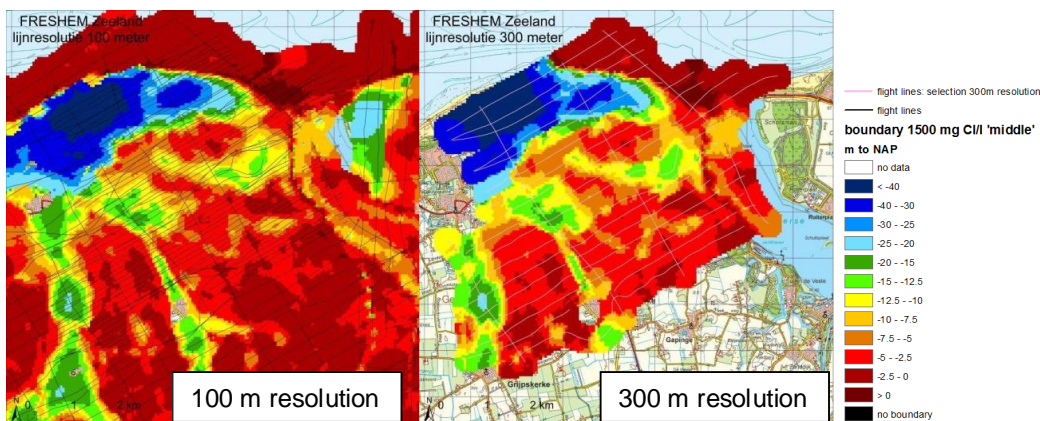


Figure 10.6 Flightline resolution: a. 100 metre between the flightlines (pink and black lines) and b. 300 metre between the flightlines (only pink lines) for the test area Walcheren.

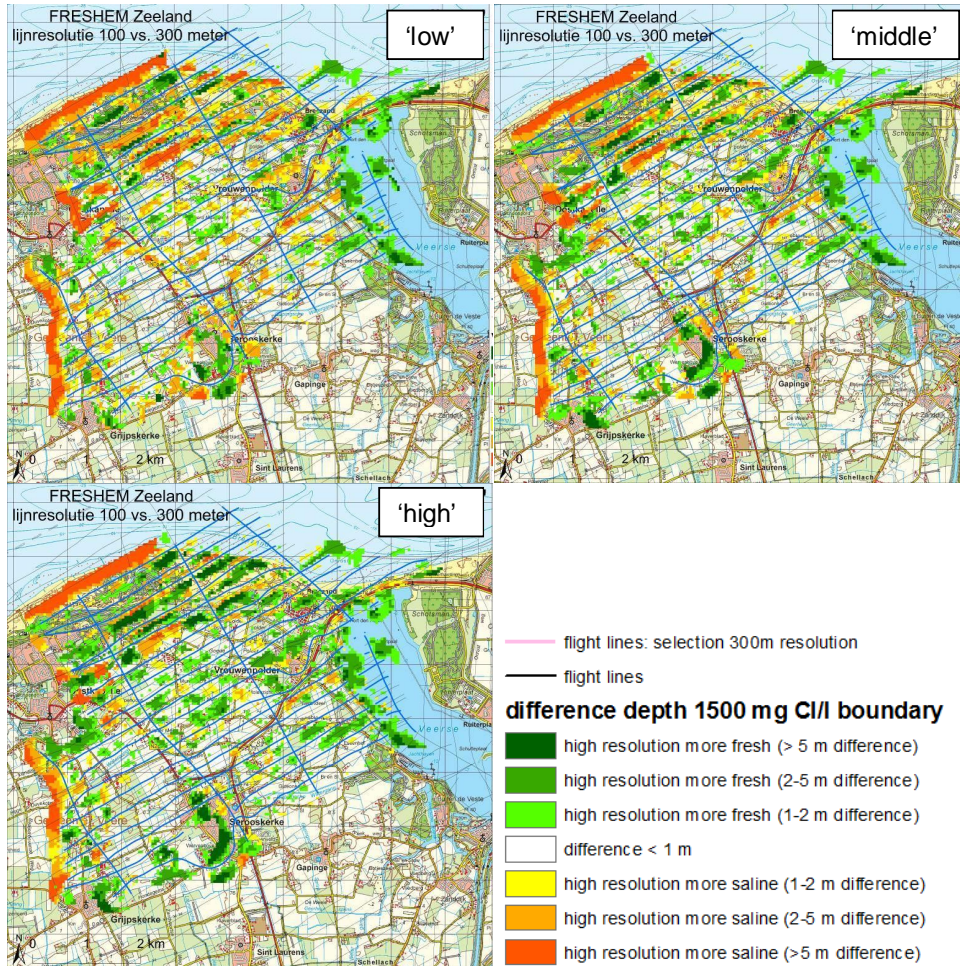


Figure 10.7 Flightline resolution: difference between the 100m and 300m resolution (distance between the flightlines) for a. FRESHEM 'low'; b. FRESHEM 'middle' and c. FRESHEM 'high'.

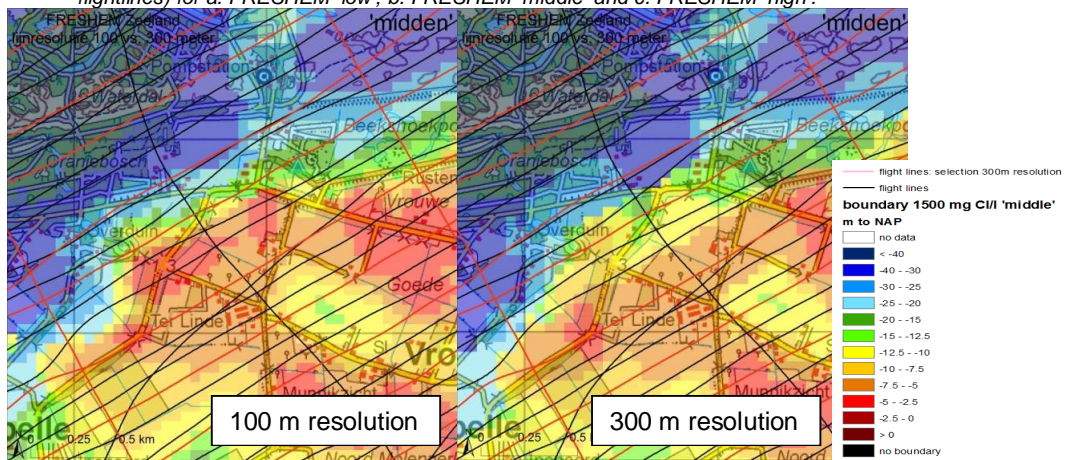


Figure 10.8 Flightline resolution: a. 100 metre between the flightlines (red and black lines) and b. 300 metre between the flightlines (only red lines). The high flightline resolution results in the mapping of the saline seepage area near the dunes (in the middle of the figures).

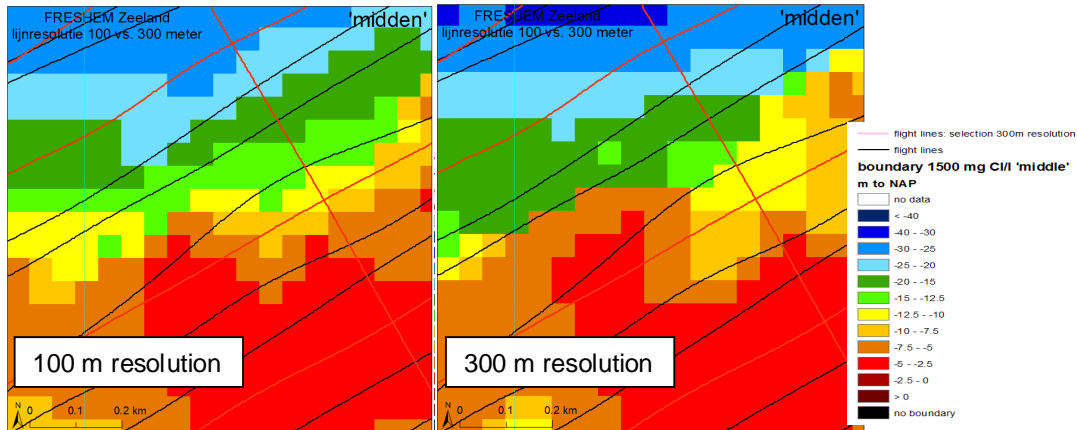


Figure 10.9 Flightline resolution: a. 100 metre (red and black lines) and b. 300 metre between the flightlines (only red lines). The high flightline resolution results in the mapping of the sw-ne freshwater lens.

11 Results

The first part of this chapter describes the products from FRESHEM Zeeland:

1. 2D chloride concentration along the flightlines (section 11.2),
2. 3D chloride concentration voxel model (section 11.3),
3. Boundary maps (section 11.4).

For each product the uncertainty is displayed by the results of 'low' and 'high' as explained in section 11.1.

The second part of this chapter describes new insights in the groundwater system and lithology of Zeeland based on these products:

1. Comparison with previous maps (11.5),
2. Fresh below saline groundwater (section 11.6),
3. New insights lithology (section 11.7).

The final part of this chapter describes new insights for future projects:

1. Comparison with fixed Ω_m boundary (section 11.8)

11.1 Uncertainty: 'low', 'middle' and 'high'

FRESHEM does not map absolute values of the chloride concentration of the groundwater, but rather probability density functions of the chloride concentration. In FRESHEM uncertainties stemming from (section 8.3 and chapter 9):

1. mathematical inversion
2. lithology (GeoTOP)
3. formation factor
4. surface conductivity
5. salinity – chloride concentration relation and
6. 3D interpolation

were characterised and combined to quantify the total uncertainty in the end-result.

A data error based on a statistical variation of repeated measurements is not available for HEM data, because all the measurements consist of single values. Therefore, an error value was derived for all measurements which resulted in the discrete marker QCPM (section 6.6). Where the data quality is too low for a reliable data interpretation, the data will be removed from the 2D result.

Every 2D or 3D cell or voxel hence contains a probability density function of the chloride concentration. The p50 (median) value of this distribution is called 'middle' in FRESHEM. The p25 value is called the 'low' value and the p75 value is called the 'high' value. The range between 'low' and 'high' only encompasses part of the uncertainty. However, by using the p25 and p75 the 'low' and 'high' values are still workable for users of the FRESHEM dataset. Chloride concentrations with a lower chance of occurrence are not visualised by 'low' and 'high'.

11.2 2D result FRESHEM Zeeland

The first product of FRESHEM Zeeland consists of the chloride distribution along the flightlines with a horizontal resolution of ~4 m and 20 layers with different thickness (vertical resolution higher near the surface). The depth of the bottom of the profile is between the 30 and 160 metre below surface elevation and depends on the lithology and chloride

concentration of the groundwater. In general there are only shallow results in clayey areas with saline groundwater and deep results in sandy areas with fresh groundwater.

There is no data if the quality criterion (section 6.6) is not met or if no data was collected. Uncertainties incorporated in the 2D results are stemming from mathematical inversion, lithology, formation factor, surface conductivity and the salinity-chloride concentration relation.

The data file with the chloride concentration contains 14 chloride classes, see Table 11.1. This classification is motivated by the use of water, as e.g. 150 mg/L Cl is a limit for drinking water, and 1500 mg/L Cl is a limit for agrarian use. Additional details in the classes are added for research and engineering purposes. For each flightline a figure is produced containing the results for 'low', 'middle' and 'high'. Because of the high horizontal resolution this is called the 2D high resolution result of FRESHEM Zeeland.

Table 11.1 Chloride classes in data files 2D and 3D FRESHEM result.

Value in data file	class
0	0 – 150 mg Cl/l
150	150 – 300 mg Cl/l
300	300 – 500 mg Cl/l
500	500 – 750 mg Cl/l
750	750 – 1000 mg Cl/l
1000	1000 – 1250 mg Cl/l
1250	1250 – 1500 mg Cl/l
1500	1500 – 2000 mg Cl/l
2000	2000 – 3000 mg Cl/l
3000	3000 – 5000 mg Cl/l
5000	5000 – 7500 mg Cl/l
7500	7500 – 10000 mg Cl/l
10000	10000 – 15000 mg Cl/l
15000	> 15000 mg Cl/l

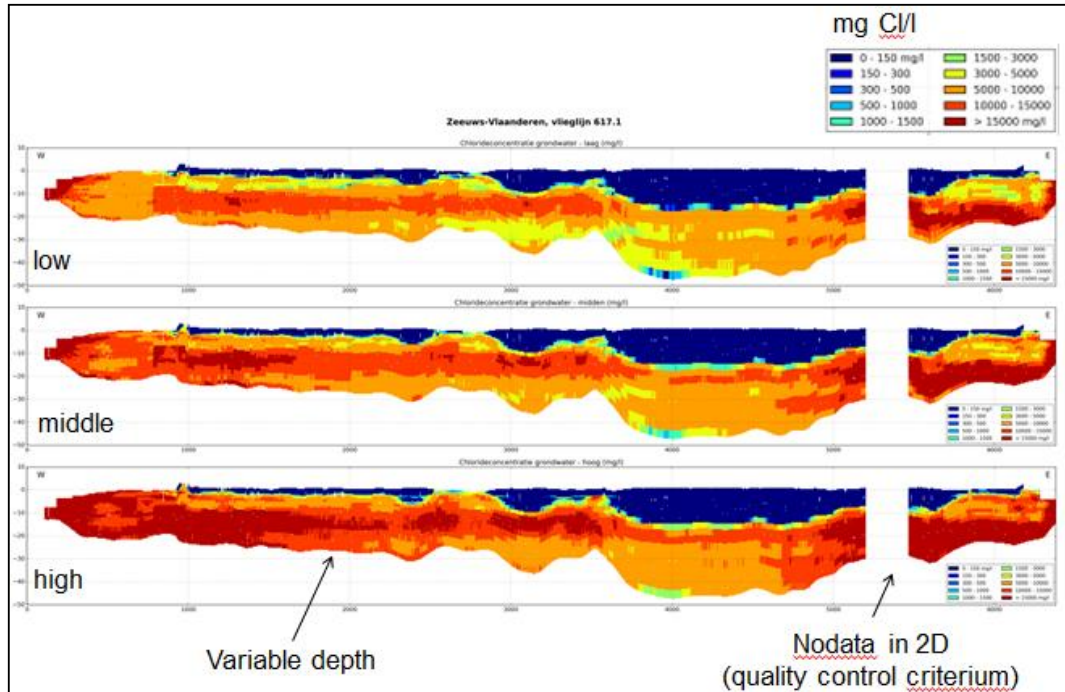


Figure 11.1 Example chloride concentration along the flightlines for 'low', 'middle' and 'high'.

11.3 3D result FRESHEM Zeeland

The second product of FRESHEM Zeeland is the three dimensional distribution of chloride concentration of the groundwater in Zeeland. This is a voxel model with a horizontal resolution of 50*50 m² and a vertical resolution of 0.5 m. The data files with the chloride concentration contain 14 chloride classes, see Table 11.1. The uncertainties incorporated in the 2D result are combined with the uncertainties from the 3D interpolation. Therefore each voxel has 3 values: 'low', 'middle' and 'high'. The data files are produced in *.asc format per layer for GIS, *.idf format per layer for iMOD and as a *.csv file containing all data. Some examples (visualized in iMOD) are shown in Figure 11.2, Figure 11.3 and Figure 11.4.

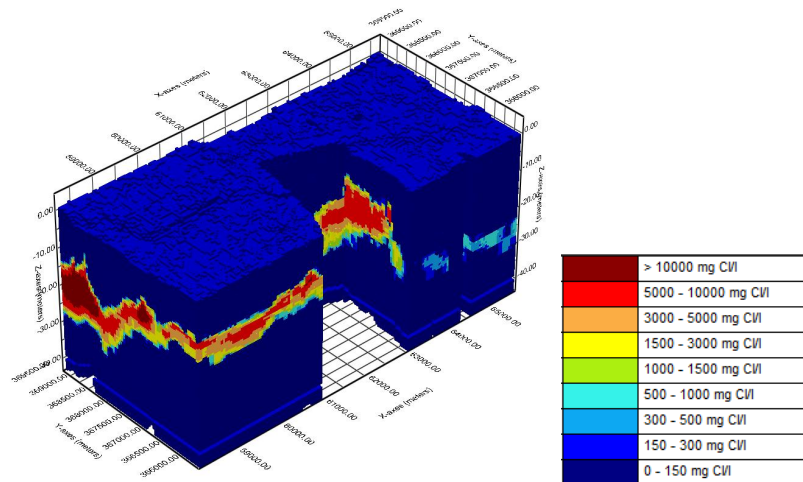


Figure 11.2 3D Example FRESHEM 'middle' for part of Zeeuws Vlaanderen.

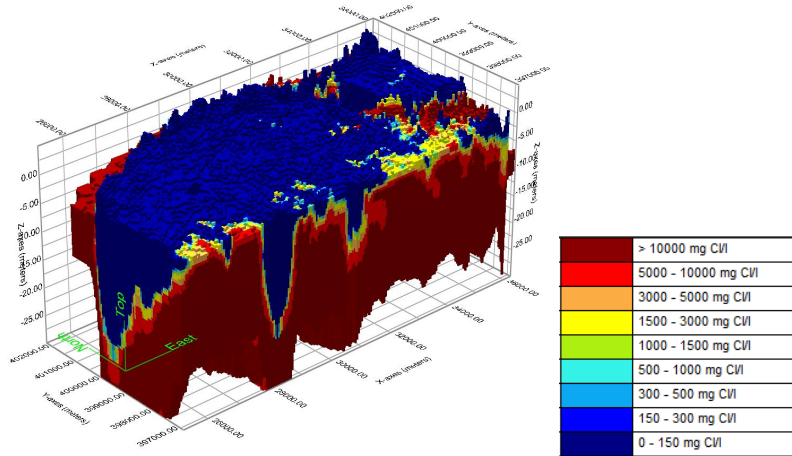


Figure 11.3 3D example FRESHM 'middle' for part of Walcheren. West the dune area Oranjezon and in the south two sandy creek ridges near Serooskerke.

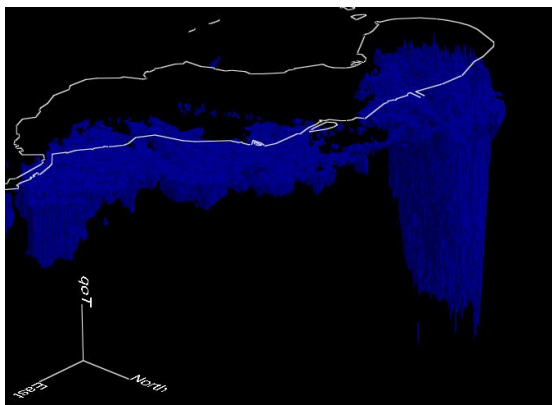


Figure 11.4 3D example showing only freshwater occurrence 'middle' for island Schouwen-Duiveland. Blue is fresh groundwater (<1500 mg Cl/l), visualized in iMOD. West (right) the dune area of Schouwen-Duiveland with a large freshwater lens.

11.4 Boundary maps

From the 3D FRESHM Zeeland result boundary maps were derived with the depth of a fixed chloride concentration with respect to NAP or surface elevation. Maps were derived for the values 150, 300, 1000, 1500, 3000 and 10000 mg Cl/l for the 'low', 'middle' and 'high' chloride distribution. Uncertainties stemming from mathematical inversion, lithology, formation factor, surface conductivity, salinity-chloride concentration relation and 3D interpolation are incorporated in these boundary maps. The no data areas from the 2D result based on the quality criterion of the data were filled up by the 3D interpolation. Therefore areas with a lack of data or areas with no reliable data have a larger uncertainty. Figure 11.5 shows an example of a boundary map.

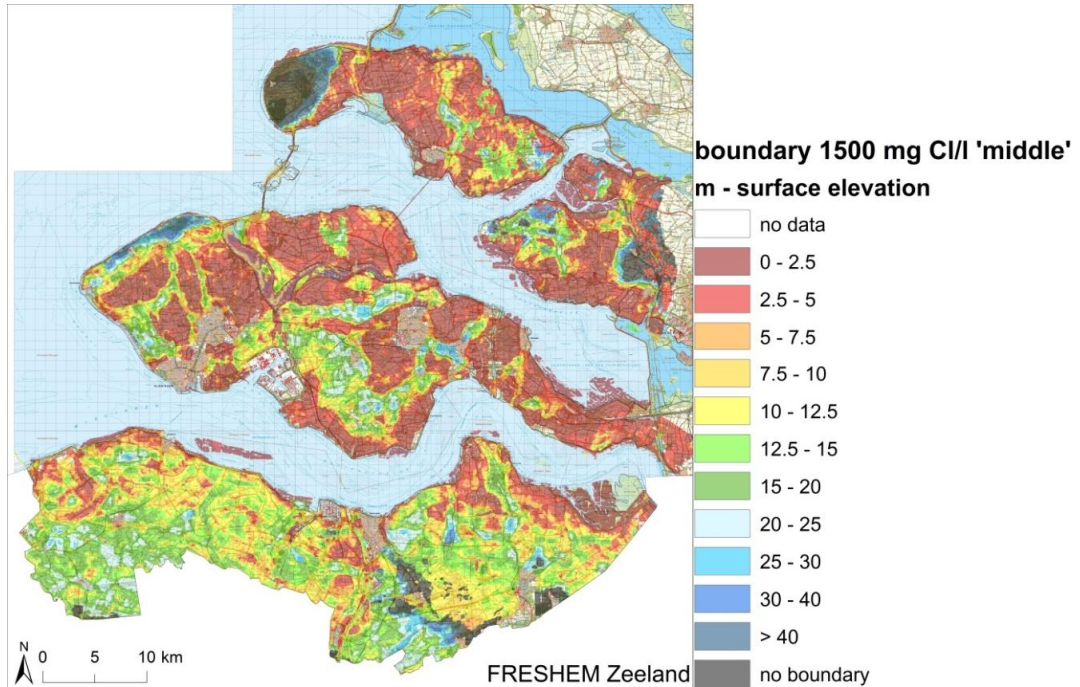


Figure 11.5 Depth of the 1500 mg Cl/l 'middle' boundary relative to surface elevation.

11.4.1 Fresh groundwater

For water supply for agriculture mainly fresh groundwater lenses of more than 15 m thickness are of interest. Smaller lenses can be used for irrigation purposes as well, but under more strict conditions to prevent salinisation of the groundwater. Location and total area where the fresh groundwater lens is at least 15 m thick can be found in Table 11.2 and Figure 11.6. More information about sustainable use of fresh groundwater resources and measures freshwater supply in Zeeland the reader is referred to (Pauw, 2015; Zuurbier, 2016; Oude Essink 2014).

Table 11.2: Areas in Zeeland with more than 15 metre fresh groundwater.

Areas with > 15 m fresh groundwater (<1500 mg Cl/l)	Km ²	% of Zeeland
'low'	550	30
'middle'	425	25
'high'	325	20

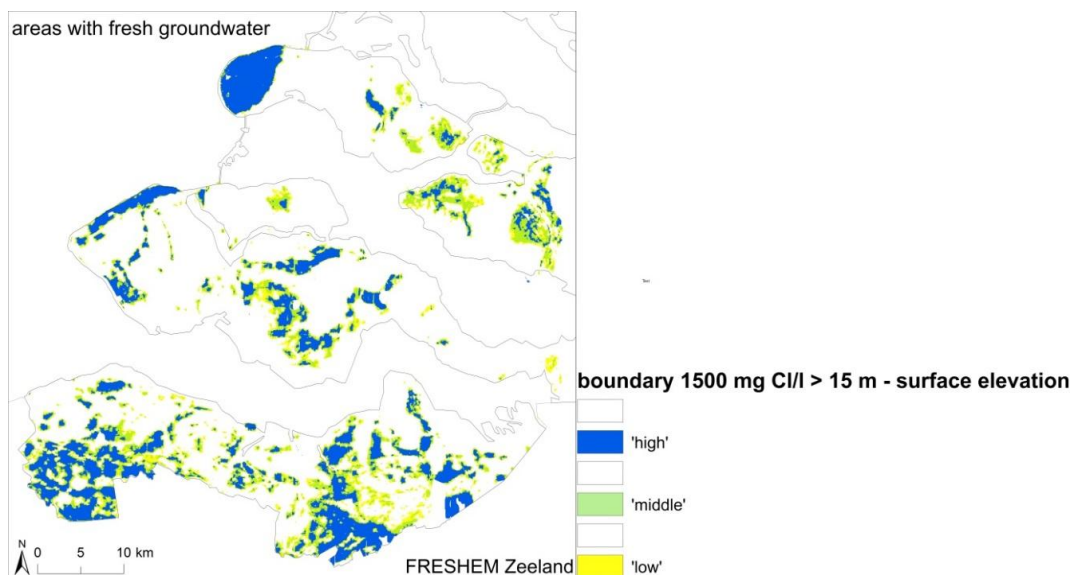


Figure 11.6: Areas in Zeeland with more than 15 metre fresh (<1500 mg Cl/l) groundwater for 'low', 'middle' and 'high'.

11.4.2 Saline areas

Agriculture or 'fresh' nature might be difficult in areas with a lack of fresh groundwater. Figure 11.7 shows the locations in Zeeland with a fresh groundwater lens of less than 5 m thickness. Table 11.3 shows the total area of Zeeland with only limited (or no) fresh groundwater for 'low', 'middle' and 'high'. More information about saline seepage areas in Zeeland can be found in (De Louw, 2011; De Louw, 2013). More information about increasing the thickness of these small fresh groundwater lenses can be found in (Oude Essink, 2014).

Table 11.3: Areas in Zeeland with less than 5 metre fresh groundwater.

Areas with < 5 m fresh groundwater (<1500 mg Cl/l)	Km ²	% of Zeeland
'low'	625	35
'middle'	750	40
'high'	850	50

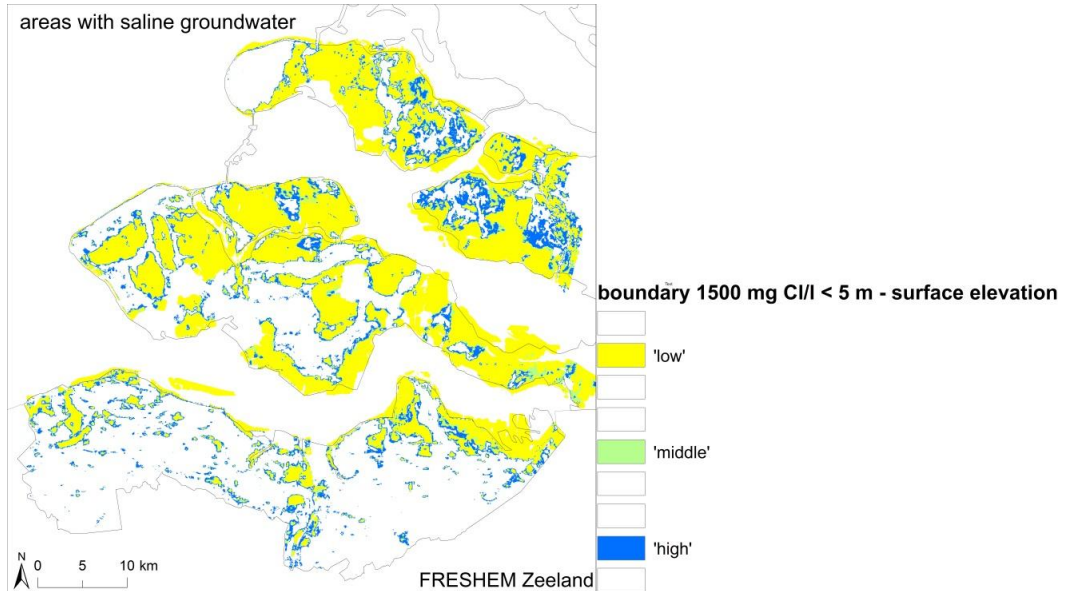


Figure 11.7 Areas in Zeeland with more less than 5 metre fresh (<1500 mg Cl/l) groundwater for 'low', 'middle' and 'high'.

11.4.3 Uncertainty

In Chapter 10 the main causes for uncertainty were shown for the 2D result and the additional uncertainty due to 3D interpolation. Figure 11.8 shows the difference of the depth of the 1500 mg Cl/l boundary (as reference to surface elevation) of 'low' and 'high' as percentage of the depth of the 1500 mg Cl/l boundary of 'middle'. The uncertainty increases in areas with no-data: above power lines, railways, roads, build-up areas, radar and canals with boats with radar. Examples are shown in Figure 11.9 and Figure 11.10a. The uncertainty increases as well at the (horizontal) borders of fresh groundwater lenses (example in Figure 11.10b).

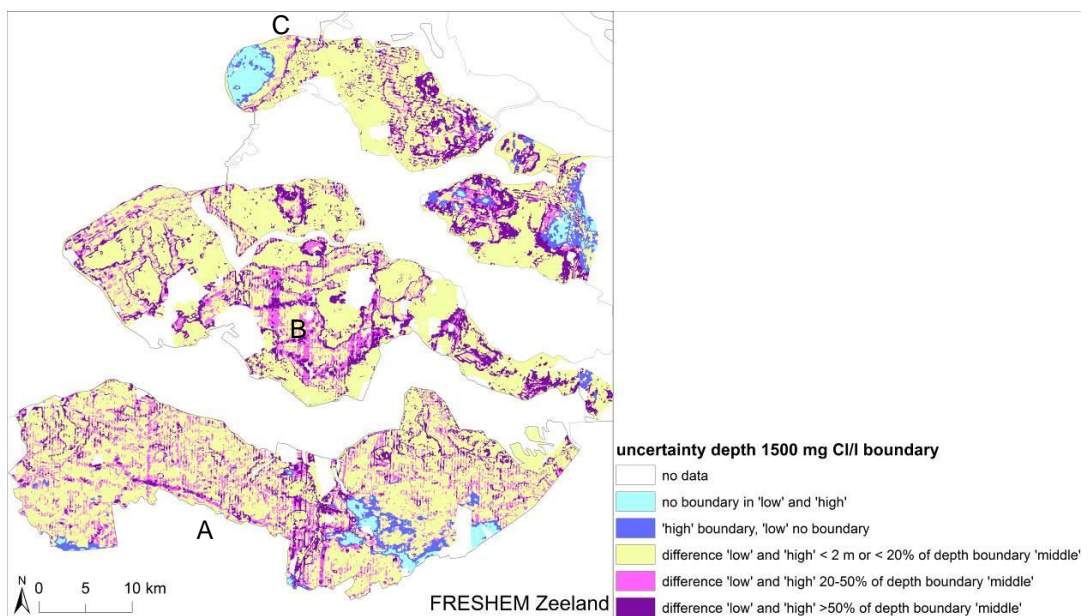


Figure 11.8 Uncertainty depth 1500 mg Cl/l boundary: difference depth 'low' and 'high' as % of depth 'middle'.



Figure 11.9 Uncertainty depth 1500 mg Cl/l boundary: difference depth 'low' and 'high' as % of depth 'middle'. For location (A) and legend, see Figure 11.8. Visualized are the flightlines and the no-data gaps in the flightlines. The uncertainty increases above the power line.

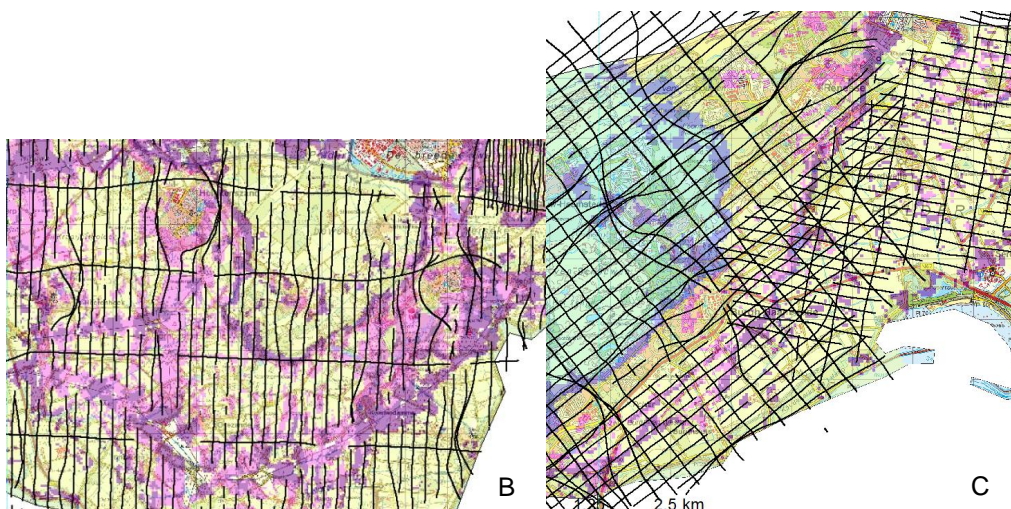


Figure 11.10 Uncertainty depth 1500 mg Cl/l boundary: difference depth 'low' and 'high' as % of depth 'middle'. Visualized are the flightlines and the no-data gaps in the flightlines. For location (B and C) and legend, see Figure 11.8. Figure a. Zuid-Beveland: the uncertainty increases above power lines, roads, rail ways and build-up areas. Figure b. Schouwen-Duiveland: the uncertainty increases and the horizontal boundary of the fresh groundwater lens.

11.5 Comparison with previous maps

11.5.1 Density dependent groundwater model

One of the previous maps of the depth of the fresh-salt boundary is based on a density dependent groundwater model of Zeeland (van Baaren, 2016). The current situation of the chloride distribution (year 2010) of this groundwater model was constructed in three steps: 1. Interpolation of point measurements including among others VES and ECPT's (Pebesma, 2009); 2. Inclusion of REGIS 2D boundaries 150 mg Cl/l and 1000 mg Cl/l (Goes, 2009 and Goes and Vernes, 2010) and 3. Removal of numerical instabilities by a density dependent calculation with high molecular diffusion. The strength of this chloride distribution is the use of point measurements in combination with system knowledge. Weaknesses of this chloride distribution are the locations without point measurements or locations where multiple interpretations of the groundwater system exist. From this chloride distribution the depth of the 1500 mg Cl/l boundary was derived (Figure 11.11b) and compared with the 1500 mg Cl/l

boundary of FRESHEM Zeeland 'middle' (Figure 11.11a). The differences are shown in Figure 11.12.

This results in the following –not complete- new insights of the groundwater system of Zeeland (for location see Figure 11.11a):

- More fresh groundwater north west Tholen (1);
- Shallow saline groundwater near the Eendracht and near Brabantse Wal (2);
- Significant fresh water lens Noord-Beveland (3);
- Significant fresh water lens east of Schouwen-Duiveland (4);
- Smaller fresh water lens sandy creek centre of Schouwen-Duiveland (5);
- Upconing of saline groundwater below ditches that cross a sandy creek ridge (6 and Figure 11.13);
- More fresh groundwater stored in the dune area of Walcheren (7);
- Local differences in Zeeuws-Vlaanderen (8);
- Land van Saeftinge does not contain fresh groundwater (9);
- More fresh groundwater in sandy creek ridges in Walcheren (10).

New insights with respect to fresh groundwater below saline groundwater are described in section 11.6.

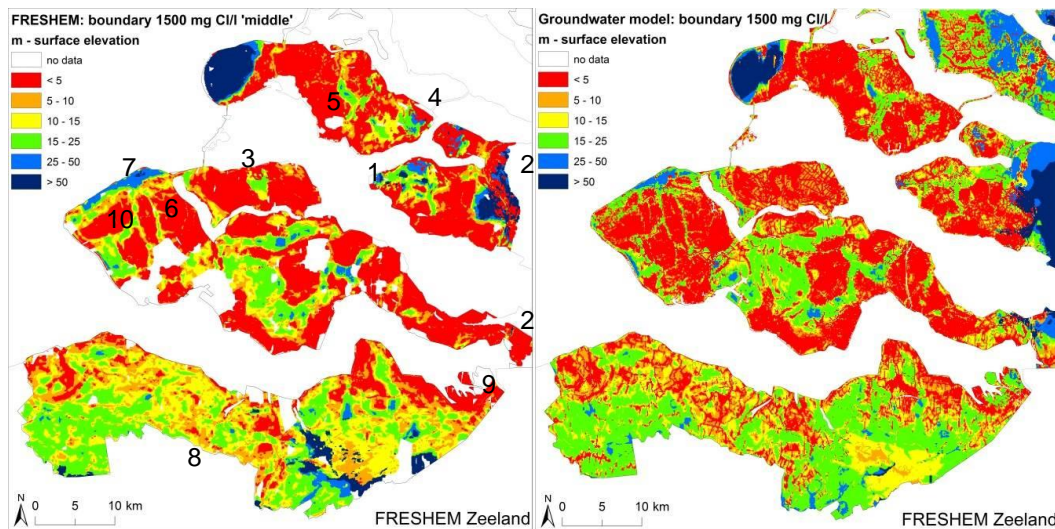


Figure 11.11 a. Depth 1500 mg Cl/l boundary FRESHEM Zeeland 'middle' and b. depth 1500 mg Cl/l boundary Groundwater model (the 'old' map).

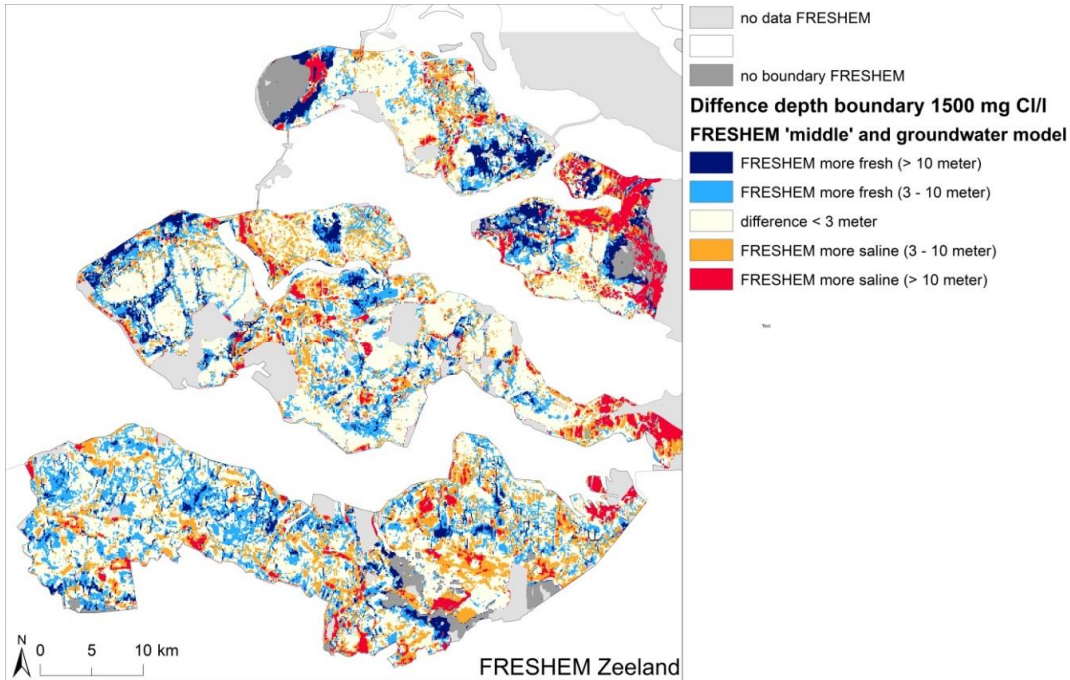


Figure 11.12 Difference in depth 1500 mg Cl/l boundary of the FRESHEM result and the 'old' map derived for the density dependent groundwater model.

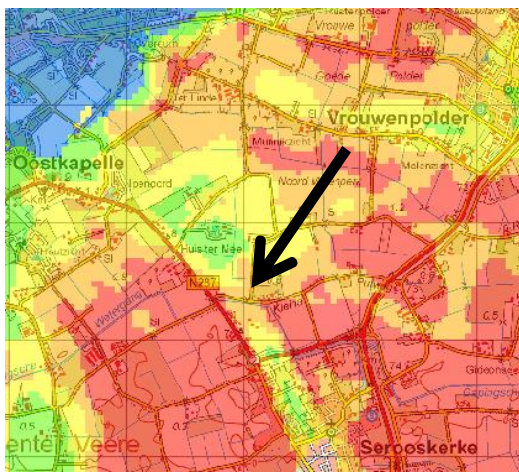


Figure 11.13 Depth 1500 mg Cl/l boundary FRESHEM Zeeland 'middle'. For legend and location see Figure 11.11.

11.5.2 Map of Waterboard Scheldestromen used for groundwater extraction permits

Waterboard Scheldestromen in Zeeland in the Netherlands uses the map 'Fresh groundwater bodies' with locations where the fresh groundwater lens has a thickness of at least 15 metre or where sufficient recharge of fresh water is assumed. Based on this map permits for groundwater extractions are evaluated. Figure 11.14 shows the areas in Zeeland with more than 15 metre fresh groundwater (<1500 mg Cl/l) based on FRESHEM Zeeland in combination with the map 'Fresh groundwater bodies' from Scheldestromen. FRESHEM results in new insights in the fresh groundwater bodies: new discovered bodies in eastern

Schouwen-Duiveland and Tholen (see A in Figure 11.14) and a necessity of reconsidering the bodies in Zeeuws-Vlaanderen and Zuid-Beveland (see B in Figure 11.14).

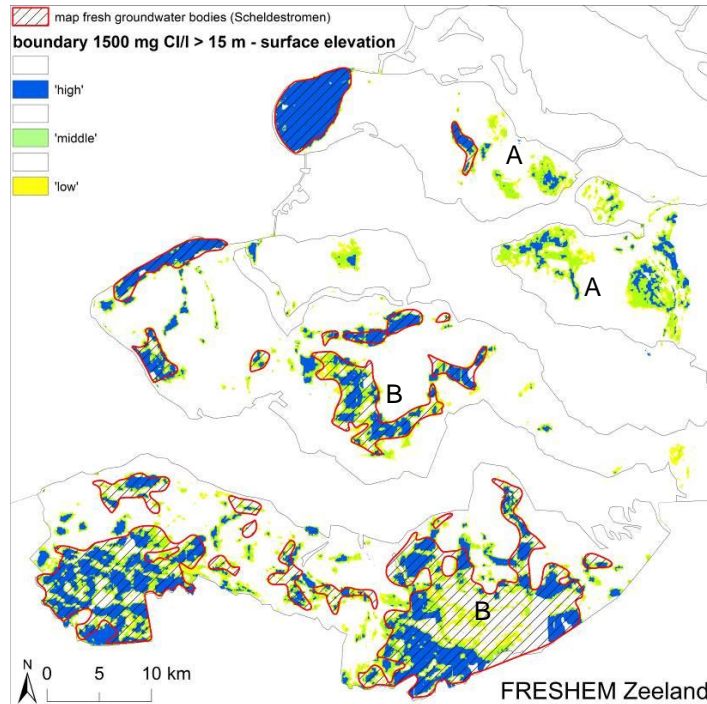


Figure 11.14 Areas in Zeeland with more than 15 metre fresh (<1500 mg Cl/l) groundwater for 'low', 'middle' and 'high' combined with the map 'fresh groundwater bodies' from Waterboard Scheldestromen.

11.6 Fresh below saline groundwater

11.6.1 Introduction

The FRESHM results show that fresh groundwater is present below saline groundwater at various locations in the province of Zeeland. In this situation the density distribution of the groundwater is unstable; the saline groundwater is heavier than the underlying fresh groundwater. In absence of low permeable (clay) layers this will result in the downward movement of the saline groundwater, thereby salinising the fresh groundwater. This process is known as free convection.

An unstable density distribution is less common than a stable density distribution, as for example is the case in a freshwater lens. Therefore, the unstable density distribution is typically referred to as 'inversion' (not to be confused with the mathematical inversion process used to derive vertical resistivity distributions from raw HEM data in chapter 7). This section gives an overview of the most important inversions present in the HEM data. Each type or location of the inversion is described and supported by independent geophysical data, chloride analyses of the groundwater or literature.

11.6.2 Method

The inversions have been analysed and mapped using the 2D and 3D FRESHM results (chloride concentrations) of the p50 (result 'middle'). An inversion is defined as fresh below saline groundwater, where different definitions of fresh and saline can be used. Figure 11.15 shows the inversions that have been found in the 3D chloride concentration result of the p50.

Note that FRESHEM maps the minimum area of Zeeland with inversions: additional areas with fresh below saline groundwater might exist but were not mapped because of the limited depth of the HEM measurements.

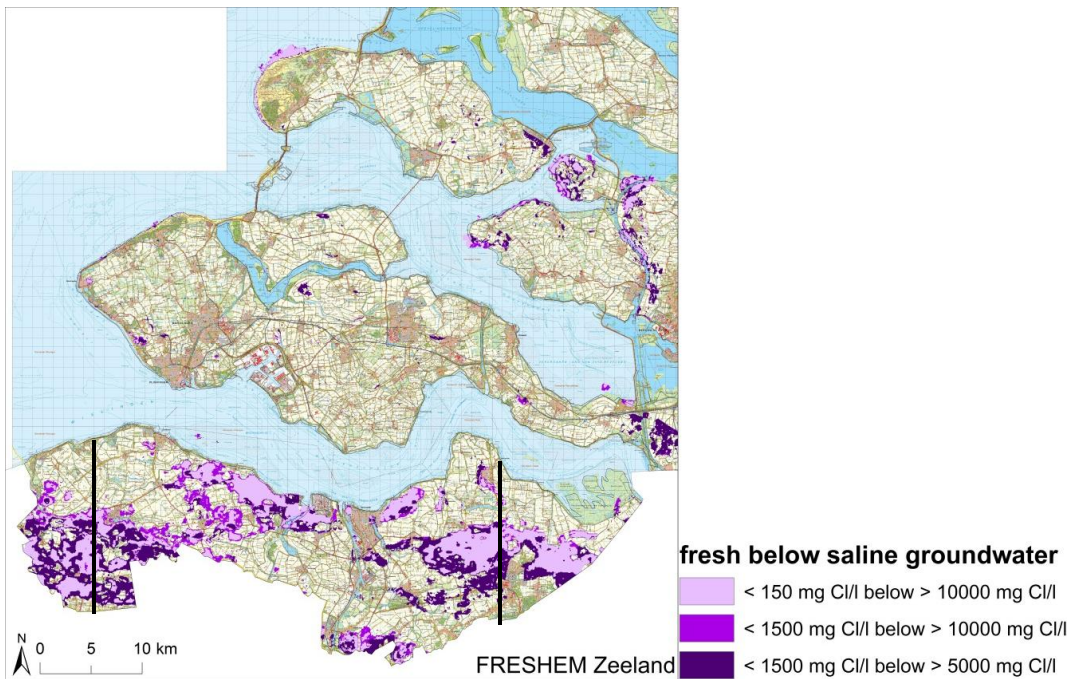


Figure 11.15: Inversions in the 3D chloride concentration model ("middle"). Black lines are the locations of the cross sections of Zeeuws-Vlaanderen in section 11.6.3.4.

The clear inversions have been subdivided into different types of systems and areas. Per system/type, independent geophysical data and chloride concentrations of the groundwater have been used to confirm or discuss the inversions.

11.6.3 Results

11.6.3.1 Fresh groundwater extending out into the sea

On Schouwen-Duiveland, and to a lesser extent on Walcheren, inversions are present below the beach and below the seabed. An example of such an inversion is presented in Figure 11.16, which shows a shore-normal profile of flightline 128.9 (Schouwen-Duiveland). In the REGIS Zeeland report (subreport C) the presence of this type of inversion on Schouwen-Duiveland has also been indicated (Goes and Vernes, 2010).

This type of inversion at the beach has been described for the first time in the scientific literature along the Belgium coast (Lebbe, 1978). The inversion is the result of the infiltration of saline water on the beach and the underlying flow of fresh groundwater from the dunes into the offshore direction. This situation can even occur without the presence of a low permeable layer, especially in case the (vertical) hydraulic conductivity is low and the flux of fresh groundwater from the inland is high (Greskowiak, 2014). At several locations in the provinces of Noord-Holland and Zuid-Holland, this type of inversion is also present (Pauw et al., 2017). At these locations, clay layers play an important role in preventing salinisation by free convection.

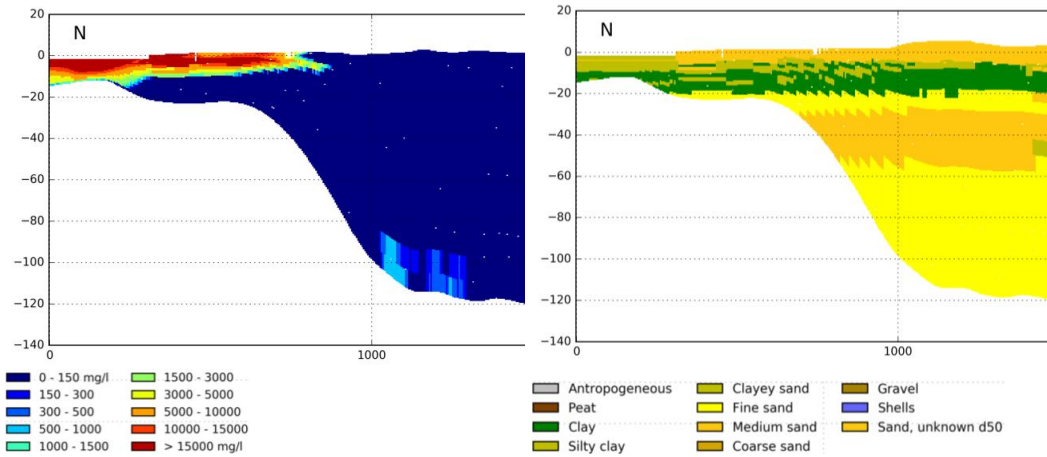


Figure 11.16: Inversion along the coast in flightline 128.9, perpendicular to the coast of Schouwen-Duiveland.

Figure 11.16 shows that also further offshore the inversion is present. The clay layer functions as a barrier against free convection. Without the clay layer fresh groundwater would probably not be present offshore. The fresh groundwater below the clay layer offshore can be explained by two processes:

- 1) The flow of fresh groundwater from the inland into the offshore direction (Figure 11.17).
- 2) Paleo-groundwater. The fresh groundwater offshore can also be a relic of historic periods, for example Pleistocene ice ages when the coastline was situated further westward compared to the current position of the coastline and fresh groundwater could infiltrate into the subsurface. In the literature several examples of fresh paleo-groundwater have been described, such as offshore the coast of Surinam (Kooi en Groen, 2003).

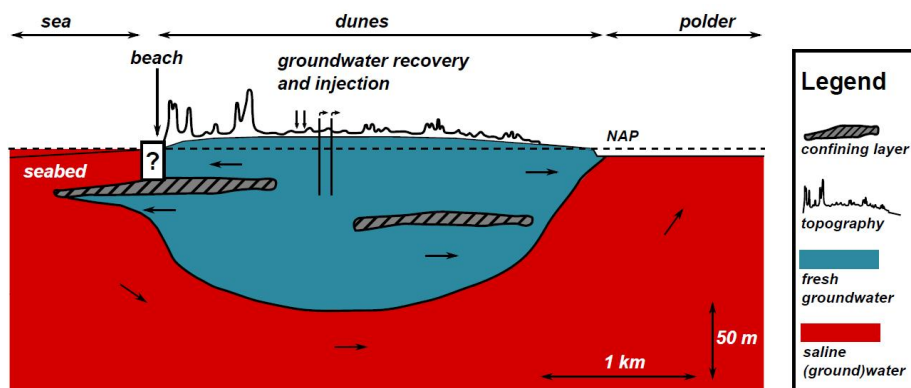


Figure 11.17: Concept of the groundwater salinity distribution along the Dutch coast (Pauw et al., 2017). Below the beach the groundwater salinity has been omitted and marked with a '?'. Saline groundwater also comprised brackish groundwater is this concept.

11.6.3.2 Flow of fresh groundwater below low permeable sediments along the landward side of the dunes and below the creek ridges.

At the inland boundaries of the dune areas of Schouwen-Duiveland and Walcheren, and along several creek ridges in the province of Zeeland inversions are present below a low permeable layer. The salinity of the low permeable layer is higher than 'fresh'. Examples are given in Figure 11.18.

There are no chloride analyses available that confirm or reject the inversions. A CVES measurement near Grijpskerke (Figure 11.19) also indicates fresh groundwater below the clayey sediments along the side of the creek ridge. The clayey sediments were deposited during the Holocene in a brackish / saline environment, and can still contain some of this water because the permeability of the sediments is low. In the sandy, more permeable layers freshening has occurred much faster than in the low permeable layer. This is shown in concept in Figure 11.20.

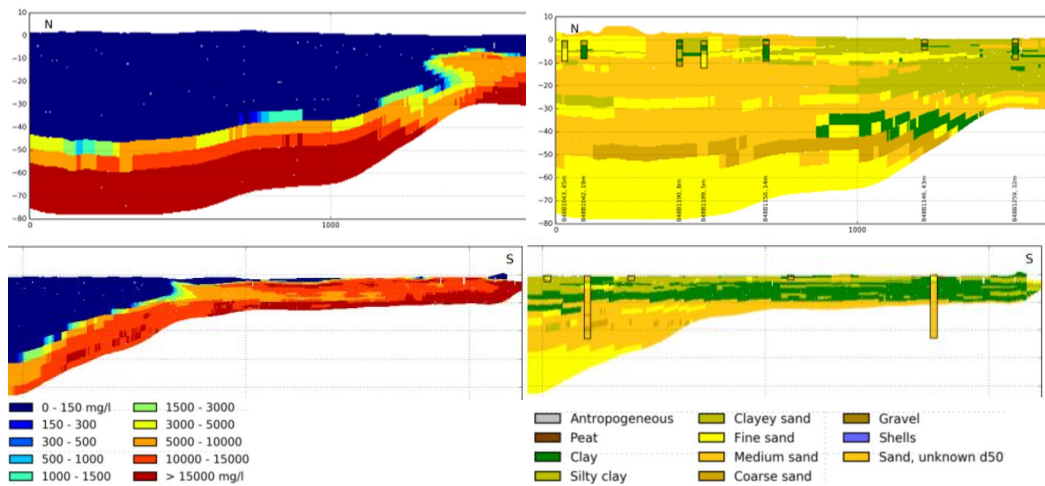


Figure 11.18: Inversions along the inland boundary of the dune areas of Oranjezon (Walcheren) (above) in flightline 109.9, and Schouwen-Duiveland (below) in flightline 126.9.

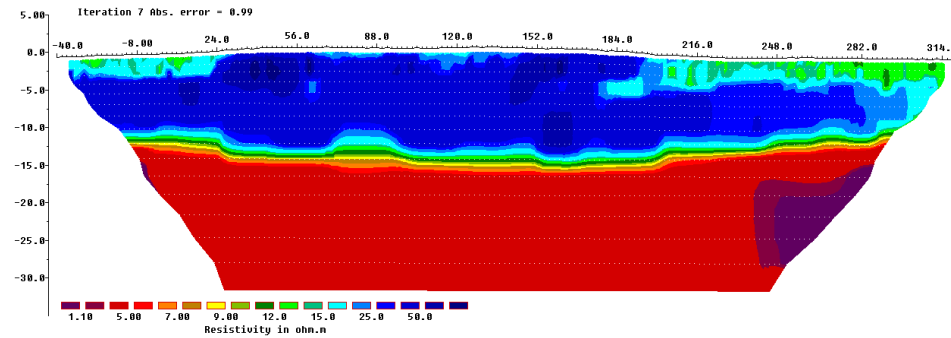


Figure 11.19: Inversion result of a CVES measurement along a creek ridge south of Grijpskerke (Walcheren).

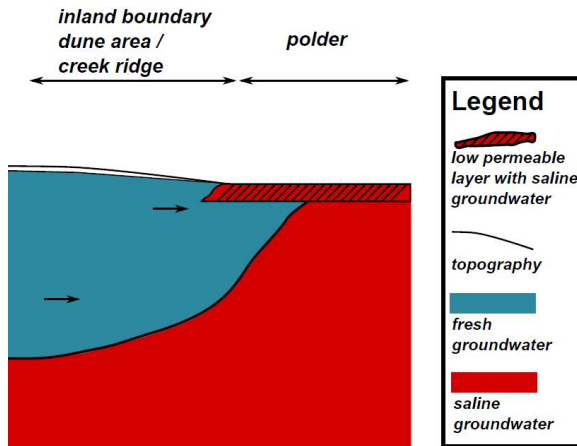


Figure 11.20: Concept of the inversion along the inland boundary of the dune area and next to the creek ridges.

11.6.3.3 *Thin layer of saline groundwater in the clay and peat layer near Bruinisse (Schouwen-Duiveland), Tholen, St. Philipsland, East of Schelde-Rijnkanaal (Noord Brabant), and at the Brabantse Wal.*

Figure 11.15 indicates shallow (here: ~ -5 to -15 m NAP) inversions at several locations at Bruinisse (Schouwen-Duiveland), Tholen, St. Philipsland, East of Schelde-Rijnkanaal (Noord Brabant), and at the Brabantse Wal. In Figure 11.21 an example is given in a vertical cross section. 1000 years ago, these areas were in open connection to the sea and sedimentation, erosion, and infiltration of seawater took place (Vos en de Vries, 2013; Figure 2.4c). The saline clay and peat deposits that currently lie near the surface above the fresh groundwater originate from this period. Part of these sediments have freshened after the embankments by mankind, part of it is still saline or brackish.

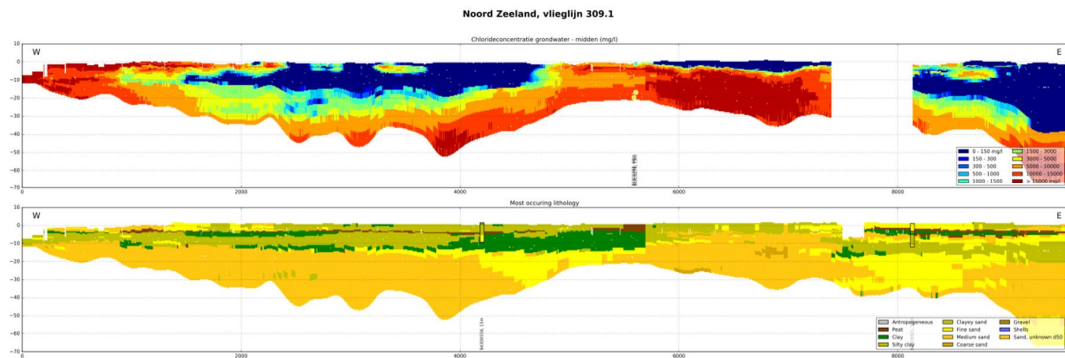


Figure 11.21: Inversion on Sint Philipsland (left) East of the Schelde-Rijnkanaal (right) in flightline 309.1.

In the sandy sediments below the saline peat and clay deposits freshening has taken place. The driving force of this freshening can be the higher hydraulic heads at the higher elevated areas, such as the creek ridge, or regional groundwater flow from the province of Noord Brabant. The latter is probably responsible for the freshening of the sediments East of de Eendracht (Schelde Rijnkanaal) and near the Brabantse Wal. Another explanation for the presence of the fresh groundwater is that this is old (pre-Holocene) groundwater which was not subjected to salinisation during the Holocene transgressions, due to the presence of a clay layer or Basal Peat. The inversions are confirmed by chloride analyses (Figure 11.22), a cone penetration test (Figure 11.23) and borehole logging measurements (Figure 11.24). Locations of the different measurements are presented in Figure 11.25.

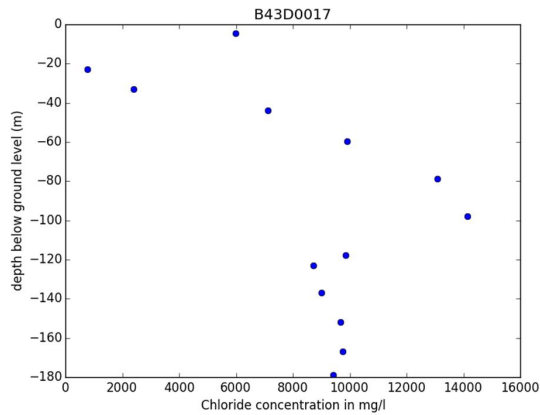


Figure 11.22: Chloride concentration of piezometre B43D0017, West of De Eendracht / Schelde Rijnkanaal. The upper filter shows brackish/saline groundwater, the filter below (21 m below ground level) is fresh. In this area also piezometres B430013, B430016, and B430021 (Figure 11.25) indicate fresh groundwater below saline groundwater in the FRESHEM result.

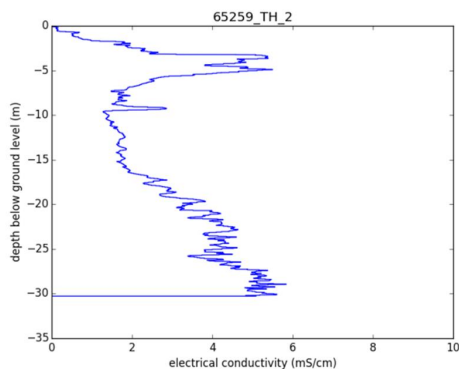


Figure 11.23: Cone penetration test at Tholen. In the upper 5 m the salinity increases, then decreases and finally increases again from ~16 m below groundlevel.

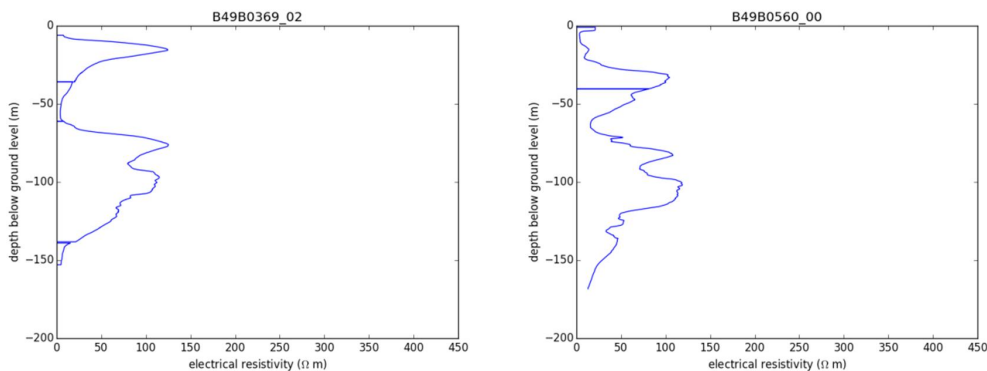


Figure 11.24: Borehole logging measurements East of De Eendracht / Schelde-Rijnkanaal (see Figure 11.25). Both measurements indicate fresh groundwater between ~60 m below ground level and ~120 m below ground level. Between ~30-40 m below ground level and ~50-60 m below ground level the groundwater at some depth is probably saline or brackish. This is probably also the case close to the surface.

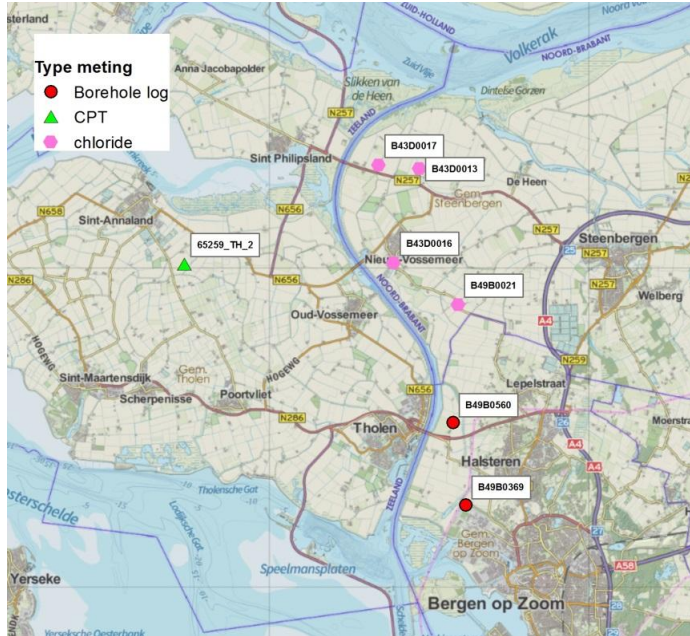
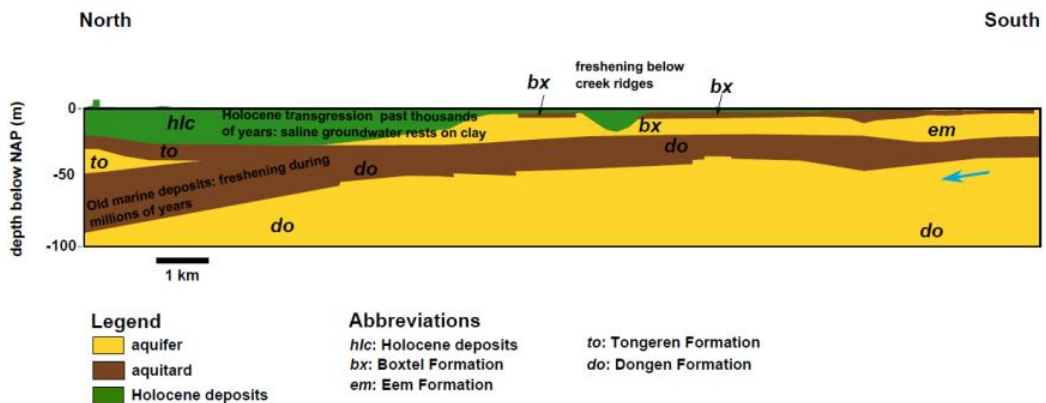


Figure 11.25: Overview of the different independent measurements around De Eendracht / Schelde-Rijnkanaal that support the presence of the inversions.

11.6.3.4 Saline groundwater on top of old marine deposits in Zeeuws-Vlaanderen

The old marine clay deposits of the Rupel Formation (Boomse Klei), Tongeren Formation, and Dongen Formation, and the confined aquifers below and in between them are probably fresh because of millions of years of freshening. Holocene transgressions resulted in the deposition of sediment in a saline environment, and infiltration of saline water on top of the old (pre-Holocene) clay deposits. After the land reclamations by mankind, freshening of the saline deposits took place. Where freshening has taken place, only just a thin layer of saline groundwater is present between the fresh groundwater above and the old clay deposits below (Figure 11.26).



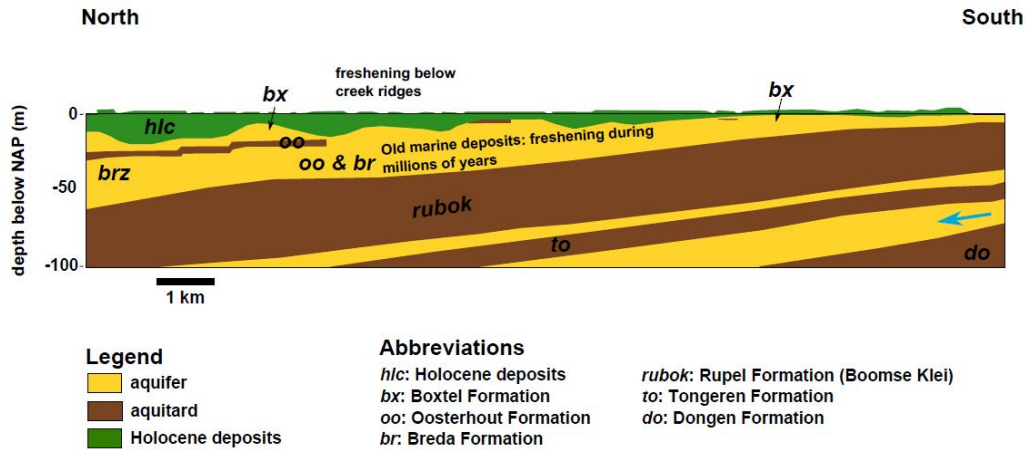


Figure 11.26: Inversions and hydrogeology in Zeeuws-Vlaanderen. See Figure 11.15 for the locations of the hydrogeological cross sections.

11.7 New insights in lithology

The FRESHEM project focusses on calculating chloride concentrations from the HEM measurements. Lithology is an important factor that is corrected for, as it has a significant imprint on resistivity values. Turning this around, the FRESHEM results can potentially be used for lithological mapping as well. It will not be straightforward to directly use the resistivity values from this project in the GeoTOP modelling procedure. Still, there is valuable lithological information enclosed in the resistivity values. Four examples are given in the text below.

11.7.1 Resistivity differences within fresh water bodies

The major difficulty in lithological mapping based on FRESHEM results is that resistivity values are controlled by chloride content rather than lithology. Where salt groundwater is present, the resistivity contrast from lithology will be overprinted by the high conductivity of the groundwater. At the fresh-salt interface, a contrast in resistivity is often better explained by a change in chloride content than a lithological change. The most promising locations to extract lithological information from resistivity results are therefore the fresh water bodies.

The dunes at the western coast of Schouwen-Duiveland have developed a fresh water lens to considerable depth. Figure 11.27 shows the p50 of the 3D chloride model at a depth of 19 m below NAP. The outline of a structure of high resistivity is indicated in Figure 11.28. Resistivity values here are likely to be controlled by lithology, this means the structure is more sandy than its surroundings. The GeoTOP prediction of lithology at this depth, based on borehole information, is shown in Figure 11.29. Within the Naaldwijk Wormer member, the line of boreholes from B42B0003 to B42B0046 indeed show a transition from clay to sand at this depth (see Figure 11.30). If the high resistivity structure is a sandy channel infill of the Naaldwijk Wormer, then the borehole locations are a bit unfortunate as only B42B0003 is located near the center line of this structure. GeoTOP therefore cannot predict the curve of the sandy channel based on borehole information. Identification of the contrast in resistivity potentially is a valuable addition to the GeoTOP workflow as it can be used to provide extra information in between borehole locations.

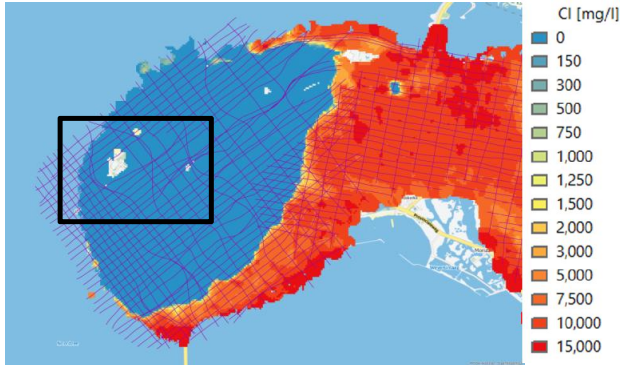


Figure 11.27 P50 of chloride concentration at the western coast of Shouwen Duiveland, at a depth of 19 m below NAP. Flightlines (purple lines) and approximate area indicated in Figure 11.28 and Figure 11.29 (black box).

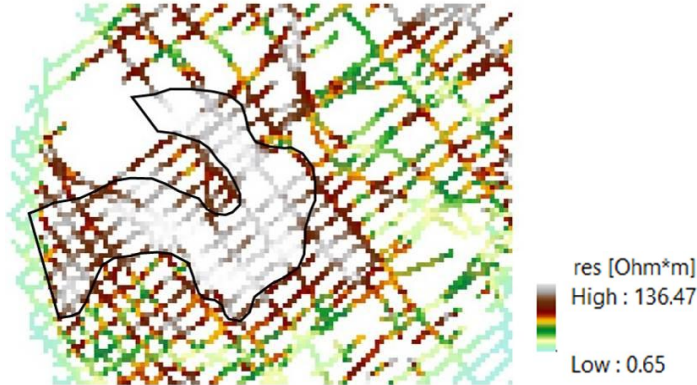


Figure 11.28 Resistivity values at flightlines at a depth of 19 m below NAP. Indicated is the interpretation of a relatively high resistivity area.

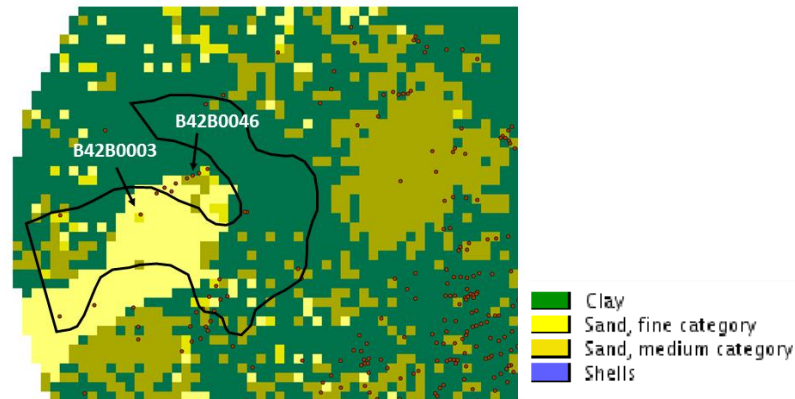


Figure 11.29 Interpretation of the high resistivity body, projected on GeoTOP lithological prediction at 19 m below NAP. Red dots are GeoTOP boreholes that at least reach the Naaldwijk Walcheren member, logs of two selected boreholes shown in Figure 11.30. See Figure 11.31 for the legend.

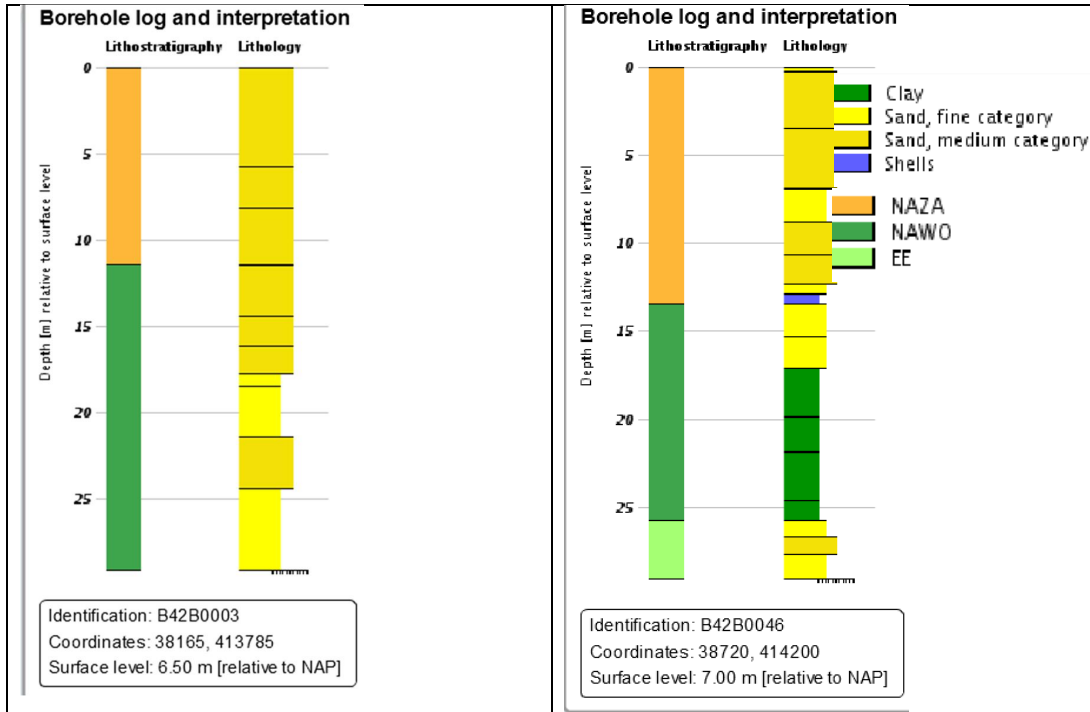


Figure 11.30 Two boreholes showing the transition from the sand to clay at 10 metres below NAP.

11.7.2 High chloride concentration as proxy for clay extent

Figure 11.31 shows the chloride concentration, resistivity and the lithological prediction from GeoTOP of a part of line 431.1. At the northern edge of the fresh water body, a 'tongue' of high chloride and low resistivity extends to the south. GeoTOP predicts a clay layer, possibly topped by peat, that extends south until termination at the sandy tidal channel infill. Replacement of initial saline groundwater by fresh water is very slow process. The resistivity of the clay here is relatively low because of its high chloride content, while sand above and below show a low resistivity. Resistivity / chloride content here is a clear proxy of hydraulic conductivity of the lithological layers. This can be used as an indication of the extent of the high hydraulic conductivity (therefore clay rich) layer. In this example, based on the observed resistivity contrast the clay layer possibly is modelled too far south into the channel.

Midden Zeeland, vlieglijn 413.1

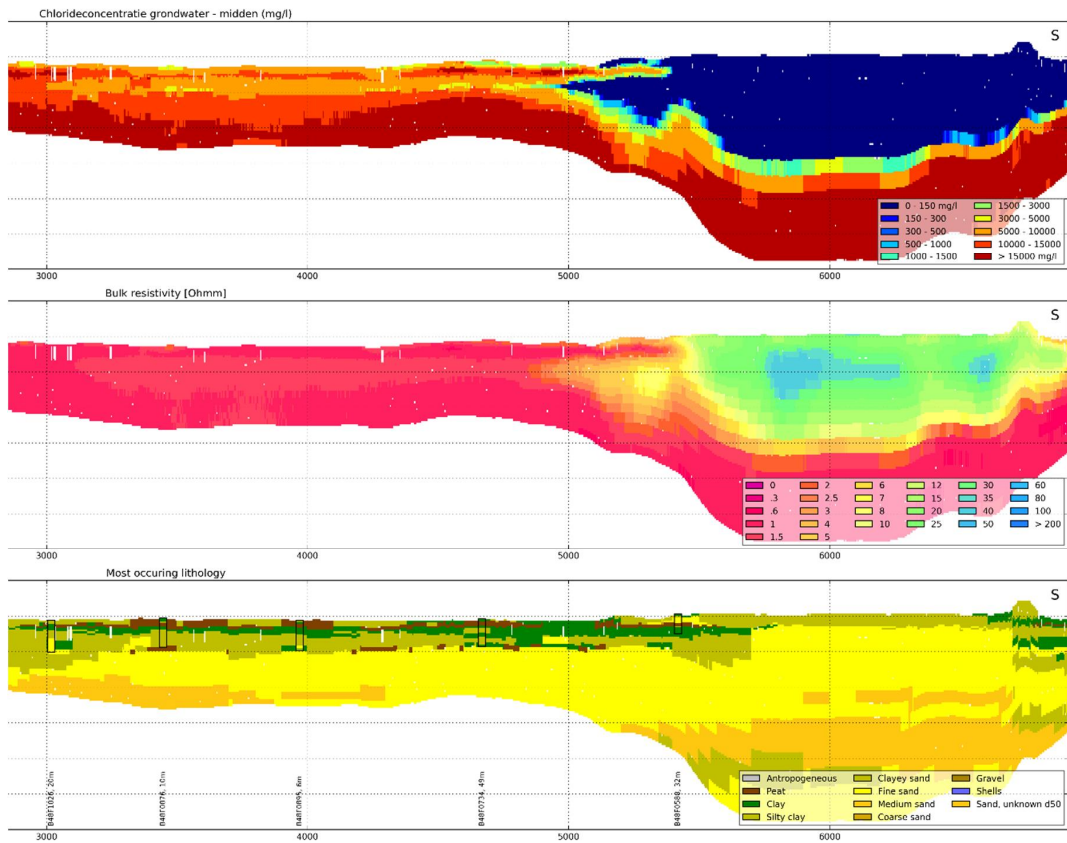


Figure 11.31 Chloride concentration, resistivity and GeoTOP lithology of part of line 431.1

11.7.3 Freshening of groundwater as a proxy for clay discontinuity

Figure 11.32 shows the process of freshening of the groundwater (orange arrows). The GeoTOP prediction at this location is a continuous clay layer at approximately 10 m below NAP. A discontinuity of this clay layer is tentatively expected, as the onset of freshening is localized around the arrows. This is confirmed by the sandy interval at this depth that is seen in borehole B49B1753. The patterns that are found in groundwater salinity distribution are therefore an indication of the continuity of clay layers, and can be used to localize discontinuities at a resolution that is hard to obtain from borehole information.

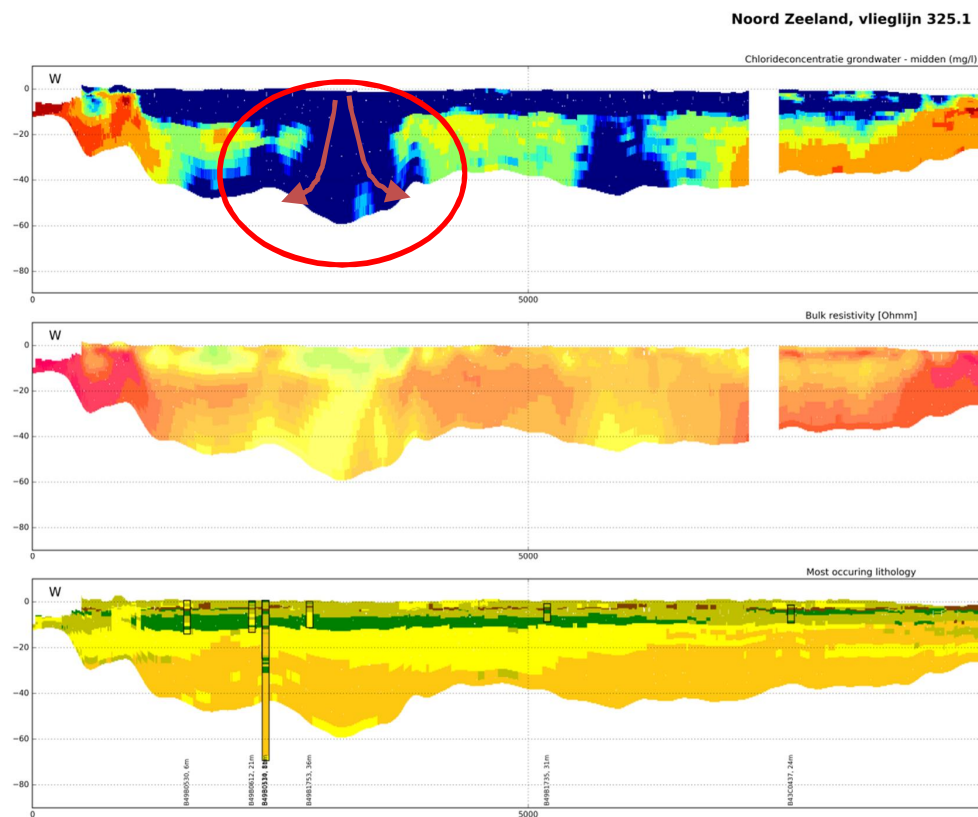


Figure 11.32 Chloride concentration, resistivity and GeoTOP lithology of part of line 325.1, see Figure 11.31 for the legend.

11.7.4 Width of the fresh water at creek ridges as an indication of clay occurrence

A creek ridge just northwest of Middelburg shows a zone where the width of the fresh water lens is smaller (see Figure 11.33). Local low hydraulic conductivity can limit the extent of the fresh water lens. The lithological prediction from GeoTOP at this depth is given in Figure 11.34. A clay rich area is predicted exactly at same location of narrowing of the fresh water lens. Where the tidal channel infill consists of clayey sediments the flow of fresh water groundwater will be limited with respect to a more sandy infill. This will hamper the development of a sizable fresh water lens. Relative changes in the fresh water lens under creek ridges might therefore be used as an indication of the lithological infill of the tidal channels.

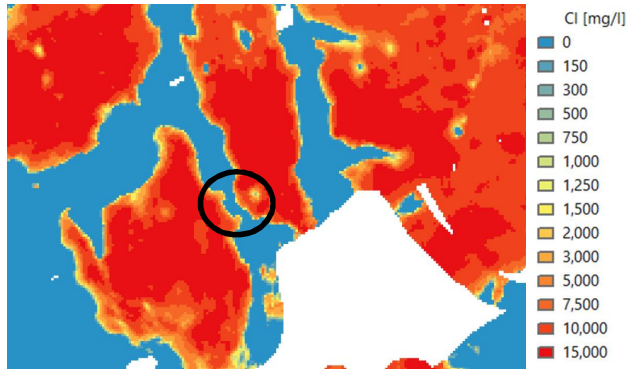


Figure 11.33 Chloride concentration at 6.75 m below NAP, a relatively narrow zone of fresh water is indicated by the black circle.

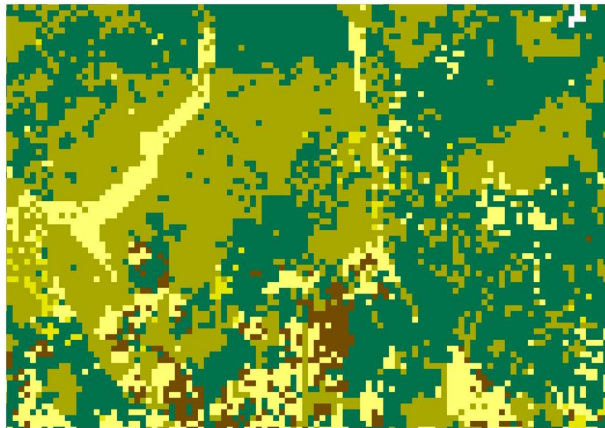


Figure 11.34: Lithological prediction from GeoTOP at 6.75 m below NAP shows a clay rich area at the same location where fresh water lens is relatively small. See Figure 11.31 for the legend.

11.8 Comparison with fixed Ω_m boundary

Previous studies about large scale airborne geophysics for fresh-salt groundwater mapping do not take into account the translation from resistivity of the groundwater and the subsoil (bulk value) into the conductivity of the groundwater or the chloride concentration of the groundwater. Several studies use the 6 Ω_m boundary (bulk value groundwater and subsoil) as fresh-salt interface of the groundwater (Schaars, 2014; Siemon 2009; Paine and Minty, 2005). In FRESHEM resistivity was translated into chloride concentration taking lithology into account and based upon that result the 150 or 1500 mg Cl/l boundary was used to determine the fresh-salt interface of the groundwater. A comparison is made between the 6 Ω_m boundary with the 150 and the 1500 mg Cl/l boundary of the 2D result of FRESHEM for all flightlines (since there is no 3D resistivity result).

In general, FRESHEM maps freshwater in clay where the 6 Ω_m approach maps saline groundwater. See Figure 11.35 for an example: FRESHEM maps fresh water lenses of several metres thickness whereas the 6 Ω_m boundary is not present. One of the main benefits of FRESHEM is the distinction between areas without fresh groundwater and areas with fresh groundwater lenses of several metres thickness. Another benefit of FRESHEM is the mapping of brackish water in sand instead of mapping freshwater. Spatial differences are shown in Figure 11.36 and Figure 11.37. In 34% the total linekm the depth of the 150 mg Cl/l boundary is different than the depth of the 6 Ω_m boundary. While compared with the 1500 mg

cl/l boundary this percentage is 44% (Table 11.4). In 11% of the total line kilometre FRESHEM did find a freshwater lens whereas the 6 Ω m boundary was not present (Table 11.5).

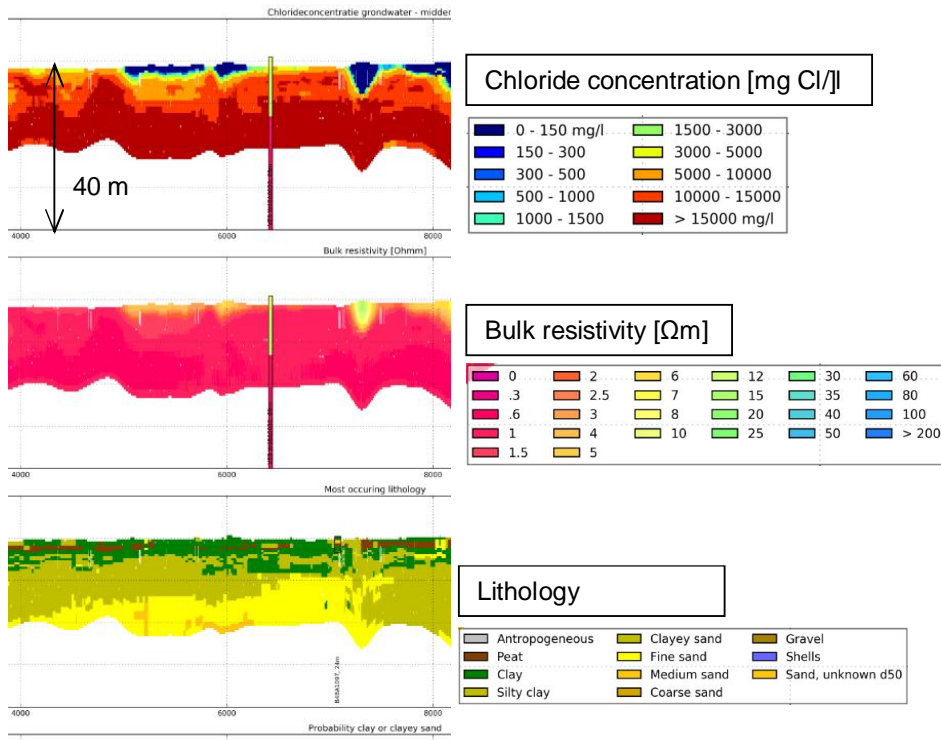


Figure 11.35: example (flightline 11.1 Midden Zeeland) of the mapping of fresh groundwater lenses in FRESHEM with a thickness of several metres (a) where the bulk resistivity remains below 6 Ω m (b) in areas with clay (c).

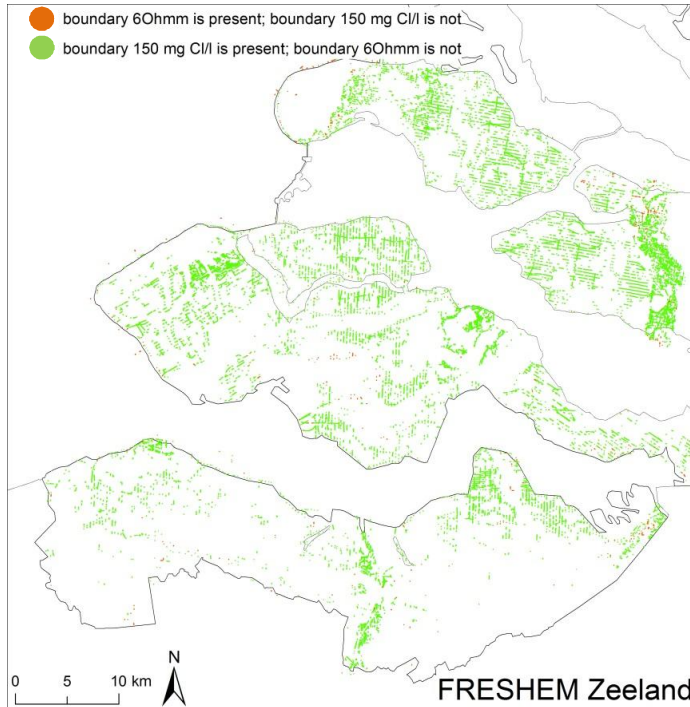


Figure 11.36 In green the locations (measurement 2D result FRESHEM) where the 150 mg Cl/l boundary is present and the 6 Ω m boundary is not present. In orange the locations where the 6 Ω m boundary is present and the 150 mg Cl/l boundary is not present.

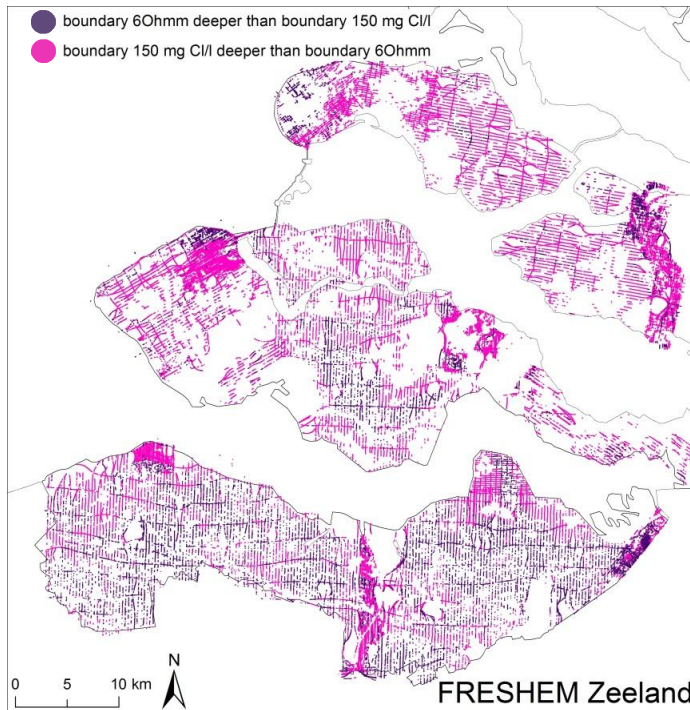


Figure 11.37 In pink the locations (measurement 2D result FRESHEM) where the 150 mg Cl/l boundary is deeper than the 6 Ω m boundary. In purple the locations where the 6 Ω m boundary is deeper than the 150 mg Cl/l boundary.

Table 11.4 Number of line kilometre and % of total line kilometre indicating differences between the 6 Ωm as fresh-salt boundary and the 150 or 1500 mg Cl/l as fresh-salt boundary.

	Line km	% of total linekm
6 Ωm boundary deeper than 150 mg Cl/l boundary	650	7
150 mg Cl/l boundary deeper than 6 Ω boundary	2350	27
6 Ωm boundary deeper than 1500 mg Cl/l boundary	125	1
1500 mg Cl/l boundary deeper than 6 Ω boundary	3775	43

Table 11.5 Number of line kilometre and % of total line kilometre indicating differences between the presence of the 6 Ωm boundary and the 150 or 1500 mg Cl/l boundary.

	linekm	% of total linekm
Freshwater lens present for 150 mg Cl/l boundary, no freshwater lens for 6 Ωm boundary	950	11
Freshwater lens present for 6 Ωm boundary, no freshwater lens for 150 mg Cl/l boundary	12	0
Freshwater lens present for 1500 mg Cl/l boundary, no freshwater lens for 6 Ωm boundary	1375	15
Freshwater lens present for 6 Ωm boundary, no freshwater lens for 1500 mg Cl/l boundary	5	0

12 Validation

12.1 Summary

Quantitative validation is required to judge the quality of the FRESHEM result and to guide the usage of the FRESHEM result. This validation was performed by comparison of the FRESHEM result with other available (direct) measurements.

There are essentially two types of measurements available in Zeeland to validate the FRESHEM result: chloride concentrations measured in samples from monitoring wells (hereafter called 'chloride measurements') and 'ground measurements' that give a chloride profile over depth. The ground measurements can be subdivided further into (Chapter 3):

1. TEC probe
2. Electrical cone penetration tests (ECPT)
3. Geo-electrical bore hole measurements
4. SlimFlex
5. VES, CVES

The chloride measurements and ground measurements have been used to quantitatively validate the FRESHEM result as follows:

1. After classification into chloride classes, FRESHEM result and chloride measurements have been compared. Data of 1294 monitoring wells have been compared to the FRESHEM result at those locations.
2. The ground measurements and the FRESHEM result have been used to determine the starting depth and thickness of the fresh-saline mixing zone, and these depths have been compared. The starting depth has been compared at 178 points, and the thickness at 153 points (the end of the mixing zone was not present in the remaining 25 points).
3. TEC probe results have been used to determine the presence of saline groundwater in the upper 4 m of the soil, and compared with whether the FRESHEM result also shows the presence of saline groundwater.
4. The effect of the 3D interpolation on the quality of the FRESHEM result has been estimated by comparing a selection of chloride and ground measurements with the 2D HEM flight line result: only measurements within 25 m from a flight line have been selected for validation.

These validation steps are described in detail in the following subchapters. The result of the validation can be briefly summarised as:

1. Using a classification of 'fresh' (< 1500 mg/L Cl), 'brackish' (1500 – 10000 mg/L Cl), and 'salt' (>10000 mg/L Cl), 78% of measured chloride points are in agreement with the HEM 'middle' result (88% of measured chloride points fall within bounds given by FRESHEM result 'low' and 'high').
2. For 80% of the ground measurement points, the top of the fresh-saline boundary falls within 2 metres plus ten percent of the depth of the fresh-salt boundary in the FRESHEM 'middle' result.
3. The FRESHEM result agrees with 88% of the selected TEC probe measurement locations in terms of top soil saline or fresh groundwater.

The following should be kept in mind when using the FRESHEM result. The FRESHEM result gives accurate, but not perfectly accurate information on the chloride distribution in Zeeland. The result is more reliable in fresh and saline zones, and less reliable in brackish zones. The result should be interpreted cautiously when looking at local features: it should for example not be used to estimate the chloride distribution around ditches. The equation above can be

used to provide a conservative estimate of the starting depth of the fresh-saline mixing zone. All these prescriptions are probabilistic in nature and consequently, the FRESHEM result should not be used in isolation at a specific site, but in combination with all available data.

12.2 Chloride measurements

12.2.1 Data and methods

Chloride measurements from a total of 1294 monitoring well screens have been used for the entirety of Zeeland. The screening depth of the screens varies from 0.6 m to 139 m below surface, and the year of last sampling of the oldest chloride measurements date back to 1910. The median chloride concentration has been taken when multiple chloride concentrations are available for a single well screen. These median chloride concentrations range from fresh (15 mg/L) to salt (20215 mg/L). Relatively many monitoring well filters are located in fresh groundwater. See Figure 12.1, Figure 12.2 and Figure 12.3.

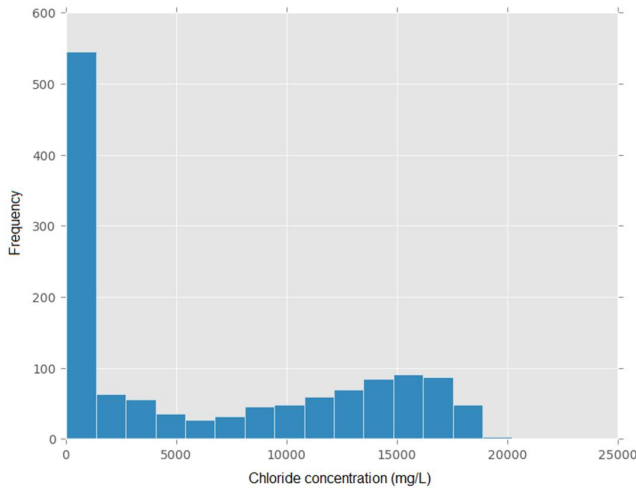


Figure 12.1 Histogram of chloride concentrations (median per well screen).

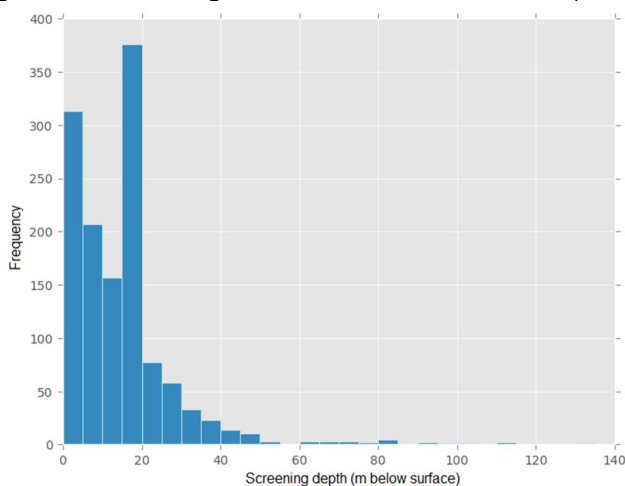


Figure 12.2 Histogram of screening depth of monitoring wells.

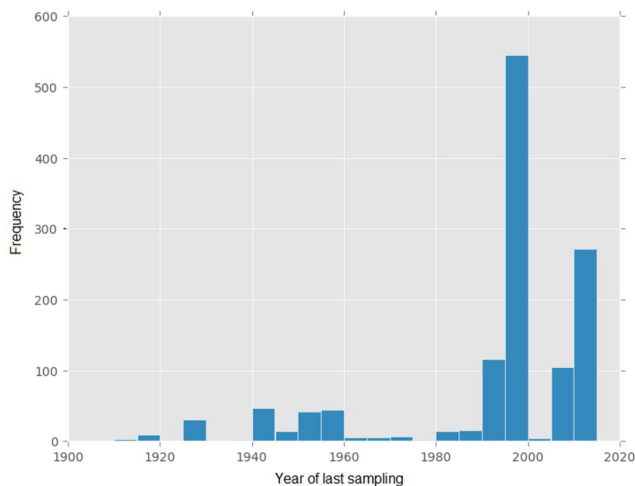


Figure 12.3 Year of last sampling of the monitoring wells. Some monitoring wells are no longer sampled; many have last been sampled in the second half of the decade 1990-2000.

The chloride concentrations have not been directly compared, but classified into nine classes. This classification is motivated by the use of water, as e.g. 150 mg/L Cl is a limit for drinking water, and 1500 mg/L Cl is a limit for agrarian use. The nine chloride classes are: < 150, 150-300, 500-1000, 1000-1500, 1500-3000, 3000-5000, 5000-10000, and > 10000 mg/L Cl. Additionally, a simplified classification has been considered as well, consisting of three classes: <1500, 1500-10000, and > 10000 mg/L Cl.

The 3D FRESHEM result was validated by point-to-point comparison with available measurement data. Where monitoring screens extend over multiple layers in the 3D result, the mean was taken over the different layer values. For this validation step the chloride measurements classes have been compared with the HEM p50 class, and whether they fall within the class bounds given the p25 and p75 class, and the bounds given by the p10 and p90 class. Note that p25 corresponds with FRESHEM 'low' and p75 corresponds with FRESHEM 'high'.

A sizeable number of data have been used to validate the FRESHEM results, and some data are older than 100 years. In contrast, the FRESHEM result is a snapshot of the fresh-saline water distribution. In general salinization and freshening of the groundwater are very slow processes, which allows us to use historical data for validation. In some areas, however, there may have occurred changes that have influenced the fresh-saline groundwater distribution. Data from these areas have not been used in the validation. Specifically:

1. The dune area of Schouwen-Duiveland: all data before 1980 are omitted due to changes in drinking water extraction.
2. The dune area of Walcheren: all data before 2000 are omitted due to changes in drinking water extraction.
3. The Waterdunen area in Zeeuws-Vlaanderen: all data before 2011 are omitted due to land use changes.

12.2.2 Results

If we consider the localisation of freshwater by FRESHEM, FRESHEM results compare to available chloride measurements as follows (Figure 12.4):

- When FRESHEM result 'middle' indicates fresh water (< 1500 mg/L Cl) 83% of the chloride measurements are fresh as well. The number of chloride measurement points for this criterion is 586.
- When FRESHEM result 'high' indicates fresh water (< 1500 mg/L Cl) 87% of chloride measurements are fresh as well. The number of chloride measurement points for this criterion is 513.
- For FRESHEM result 'middle' the agreement for all 1294 points is 78%, see Figure 12.4. 88% of points fall within bounds given by 'low' and 'high', and 93% of points fall within bounds given by p10 and p90.

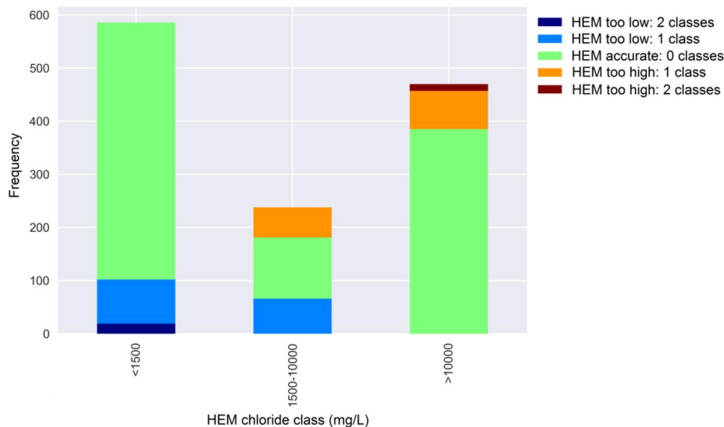


Figure 12.4 Validation result for chloride classes fresh, brackish and saline for FRESHEM result 'middle', per chloride class, absolute numbers.

When validating using all nine available (thus much more detailed) chloride classes, the result is as follows: 59% of chloride measurements fall within the class given by the 'middle' (p50) FRESHEM result at that location, 74% falls within the p25 and p75 class bounds (FRESHEM 'low' and 'high'), and 84% falls within the p10 and p90 class bounds.

Figure 12.5 shows the validation result per chloride class for the 'middle' FRESHEM result, and the validation result as per cent agreement per chloride class. Two observations stand out. There are relatively few brackish chloride classes (between 150 and 10000 mg/L Cl); this agrees with the distribution in Figure 12.1. Secondly, the majority of accurately estimated points fall within the lowest (< 150 mg/L) and highest (>10 000 mg/L) FRESHEM chloride classes. The points in the brackish FRESHEM classes (> 150 mg/L and < 10 000 mg/L) do not match very well.

Figure 12.6 shows the validation results spatially. There are no strong general spatial patterns in Zeeland. There are relatively many points giving a too low chloride classification in the upper 5 m of the soil. This coincides with brackish zones. Excluding shallow (<10 m below surface) well screen data results in roughly 5% more agreement for the given percentages: 65% for p50, 80% for p25 and p75, and 87% for p10 and p90 class bounds.

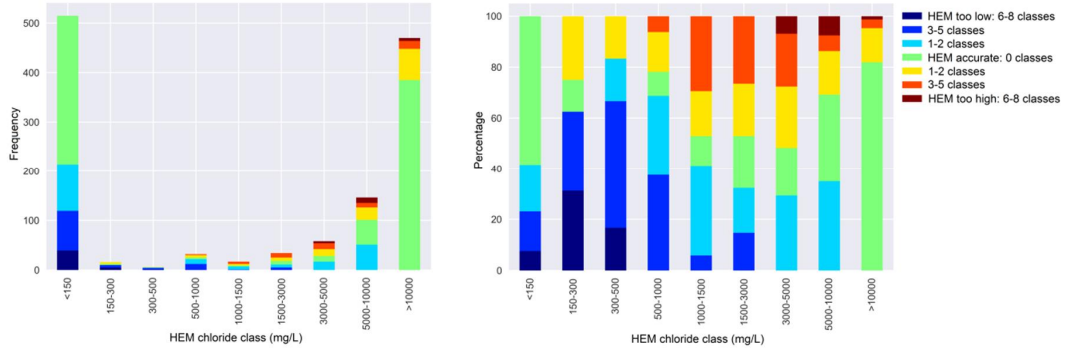


Figure 12.5 Left: validation result per chloride class for FRESHEM result 'middle', absolute number. The green bars represent 59% of the monitoring wells. Right: Validation result per chloride class for the FRESHEM result 'middle', relative per chloride class.

The median concentration of the available time series is a good estimator of the stationary chloride distribution. The median values have been computed taking only measurements after the year 2000; this amounts to 395 well screens of which the majority has been sampled many times. For the same well screens, the median values have also been computed taking all measurements. Only 7% of the well screens show more than one class difference in chloride concentrations (85% shows no difference, 8% one class difference).

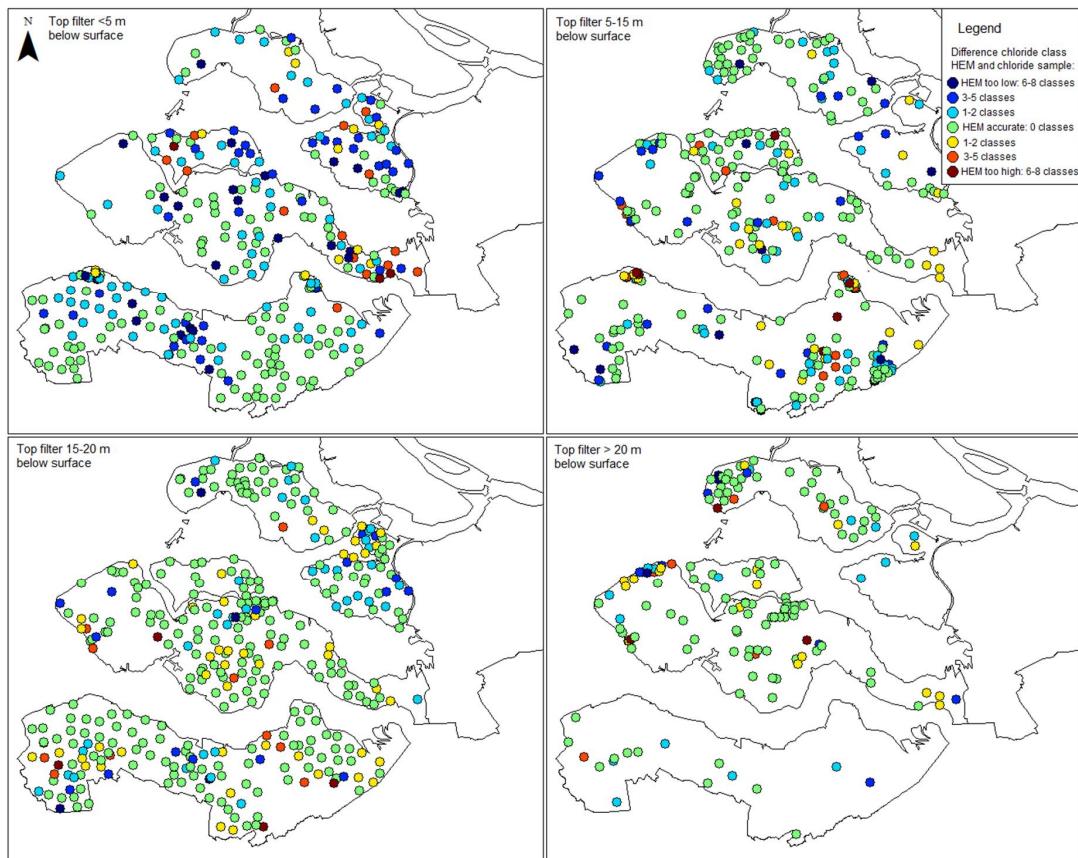


Figure 12.6: Validation chloride results for p50 FRESHEM result separated per filter depth.

12.3 Geophysical ground measurements

12.3.1 Data and methods

Table 12.1 shows an overview of available geophysical ground measurements used in this validation step. The ground measurements are originally expressed in bulk electrical conductivity (mS/cm). This bulk conductivity is not solely dependent on groundwater salinity, but also on lithology. Additionally, the absolute EC range is not consistent for the different types of measurements. Therefore, the ground measurement data could not simply be converted into the chloride classes of the FRESHEM result. Rather, the ground measurements have been used to determine the starting and end depth of the fresh-saline mixing zone. The depth of the fresh-saline mixing zone is a major focus of the FRESHEM study. A starting depth and end depth has also been estimated from the FRESHEM result, and these starting depths have been compared to further validate the FRESHEM results.

As the influence of lithology on the ground measurement results requires some geohydrological knowledge to reliably interpret the starting depth of the mixing zone, an automated procedure to determine the starting depth from the ground measurements and the FRESHEM result was impossible. Instead, the starting depth of the mixing zone was visually estimated for both the ground measurements and the FRESHEM result. An example is shown in Figure 12.8.

No clear fresh-saline mixing zone is present in many of the ground measurements. Lithology may cause an increase in conductivity without the presence of saline groundwater. Hence, a conservative approach has been used, where only ground measurement with bulk EC's exceeding 6 mS/cm have been used in the validation; an EC over 6 mS/cm almost certainly indicates chloride. For completely fresh profiles, no starting depth has been estimated. For completely salt profiles, the starting depth has been set at surface level. These choices, along with quality control, are the reason why the number of measurements used in table 1 is (much) smaller than the total number of available measurements. Areas without stable chloride distributions have been excluded also in this validation step (see the final paragraph of section 12.2.1).

VES (and CVES) data have not been used in this validation step. This has two primary reasons: firstly, the VES data are also the result of inverse modelling rather than a more direct measurement; secondly, the VES data give a sharp fresh-saline interface, which cannot be directly compared to the often gradual profiles in the FRESHEM results.

Table 12.1 Total number of available ground measurements in Zeeland, and the number of ground measurements used in the validation after all steps.

Type of ground measurement	Number available	Number used in start depth mixing zone	Percentage	Number used in thickness mixing zone	Percentage
Borehole measurement	143	39	27	35	24
CPT	213	127	60	111	52
SlimFlex	41	12	29	7	17
Total	397	178	45	153	39

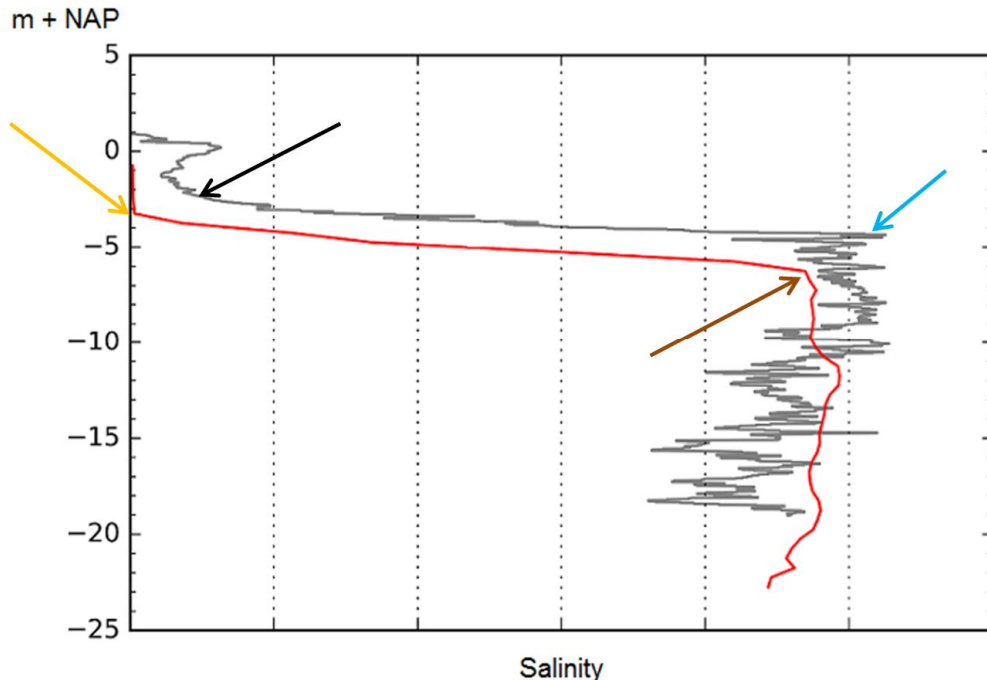


Figure 12.7 Example of visual determination of starting and end depth of fresh-saline mixing zone. The grey line is the EC profile of the ground measurement. The red line is the FRESHEM result for this location. The black arrow indicates the start of the mixing zone according to the ground measurement, at -2.0 m NAP. The orange arrow indicates the start of the mixing zone according to the FRESHEM result, at -3.0 m NAP. The brown arrow indicates the end of the mixing zone according to the FRESHEM result at -6 m NAP, and the blue arrow indicates the end of the mixing zone according to the ground measurement at -4.5 m. The increase and decrease of the EC around 0 m NAP is interpreted as a lithological feature, and not as the presence of saline groundwater; the noisy profile deeper than -4.5 m NAP is also caused by lithology rather than by fluctuating chloride concentrations.

12.3.2 Results

Quantitative validation results are shown in Table 12.2. Most of the FRESHEM starting mixing depths are close to those estimated from the ground measurements, as the mean absolute error is 1.5 m. There is slight bias in the FRESHEM result: depth of the fresh-saline mixing zone is somewhat overestimated. The histogram in Figure 12.8 and the qualitative validation results in Table 12.3 reinforce this notion: the majority of points is nicely in the zero class, but somewhat skewed towards positive numbers (the FRESHEM starting depth is deeper). Figure 12.10 shows the result spatially: there are no clear spatial patterns apparent on this scale. Looking more closely at the spatial pattern: ground measurements are biased towards 'easy-access locations', and therefore perhaps also biased towards locations with a somewhat different salinity distribution due to the presence of ditches, dikes, etc.

Table 12.2 shows that the predicted thickness of the mixing zone is also slightly overestimated in the FRESHEM results. Figure 12.9 shows the majority of points in the zero class, but the histogram is somewhat positively skewed. This may result from the footprint of the HEM measurements and the lower vertical resolution of FRESHEM when compared to ground measurements.

Table 12.2 Quantitative validation results of the FRESHEM result compared with ground measurements in terms of starting depth of the mixing zone.

	Mean absolute error (m)	Mean error or bias (m)*
Starting depth mixing zone	1.50	0.56
Starting dept mixing zone, worst 10% excluded	1.16	0.41
Thickness mixing zone	2.7	0.41
Thickness mixing zone, Worst 10% excluded	1.8	0.52

* Error is calculated as: starting depth FRESHEM – starting depth ground measurement. Positive error therefore indicates a larger value of the starting depth in the FRESHEM result compared to the ground measurement.

Table 12.3 Qualitative validation results of the FRESHEM result compared with ground measurements in terms of starting depth of the mixing zone.

Starting depth mixing zone HEM is ... than ground measurement	Number (total = 178)	Percentage
Less deep	43	24
Equal (<0.25 m)	54	30
Deeper	81	46

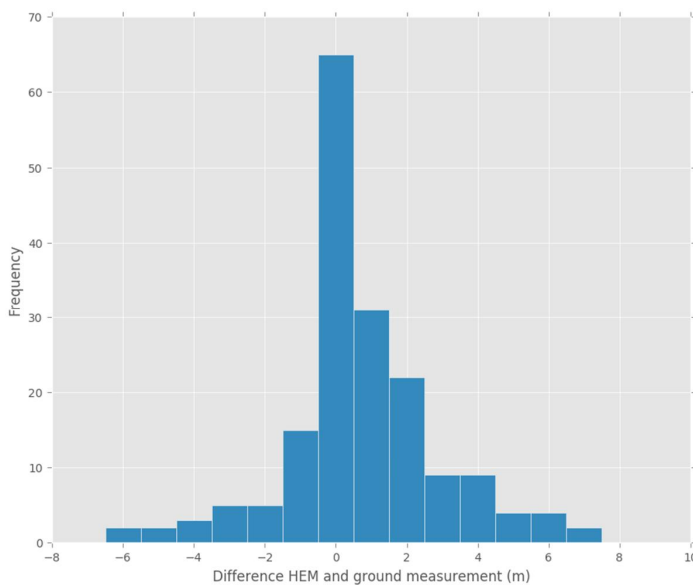


Figure 12.8 Histogram of the difference between the starting depth of the fresh-saline mixing zone as determined from the 3D FRESHEM result, and from the ground measurements. Positive values indicate larger value of the starting depth in the 3D FRESHEM result compared to the ground measurement.

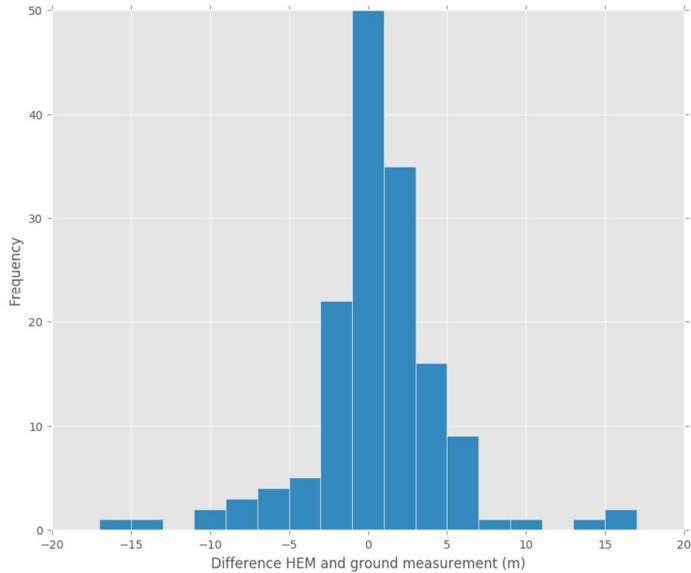


Figure 12.9 Histogram of the difference between the fresh-saline mixing zone thickness as determined from the 3D FRESHEM result, and from the ground measurements. Positive values indicate larger value of the mixing zone thickness in the 3D FRESHEM result compared to the ground measurement.

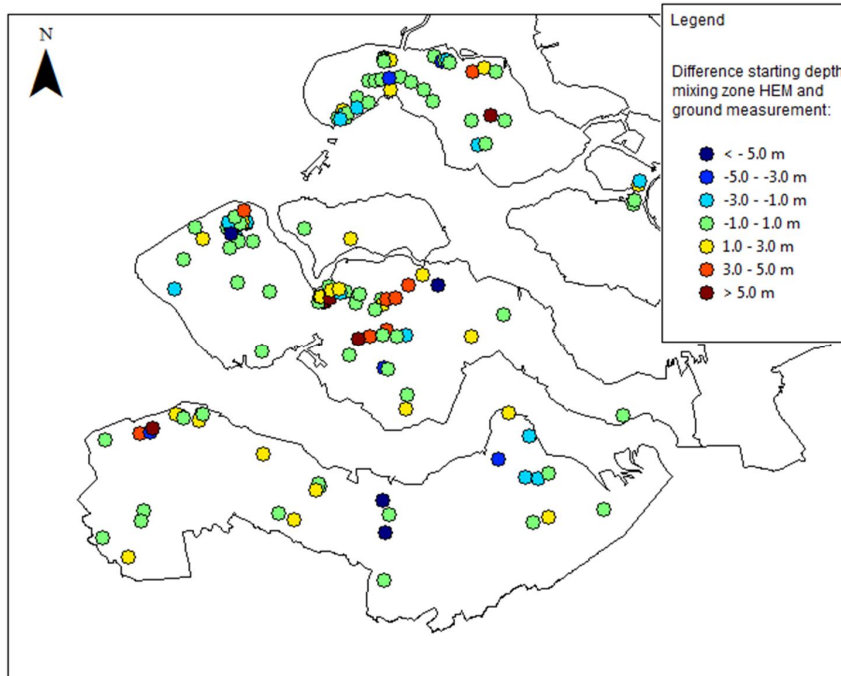


Figure 12.10 Validation result difference starting depth of fresh-saline mixing zone. Positive values indicate larger value of the mixing zone starting depth in the 3D FRESHEM result compared to the ground measurement.

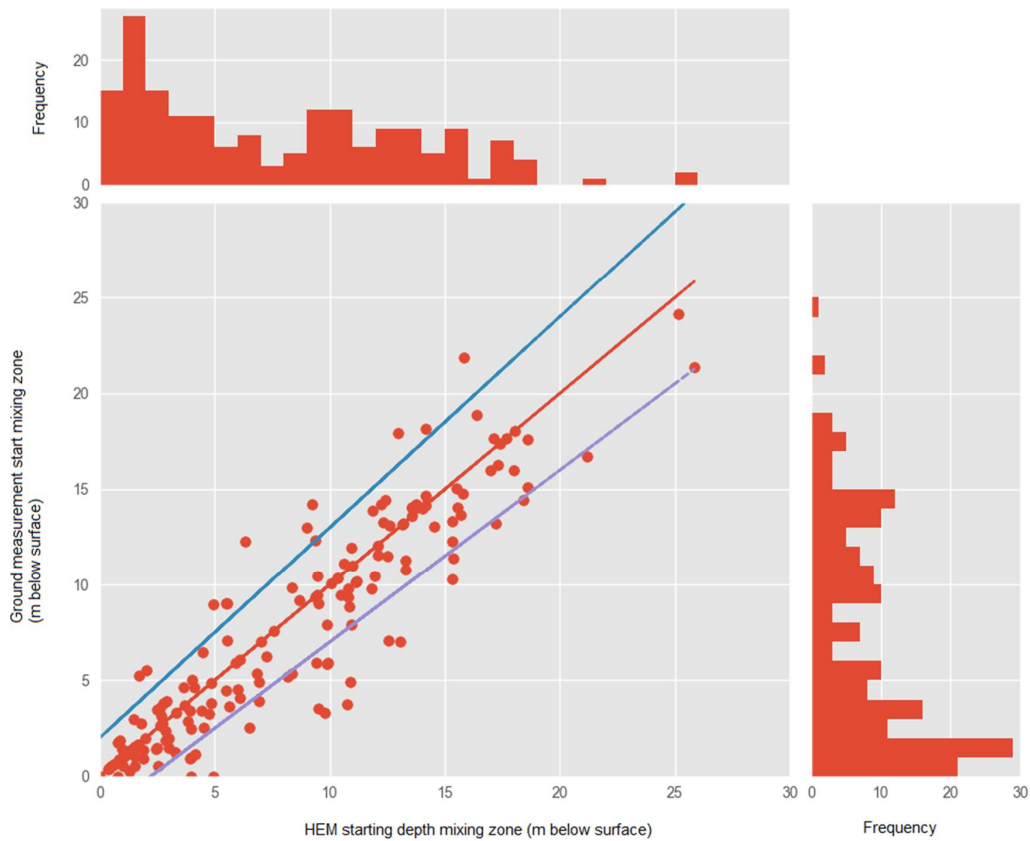


Figure 12.11 Scatterplot of HEM starting depth of the fresh salt-mixing zone versus ground measurement starting depth. The red line indicates the 1:1 relationship. The blue line gives an upper bound estimate on the starting depth of the mixing zone, and the purple line gives a lower bound estimate. Marginal histograms at the top and right show the distribution of the starting depths: many starting depths are shallow.

Figure 12.11 shows a scatterplot of the FRESHEM starting depth versus the ground measurement starting depth with upper and lower bounds. The bounds serve to give a simple estimate of uncertainty around the FRESHEM starting depth and were fitted visually. These bounds, in m below surface, are given by:

$$HEM_{bounds} = Depth_{HEM} \pm (2 + 0.1 \times Depth_{HEM}) \quad (12.1)$$

Where HEM_{bounds} (m below surface) are the upper and low HEM estimates of the starting depth, and $Depth_{HEM}$ (m below surface) is the 'middle' HEM estimate of the starting depth.

Essentially, uncertainty is equal to 2 m, increased by 10% of the HEM depth of the fresh-saline mixing zone; 80% of the ground measurements fall within these bounds (the area delineated by the blue and purple lines in Figure 12.11).

12.4 TEC probe

12.4.1 Data and methods

The results of the TEC probe have not been used to estimate the starting depth of the mixing zone, due to the limited measurement depth of this technique. Instead, these measurements have been used to indicate whether there is saline groundwater in the upper 1.5 - 4 m of the subsurface. There are 59 measurement points for the TEC probe available in Zeeland, and these measurements have been classified into 'fresh', 'saline', and 'unclear':

- 1 A measurement is classified 'fresh' when the EC does not exceed 4 mS/cm at any depth. This amounts to 19 points.
- 2 A measurement is classified 'saline' when the EC exceeds 6 mS/cm at some depth. This amounts to 22 points.
- 3 The remaining points are classified as 'unclear'. There might be saline water in the upper 4 m of the subsurface, causing an EC of over 4 mS/cm, or it might be due to lithology. Alternatively, the point is outside of the FRESHEM result or the data quality is insufficient.

Only the fresh and saline points are used in this validation step. These points are overlaid on a map of the 1500 mg/L Cl interface depth of the FRESHEM result. Figure 12.12 shows an example of two TEC probe overlaid on the fresh-saline water interface.

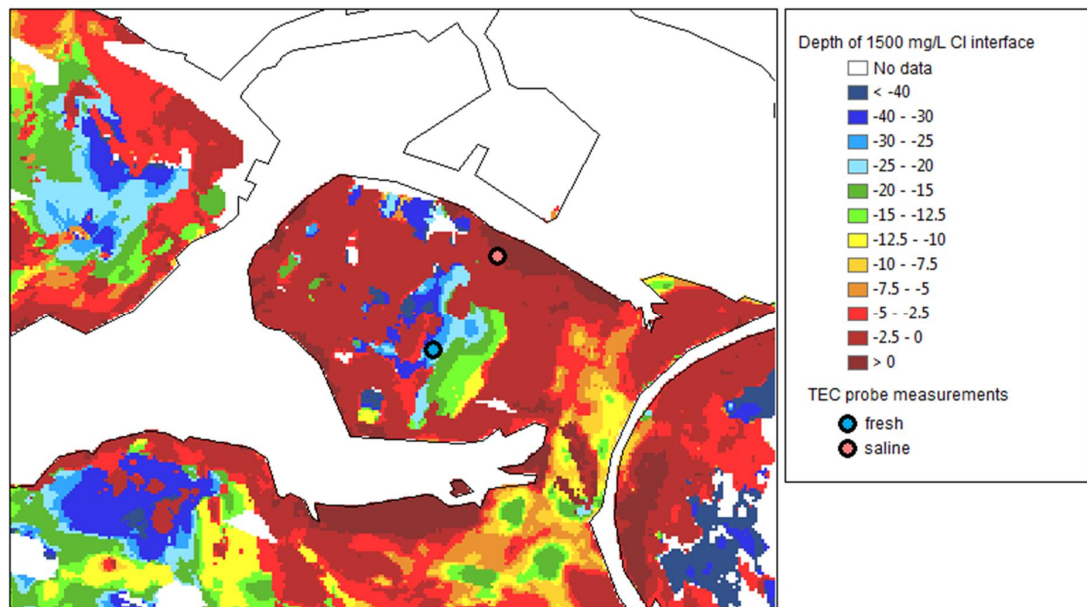


Figure 12.12 Example of two TEC probe measurements in St. Philipsland, Zeeland, overlaid on the depth below surface of the fresh-saline interface (defined by 1500 mg/L).

12.4.2 Results

19 of 22 (86%) TEC probe points classified as fresh are in an area that the FRESHEM results show as having a fresh-saline interface below 5 m; 17 of 19 (89 %) qualified as saline are in areas showing a fresh-saline interface within 5 m. Agreement for both fresh and saline points is 88%.

12.5 Discussion

12.5.1 Chloride measurements

Using the FRESHEM result, the following numbers may be useful to keep in mind. For the entirety of Zeeland, the 'middle' FRESHEM result provides chloride concentrations in detailed classes, which agree with available chloride measurements in roughly 60%; taking 'low' and 'high' FRESHEM results into account, agreement becomes 75%. When using FRESHEM as a predictor of fresh, brackish or saline water, agreement is roughly 80% for the 'middle' result, and roughly 90% when taking 'low' and 'high' into account. The reliability is lower in brackish zones, and the results should be used cautiously when looking at the chloride distribution around local features such as ditches. The FRESHEM result should not be used in isolation at a specific site, but in combination with all available data.

The chloride classes of the middle FRESHEM result agree for the majority of the points (59%) with the concentrations of the chloride measurements. However, it is important to note that even with perfect accuracy the FRESHEM result would not agree 100% with the chloride measurements. Errors in the chloride measurements aside, measured chloride concentrations represent a small volume, while the HEM measurements represent a far larger volume. Furthermore, monitoring wells are often immediately next to dikes or ditches, where the fresh-saline interface is generally shallower than in the surrounding area. This is a limitation of point measurements, and this is not represented by the uncertainty bounds of the FRESHEM result.

In general, the FRESHEM result show better agreement for either 'fresh' or 'saline', than for intermediate, brackish, chloride concentrations. This has three causes:

- 4 The brackish zone is a relatively small part of the subsurface and the brackish classes are quite narrow. An error of one metre in the fresh-saline interface will lead less quickly to differing chloride classes in the fresh and saline zone than in the brackish zone.
- 5 A saline zone is sometimes a very local feature, for example upconing of saline groundwater below ditches, while the footprint of a HEM measurement is much larger. The FRESHEM result effectively shows an averaged chloride concentration over a large area: fresh combined with the saline water under the ditch (hence brackish), while the chloride concentration in a monitoring well is a very local measurement: saline when very close to the ditch.
- 6 The effect of lithology on conductivity is sometimes difficult to separate from the effect of chloride: a low conductivity might indicate absence of clay and chloride, and a high conductivity indicates presence of chloride, but a medium conductivity may be caused both by clay and by chloride. The geological data does not have sufficient resolution to distinguish every clay layer.

Note that no quality control of the chloride measurements was performed, and e.g. typos could result in strange chloride concentrations, although the use of the median in time appears to give reliable concentrations. The majority of monitoring well filters is located in aquifers (sand), so effectively this step has not validated chloride concentrations in clay layers.

12.5.2 Geophysical ground measurements

Much of the chloride measurement validation discussion applies also to the ground measurements. The mean absolute error of the top of the FRESHEM fresh-salt boundary ('middle') compared to ground measurements is 1.5 m, 80% of the tops of the fresh-salt boundary in ground measurements fall within the bounds given in Figure 12.11. We did not

quantify the agreement given the range between the 'low' and the 'high' FRESHEM result due to the labour intensive process of visually estimating the depth of the mixing zone. Note again that FRESHEM results will always differ to some extent with ground measurements, for the reasons noted in section 12.5.1 (locality of features compared to HEM footprint, lithology, biased location of ground measurements).

For example, Figure 12.13 shows an example of two ground measurements in Zeeland. The difference between the starting depths with FRESHEM for the red point on the right is 5 m, while the difference with the green point on the left is only 1 m. This may be expected: the red point is between two ditches, and the shortest distance to the nearest flight line is 100 m. Neither the HEM measurement nor the interpolation procedure can accommodate for such local anomalies. Nonetheless, for the area on the whole, the FRESHEM result may give a more accurate estimate of the starting depth of the fresh-saline mixing zone than the ground measurement located at the red point: the FRESHEM result agrees with the other ground measurement at the green point.

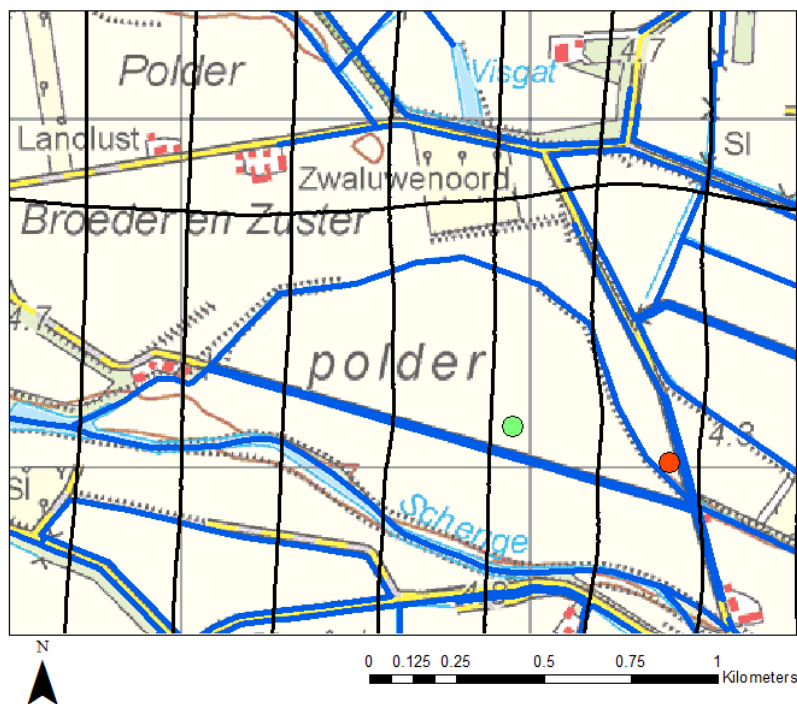


Figure 12.13 Location of two ground measurements in Schouwen-Duiveland, a kilometre north of Eindhoven. Thick black lines indicate flight lines of the HEM measurements and thick blue lines indicate ditches. The green point indicates a ground measurement where the difference between starting depths is 1 m; the red point indicates a ground measurement where the difference between starting depths is 5 m.

12.5.3 TEC probe

The TEC probe data were only suitable for a more qualitative validation approach, but the high percentages are in line with the results of the chloride and ground measurements.

13 Conclusions and recommendations

13.1 General conclusions

- FRESHEM approach produced the desired result: a spatially consistent, detailed, validated dataset of fresh-brackish-saline groundwater for the entire Province of Zeeland.
- The FRESHEM airborne surveys were flown within three two-week periods in 2014 and 2015 in addition to the two one-week surveys of the CLIWAT project flown in 2009.
- 9640 flight kilometres resulted in 1700 km² of mapped chloride distribution of the groundwater.
- The total number of data points collected by the helicopter during the FRESHEM Zeeland project was 13.6 million; this was added to the 0.8 million data points from the 2009 CLIWAT project.
- The full flight plan has been completed, including 8 high resolution areas. The flight-line separation was 100, 200 or 300 m.
- The FRESHEM dataset consists of:
 - 2D results of probability of groundwater chloride concentration classes along flightlines, ~4m horizontal resolution, vertical resolution ranging from 0.5 to several metres,
 - 3D results of probability of groundwater chloride concentration classes, 50*50m² horizontal resolution, 0.5 m vertical resolution,
 - derived maps such as depth of 150 mg Cl/l and 1500 mg Cl/l boundary.
- The depth range of the FRESHEM datasets varies between 30 metre in clay areas with saline groundwater up to 160 metres in sandy areas with fresh groundwater.
- The p50 value of the probability function of the groundwater chloride concentration is called the 'middle' value. The p25 value is the 'low' value and p75 the 'high' value.
- The transformation of bulk conductivity to groundwater chloride concentration was based on an elaborate dataset of 71 typical Zeeland soil samples. Samples were collected in the field and the intrinsic formation factor and surface conductivity was determined in the laboratory. All lithology types (including fine sand) show significant surface conductivity; surface conductivity must therefore be accounted for to correctly obtain groundwater chloride concentrations from bulk conductivity.

13.2 Conclusions regarding the result in Zeeland

- 25% (20-30% including uncertainty) of Zeeland has a fresh groundwater lens (<1500 mg Cl/l) with a thickness of more than 15 m.
- 40% (35-50%) of Zeeland has no or only a small fresh groundwater lens (<1500 mg Cl/l).
- FRESHEM resulted in new insights in the groundwater system of Zeeland:
 - More fresh groundwater in areas of Noord-Beveland, Tholen, Eastern part of Schouwen-Duiveland and the dune area and sandy creek ridges of Walcheren.
 - Shallow saline groundwater in the eastern part of Zeeland and less fresh groundwater than expected in Schouwen-Duiveland and the western part of Noord-Beveland.
 - Large extents of freshwater occurring below saline groundwater.
 - Off-shore fresh groundwater.
- FRESHEM showed that HEM measurements are promising to identify lithological units in Zeeland:
 - Resistivity differences within fresh water bodies can be used to identify clayey and sandy units.

- Layers with a low resistivity (currently interpreted as a high chloride concentration) in a freshening environment can serve as a proxy for clay content.
- Location of freshening of groundwater as a proxy for clay discontinuity.
- Width of the fresh water at creek ridges as an indication of clay occurrence

13.3 How does the FRESHEM result compare to ground-truth measurements?

- The final 3D result was validated with the chloride concentration from 1294 monitoring wells, the thickness of the freshwater lens from 178 geophysical ground-truth measurements and the presence of saline groundwater in the shallow subsurface from 41 TEC probe measurements.
- All ground truth measurements from the year 1900 until 2016 were used in the validation, except for local areas with significant salinisation or freshening in the past. There was no correction for the location of the ground truth measurement (often next to a ditch or dike since this makes access easier). There was no correction for the footprint of the HEM measurements.
- Using a classification of 'fresh' (< 1500 mg/L Cl), 'brackish' (1500 – 10000 mg/L Cl), and 'salt' (>10000 mg/L Cl), 78% of measured chloride points from monitoring wells are in agreement with the HEM 'middle' result (88% of measured chloride points fall within bounds given by HEM result 'low' and 'high'). These percentages increase with depth since local effects are often only present at shallow depth.
- For 80% of the ground-truth geophysical measurements, the depth of the top of the fresh-salt boundary falls within the bounds given by the following equation:

$$HEM_{bounds} = Depth_{HEM} \pm (2 + 0.1 \times Depth_{HEM})$$

Where HEM_{bounds} (m below surface) are the upper and low HEM estimates of the top of the fresh-salt boundary, and $Depth_{HEM}$ (m below surface) is the 'middle' HEM estimate of the top of the fresh-salt boundary.

- The HEM result agrees with 88% of the selected TEC probe measurement locations in terms of the shallow (within 4m from ground surface) occurrence of saline or fresh groundwater.
- The uncertainty in the thickness of the fresh groundwater lens increases in areas with no-data: above power lines, railways, roads, build-up areas, radar and canals with boats with radar. In areas with good data collection the uncertainty is in general less than 2 metre or less than 20% of the depth of the fresh-salt boundary of FRESHEM 'middle'.
- The following should be kept in mind when using the FRESHEM result. The FRESHEM result gives accurate, but not perfectly accurate information on the chloride distribution in Zeeland. The result is more reliable in fresh and saline zones, and less reliable in brackish zones. The result should be interpreted cautiously when looking at local features: it should for example not be used to estimate the chloride distribution around ditches.

13.4 What methodological advances were made in FRESHEM?

FRESHEM developed and applied novel approaches:

- to translate bulk resistivity in groundwater salinity using detailed lithological information and a novel set of formation factors and surface conductivity.
 - Freshwater occurrences in clayey sediments could be better discerned than applying the commonly used 6 Ωm bulk resistivity boundary. In 11% of the total line kilometres a freshwater lens (<150 mg Cl/l) was present where the 6 Ωm boundary was not present. For the 1500 mg Cl/l boundary this percentage is 15.
 - There is a difference in depth between the 6 Ωm boundary and the 150 mg Cl/l boundary in 34% of the survey area. For the 1500 mg Cl/l boundary the depth is different in 44 % of the survey area.

- This method improves the mapping of fresh groundwater in clay (previously mapped as saline) and brackish water in sand (previously mapped as fresh).
- This approach results in a chloride distribution of the groundwater, a parameter that is more suitable for use by stakeholders, given for example the different restrictions in absolute value of the salinity of the groundwater (horticulture, fruit cultivation, arable farming, drinking water, aquaculture, fresh and saline nature).
- to 3D interpolation, specifically designed to preserve features of the FRESHEM dataset.
 - Preserving the bimodal chloride distribution (groundwater is mostly fresh or saline, only a small percentage is brackish) in the interpolation prevented the incorrect mapping of brackish groundwater.
 - The developed guided-anisotropic interpolation procedure was able to preserve small scale features such as creek ridges in the 3D voxel model.
 - Uncertainty in the 3D model would be 30% higher if interpolation had been performed without the guided-anisotropy approach.
- to estimate and assess uncertainty of the different methodological steps in results.
 - Uncertainty stemming from the mathematical inversion, lithology (GeoTOP), formation factor and surface conductivity, the salinity – chloride concentration relation and the 3D interpolation was characterised and combined to quantify the total uncertainty in the end-result.
 - Uncertainty is mainly caused by the inversion, surface conductivity, lithology and interpolation, less by the formation factor and the salinity-chloride relation.
 - The quantification of the uncertainty can guide the use of the FRESHEM results, for instance when planning and designing measures.
- in the use of inverse models to interpret raw electromagnetic measurements.
 - The most reasonable results within this study were achieved using the inverse methods SSI and LCI (both standard and sharp). These models are different but one is not 'provable' better. Therefore FRESHEM used 3 different inverse methods to include in the uncertainty.
 - The performance of different inverse models and model parameters was quantitatively assessed by comparison to two ERT profiles, conducted on flightlines. Resulting differences in RMS error between the different parameter sets were, however, either small, or inconclusive between the different inverse models.
 - The results of these models depend on the settings, but there are no settings that are 'provable' or in all circumstances better.
 - Point measurements as a-priori data are only locally beneficial: as 1294 chloride samples represent only 0.009% of the 14 million data points collected with the helicopter, this was not considered worthwhile to pursue.
 - Spatial a-priori data were not beneficial if used as area wide starting model. The starting models are too dominant in the inversion and decreased, not increased the quality of the inversion.
- The survey plan was designed with the help of a-priori information about the expected shape of fresh groundwater features.
 - The flight-line separation was 100, 200 or 300 m. Tie-line separation was 200, 1000 or 2000 m.
 - The flightlines were located perpendicular to (expected) small features or (expected) horizontal differences in salinity.
 - A flight-line separation of 100 m results in less uncertainty than a flight-line separation of 300 m.

- Validation with different types of ground truth measurements:
 - Chloride concentration from monitoring wells can be used to compare the absolute values after classification into chloride classes.
 - Geophysical ground-truth measurements can be used to validate the thickness of the freshwater lens or start of the brackish zone.
 - TEC probe measurements can be used to validate the presence or absence of shallow saline groundwater.

13.5 Recommendations for freshwater management in Zeeland

The detailed knowledge on the groundwater salinity distribution provided by FRESHEM Zeeland is a basis for improved groundwater management:

- Licensing of groundwater extraction wells should reflect the new information on the occurrence of freshwater. Licensing guidelines should be checked to ensure that they continue to guarantee a sustainable use of the available freshwater.
- The groundwater salinity distribution is an important parameter for the suitability of a certain location for either different measures, or the potential for the growth of certain crops. Opportunity maps for different measures and suitability maps for different crops can be improved using the improved groundwater salinity distribution.
- A regional water management plan should ensure sustainable freshwater use by promoting measures that increase freshwater availability, e.g. by storing fresh water in the subsurface.
- The groundwater salinity distribution serves as an improved starting point for other and new projects in the freshwater laboratory of the Province of Zeeland.
- We recommend to update the density dependent groundwater model of the Province of Zeeland with the measured groundwater salinity distribution. This will improve the prediction of effects of climate change, sea level rise, the increase in groundwater extractions, regional effects of local freshwater measures. The update will also improve the analysis of possible tipping points in water management.
- Update current monitoring strategies to reflect the latest insights in where we can expect either salinisation or freshening.
- Investigate whether the identified fresh groundwater present below saline groundwater in Zeeuws-Vlaanderen can be used as a strategic freshwater reserve, or perhaps in sustainable aquifer-storage-and-recovery schemes.
- We recommend to repeat the survey in the year 2035 in order to determine salinisation and freshening of the groundwater system.

13.6 Recommendations for future Airborne EM surveys

- Since line kilometres are expensive it is recommended to carefully design the flight plan. In areas where no small freshwater lenses are expected, it is recommended to choose a bigger distance between the flightlines. In areas where differences are expected (for example large groundwater extractions, sandy creek ridges) it is recommended to fly across and perpendicular to the fresh or saline feature. In areas where differences between fresh and saline groundwater are expected but the exact location is unknown (but important), 100 metre between the flightlines is recommended.
- Further research is necessary to apply the FRESHEM approach to other, more data-scarce areas. For example, the developed approach relies on detailed information on the lithological make-up of the shallow subsurface, information that is not always available. As there is still a significant range in surface conductivity within defined GeoTOP lithoclasses, it may well be that the characterised uncertainties in lithoclass and surface conductivity (chapter 10) overlap, and some of the added uncertainty in not exactly knowing the lithology is therefore mitigated.

- Extend the current soil-surface conductivity dataset with local soil samples to characterise the surface conductivity and intrinsic formation factor of locally occurring lithology types. Helpful in this regard may be using the normalized chargeability as a proxy for surface conductivity, as this parameter can be more easily estimated for soil samples (Revil et al., 2017).
- Combine laboratory and field approaches to better estimate the electromagnetic properties of soils: in particular the intrinsic formation factor and the non-linear behaviour of the surface conductivity at low conductivities.

13.7 Recommendations for further research

- Better investigate and thereby validate the new insights in the groundwater system that FRESHEM offered, for instance the large amounts of freshwater found below saline groundwater in amongst others Zeeuws-Vlaanderen.
- More research is needed to improve the inversion of raw measurements to vertical resistivity profiles. Possible research angles include:
 - Only 1D and pseudo-2D (LCI) algorithms were used in the inversion, but the pseudo-3D (SCI) algorithm was not fully explored. It is computational heavy, but a smaller area can be selected and benefits can be quantified. We need to make adjustments on the settings (lateral and vertical constraints, resample data every 1, 2 or more soundings, smoothness parameters). This way truly 3D effects will be taken into account and the footprint will be naturally implemented into the inversion process.
 - Attempts to use GeoTOP and groundwater model information as a-priori information did not result in better inversion results. That does not mean though that information from boreholes (SlimFlex, ECPT) or other surface geophysical data (i.e ERT) are not useful. Use of local a-priori data should be further investigated.
 - Joint-inversion with a groundwater model is a possible future research angle, to better include knowledge on groundwater flow and possibly palaeo evolution of groundwater salinity in the inversion.
 - A different approach is to even better characterise the uncertainty stemming from the inversion by including more inversion schemes than the current three in the procedure.
- Explore the use of magnetic and radiometric data, concurrently collected in the helicopter surveys. Radiometric data can provide information about the presence of clay, peat etc. We should explore how we can make use of those data. Additionally, magnetic data can be useful for archaeology as well as hydrocarbon exploration.
- Lithological information is present in the FRESHEM dataset as resistivity contrasts that are not caused by variation in groundwater salinity. The large amount of data that is collected by airborne EM systems calls for automatic, computerized algorithms to delineate meaningful spatial units (geological / hydrogeological). Clustering and Machine Learning techniques that can take into account prior knowledge about the structure and continuity of the geology can make the interpretation of the data more efficient.
- The interpolation method that had been developed for FRESHEM might be useful to model geological properties (top and base of lithological units, lithology) especially for formations that show a strong anisotropy. Fluvial deposits show a higher correlation parallel to the direction of river flow and interpolation with local anisotropy can help to make better estimates in between borehole locations.
- Extend the current relations between lithology and surface conductivity and intrinsic formation factor. Better techniques to characterise these parameters from collected soil samples must be devised, to decrease analysis times and to improve the reliability. Possibly use proxies for surface conductivity, as e.g. the cation-exchange-capacity, on

which perhaps more data exists. Measuring the normalized chargeability (Revil et al, 2017) may be helpful in this regard. Take special care to preserve the packing of the soil, especially with samples taken at greater depths.

- Explore the use of helicopter EM surveys to map the salinity of large bodies of brackish and saline surface water, and to map the bathymetry of these water bodies.

14 References

- Anderson W.L. 1989. A hybrid fast Hankel transform algorithm for electromagnetic modelling. *Geophysics* 54, 263-266.
- Archie, G., 1942. The electrical resistivity log as an aid in determining some reservoir characteristics. *Trans. AIME* 146, 54–62.
- Auken, E., Nebel, L., Sørensen, K. I., Breiner, M., Pellerin, L. and Christensen, N. B., 2002: "EMMA - A Geophysical Training and Education Tool for Electromagnetic Modelling and Analysis." *Journal of Environmental & Engineering Geophysics*, 7, 57-68.
- Auken, E. and Christiansen, A. V., 2004, Layered and laterally constrained 2D inversion of resistivity data *Geophysics*, 69, 752-761. [pdf](#)
- Auken, E., Christiansen, A. V., Jacobsen, B. H., Foged, N., and Sørensen, K. I., 2005: "Piecewise 1D Laterally Constrained Inversion of resistivity data". *Geophysical Prospecting*, 53, 497- 506.
- Auken, E. Viezzoli, A. and Christensen, A., 2009. A single software for processing, inversion, and presentation of AEM data of different systems: the Aarhus Workbench ASEG Extended Abstracts 2009(1) 1 - 5
- Baaren E.S. van, Oude Essink G.H.P., Janssen G.M.C.M., de Louw P.G.B., Heerdink R., Goes B. 2016. Verzoeting en verzilting van het grondwater in de Provincie Zeeland; Regionaal 3D model voor zoet-zout grondwater, Deltares rapport, 88 p.
- Baaren, E. van, Delsman, J., Pauw, P., Karaoulis, M., Dabekaussen, W., Gunnink, J., Siemon, B., 2016. FRESHEM Kanaalzone Gent- Terneuzen - 3D zoet-brak-zout kartering van het grondwater, Deltares rapport 1209220.
- Berendsen, H.J.A., 2000. *Landschappelijk Nederland. Vol IV, Fysische Geografie van Nederland.* Assen, van Gorcum.
- De Louw, P.G.B., Eeman, S., Siemon, B., Voortman, B.R., Gunnink, J.L., van Baaren, E.S., Oude Essink, G.H.P., 2011. Shallow rainwater lenses in deltaic areas with saline seepage. *Hydrol. Earth Syst. Sci.* 15, 3659–3678.
- De Louw, P.G.B., Eeman, S., Oude Essink, G.H.P., Vermue, E., Post, V.E.A. 2013. Rainwater lens dynamics and mixing between infiltrating rainwater and upward saline groundwater seepage beneath a tile-drained agricultural field. *J. Hydrology*, 501, 133-145, doi: 10.1016/j.jhydrol.2013.07.026
- De Louw, P.G.B., 2013. Saline seepage in deltaic areas. Preferential groundwater discharge through boils and interactions between thin rainwater lenses and upward saline seepage. Academic PhD-Thesis, Vrije Universiteit Amsterdam, ISBN/EAN 9789461085429.
- Delsman, J.R., Hu-a-ng, K.R.M., Vos, P.C., De Louw, P.G.B., Oude Essink, G.H.P., Stuyfzand, P.J., Bierkens, M.F.P., 2014. Paleo-modelling of coastal saltwater intrusion during the Holocene: an application to the Netherlands. *Hydrol. Earth Syst. Sci.* 18, 3891–3905. doi:10.5194/hess-18-3891-2014

Deutsch, C.V., and Wang, L., 1996, Hierarchical object-based stochastic modelling of fluvial reservoirs: *Math. Geol.*, v. 28, no. 7, p. 857–880.

Drabbe, J., Badon Ghijben, W., 1889. Nota in verband met de voorgenomen putboring nabij Amsterdam. *Tijdschr. Van Koninklijk Instituut Van Ingenieurs* 5, 8–22 (in Dutch).

Edzer J. Pebesma (2004) Multivariable geostatistics in S: the gstat package, *Computers & Geosciences*, Volume 30, Issue 7, August 2004, Pages 683-691.

Eeman, S., Van der Zee, S.E.A.T.M., Leijnse, A., De Louw, P.G.B., Maas, C., 2012. Response to recharge variation of thin rainwater lenses and their mixing zone with underlying saline groundwater. *Hydrol. Earth Syst. Sci. Earth Syst. Sci.* 16, 3535–3549. doi:10.5194/hess-16-3535-2012

Fraser D.C. 1978. Resistivity mapping with an airborne multicoil electromagnetic system. *Geophysics* 43, 144-172.

Gieske, J. M. J., 1991. De oorsprong van het brakke grondwater in het IJsselmeergebied: diffusie, dispersie, of dichtheidsstroming? (Origin of brackish groundwater in the IJsselmeer area: diffusion, dispersion or density-driven flow? *H2O* 24 (7), 189–193.

Goes en Vernes, 2000. REGIS Zeeland Deelrapport C: Zoet, brak en zout grondwater. TNO rapport TNO-034-UT-2010-01833/A

Goes, B.J.M., Oude Essink, G.H.P., Vernes, R.W., Sergi, F., 2009. Estimating the depth of fresh and brackish groundwater in a predominantly saline region using geophysical and hydrological methods, Zeeland, the Netherlands. *Near Surf. Geophys.* 401–412.

Greskowiak, J., 2014. Tide-induced salt-fingering during submarine groundwater discharge. *Geophys. Res. Lett.* 41, 6413–6419. doi:10.1002/2014GL061184. Received

Lebbe, L.C., 1978. Hydrogeologie van het duingebied ten westen van De Panne. Rijksuniversiteit Gent.

Goovaerts, P. (2006). *Geostatistics for natural resource evaluation*. New York: Oxford University Press.

Gunnink, J., Bosch, J.H.A. Siemon, B., Roth, B. & Auken, E., 2012. Combining ground-based and airborne EM through Artificial Neural Networks for modelling glacial till under saline groundwater conditions. *Hydrology and Earth System Sciences*, 16, 3061–3074, doi: 10.5194/hess-16-3061-2012

Hageman, B.P., 1964. *Blad Goeree en Overflakkee, Toelichting bij de Geologische Kaart van Nederland, 1 : 50.000*. Rijks Geologische Dienst Haarlem, 89 pp.

Herzberg, A., 1901. Die Wasserversorgung einiger Nordseebäder. *J. Gasbeleucht. Wasserversorgung* 44, 815-819 (in German).

Hodges G. and Siemon B. 2008. Comparative analysis of one-dimensional inversions of Helicopter-borne frequency-domain electromagnetic data. In: *Proceeding on AEM2008 – 5th International Conference on Airborne Electromagnetics*, 28-30 May 2008, Haikko Manor, Finland.

Huang H. 2008. Airborne geophysical data levelling based on line-to-line correlations. *Geophysics* 73, F83-F89.

Isaaks, E. H. and Srivastava, R. M., 1989. An Introduction to Applied Geostatistics. New York, Oxford University Press, 561 p.

Johansen H.K. and Sørensen K. 1979. The fast Hankel transform. *Geophysical Prospecting* 27, 876-901.

Kirsch R. 2006. Hydrogeophysical properties of permeable and low permeable rocks. In: Kirsch R. (Ed.) *Groundwater Geophysics – A Tool for Hydrogeology*. Springer-Verlag, Berlin, Heidelberg, 1-22.

Knödel, K, Lange, G & Voigt, H.-J., 2007. *Environmental Geology – Handbook of Field Methods and Case Studies*. Springer-Verlag Berlin-Heidelberg

Kooi, H., & Groen, J. (2001). Offshore continuation of coastal groundwater systems; predictions using sharp-interface approximations and variable-density flow modelling. *Journal of Hydrology*, 246(1-4), 19–35. doi:10.1016/S0022-1694(01)00354-7

Maas, E.V. and G.J. Hoffman, 1977. Crop Salt Tolerance - Current Assessment. *J. Irr.Drain.Div.* 1977(6):115-134.

Menke, W., 1989. *Geophysical data analysis discrete inverse theory*. International Geophysics Series, Volume 45, Academic Press, San Diego, CA.

Oude Essink GHP (1996) Impact of sea level rise on groundwater flow regimes; a sensitivity analysis for the Netherlands. PhD TU Delft, Delft Studies in Integrated Water Management No.7, 411p

Oude Essink, G.H.P., van Baaren, E.S., Zuurbier, K.G., Velstra, J., Veraart, J., Brouwer, W., Faneca Sánchez, M., Pauw, P.S., de Louw, P.G.B., Vreke, J., Schoevers, M. 2014. GO-FRESH: Valorisatie kansrijke oplossingen voor een robuuste zoetwatervoorziening, KvK 151/2014, ISBN EAN 978-94-92100-12-2, 84 p.

Paine, J.G., Minty, B.R.S., 2006, *Airborne geophysics for hydrology*

Pauw, P.S., Van Baaren, E.S., Visser, M. De Louw, P.G.B., Oude Essink, G.H.P., 2015, Increasing a freshwater lens below a creek ridge using a controlled artificial recharge and drainage system: a case study in the Netherlands, *Hydrogeology Journal*. doi: 10.1007/s10040-015-1264-z

Pauw, P.S., Groen, J., Groen, M.M.A., van der Made, K.J., Stuyfzand, P.J., Post, V.E.A., 2017. Groundwater salinity patterns along the coast of the Western Netherlands and the application of cone penetration tests. *J. Hydrol.* doi:10.1016/j.jhydrol.2017.04.021

Pebesma, E.: *Threedimensional interpolation of subsurface chloride concentrations in the Netherlands*, 2009.

Post, V. E. A. (2003). *Groundwater salinisation processes in the coastal area of the Netherlands due to transgressions during the Holocene*. PhD thesis, VU Amsterdam.

Post, V. E. a., & Simmons, C. T. (2009). Free convective controls on sequestration of salts into low-permeability strata: insights from sand tank laboratory experiments and numerical modelling. *Hydrogeology Journal*, 18(1), 39–54. doi:10.1007/s10040-009-0521-4

13 June 2017, draft

Revil, A., Glover, P., 1997. Theory of ionic-surface electrical conduction in porous media. *Phys. Rev. B* 55, 1757–1773.

Revil, A., Glover, P.W.J., 1998. Nature of surface electrical conductivity in natural sands, sandstones and clays. *Geophys. Res. Lett.* 25, 691–694.

Revil, A., Karaoulis, M., Johnson, T., Kemna, A., 2012. Review: Some low-frequency electrical methods for subsurface characterization and monitoring in hydrogeology. *Hydrogeol. J.* 20, 617–658.

Revil A., A. Coperey, Z. Shao, N. Florsch, I.L. Fabricius, J. Delsman, P. Pauw, M. Karaoulis, P. G. B. de Louw, E.S. van Baaren, W. Dabekaussen, A. Menkovic, and J. L. Gunnink. Complex conductivity in soils. accepted for publication in *Water Resour. Res.*

Schaars, F. 2014. Elektromagnetisch onderzoek vanuit de lucht ter bepaling van de verziltingstoestand van het grondwater in het oostelijk gedeelte van de kustvlakte.

Sengpiel K.P. 1983. Resistivity/depth mapping with airborne electromagnetic survey data. *Geophysics* 48, 181-196.

Sengpiel K.P. 1990. Theoretical and practical aspects of groundwater exploration using airborne electromagnetic techniques. In: Fitterman D.V. (Ed.) *Developments and application of modern electromagnetic surveys*. U.S. Geological Survey Bulletin 1925, 149-154.

Sengpiel K.P. and Siemon B. 2000. Advanced inversion methods for airborne electromagnetics. *Geophysics* 66, 1983-1992.

Siemon B. 2001. Improved and new resistivity-depth profiles for helicopter electromagnetic data. *Journal of Applied Geophysics* 38, 65-76.

Siemon B. 2006a. Electromagnetic methods – frequency domain: Airborne techniques. In: Kirsch, R. (Ed.), *Groundwater Geophysics – A Tool for Hydrogeology*. Springer-Verlag, Berlin, Heidelberg, 155-170.

Siemon B. 2006b. HEM data processing and interpretation at BGR. *Extended Abstracts Book, AEM Workshop Hannover 2006, Airborne EM Recent Activities and Future Goals*, 45-49.

Siemon B., Auken E. and Christiansen A.V. 2009a. Laterally constrained inversion of frequency-domain helicopter-borne electromagnetic data. *Journal of Applied Geophysics*, 67 (3), 259-268, doi: 10.1016/j.jappgeo.2007.11.003.

Siemon, B., Christiansen, A.V. & Auken, E., 2009b. A review of helicopter-borne electromagnetic methods for groundwater exploration. *Near Surface Geophysics*, 7, 629-646, doi: 10.3997/1873-0604.2009043.

Siemon B. 2009. Levelling of frequency-domain helicopter-borne electromagnetic data. *Journal of Applied Geophysics*, 67 (3), 206-218, doi: 10.1016/j.jappgeo.2007.11.001.

Siemon, B., Ullmann, A., Mitreiter, I., Ibs-von Seht, M., Voß, W. & Pielawa, J., 2011a. Airborne geophysical investigations of CLIWAT pilot areas – Survey area Schouwen, The Netherlands, 2009. Technical Report, Interreg IVB Project: CLIWAT – Adaptive and sustainable water management and protection of society and nature in an extreme climate, BGR Archiv-Nr. 0129932, Hannover.

Siemon, B., Ullmann, A., Mitreiter, I., Ibs-von Seht, M., Voß, W. & Pielawa, J., 2011b. Airborne geophysical investigations of CLIWAT pilot areas – Survey area Perkpolder, The Netherlands, 2009. Technical Report, Interreg IVB Project: CLIWAT – Adaptive and sustainable water management and protection of society and nature in an extreme climate, BGR Archiv-Nr. 0130011, Hannover.

Siemon, B., Steuer, A., Ullmann, A., Vasterling, M. & Voß, W., 2011c. Application of frequency-domain helicopter-borne electromagnetics for groundwater exploration in urban areas. *Journal of Physics and Chemistry of the Earth*, 36/16, 1373-1385, doi:10.1016/j.pce.2011.02.006.

Siemon, B., 2012. Accurate 1D forward and inverse modelling of high-frequency helicopter-borne electromagnetic data. *Geophysics*, 77 (4), WB81-WB87, doi: 10.1190/GEO2011-0371.1.

Siemon, B., Pielawa, J., Petersen, H., Voß, W., Balzer, H.-U. & Plath, C., 2014. Zwischenbericht Hubschraubergeophysik – Befliegung Zeeland, Teil 1: 160 Terneuzen, 161 Waterdunen, 162 Zeeuws-Vlaanderen, 163 Zeeuws-Vlaanderen-East, Oktober 2014. BGR-Bericht, Archiv-Nr. 0132295, Hannover.

Siemon, B., Costabel, S., Voß, W., Meyer, U., Deus, N., Elbracht, J., Günther, T. & Wiederhold, H., 2015a. Airborne and ground geophysical mapping of coastal clays in Eastern Friesland, Germany. *Geophysics*, 80 (3), WB21-WB34, doi: 10.1190/GEO2014-0102.1.

Siemon, B., Pielawa, J., Petersen, H., Voß, W., Balzer, H.-U. & Plath, C., 2015b. Zwischenbericht Hubschraubergeophysik – Befliegung Zeeland, Teil 2: 163 Zeeuws-Vlaanderen-East, 164 Hedwigepolder, 165 Dunes-Schouwen, 166 Duiveland, 167 Tholen, 168 Eendracht, März 2015. BGR-Bericht, Archiv-Nr. 0132585, Hannover.

Siemon, B., Pielawa, J., Petersen, H., Voß, W., Balzer, H.-U. & Plath, C., 2015c. Zwischenbericht Hubschraubergeophysik – Befliegung Zeeland, Teil 3: 163 Zeeuws-Vlaanderen-East, 165 Dunes-Schouwen, 169 Walcheren, 170 Beveland, 171 Beveland-East, 172 Waterfarm, 173 Oost-Souburg, 174 Kreek-Terug, August/September 2015. BGR-Bericht, Archiv-Nr. 0133100, Hannover.

Staffeu, J., Maljers, D., Gunnink, J.L., Menkovic, A. and Busschers, F.S., 2011. 3D modelling of the shallow subsurface of Zeeland, the Netherlands. *Netherlands Journal of Geosciences*, 90, 293-310

Steuer A., Siemon B. and Viezzoli A. 2008. Application of spatially constraint inversion on HEM and SkyTEM data. In: *Proceeding on AEM2008 – 5th International Conference on Airborne Electromagnetics*, 28-30 May 2008, Haikko Manor, Finland.

Strebelle, S., 2002, Conditional simulation of complex geological structures using multiple-point statistics: *Math. Geol.*, 34, no. 1, p. 1–21.

Stroet, C. and J. Snepvangers (2005). Mapping Curvilinear structures with Local Anisotropy Kriging. *Mathematical Geology*, 37(6), 979-988

Stuyfzand, P.J., 1986. A new hydrochemical classification of water types with examples of application to the Netherlands (in Dutch). *H2O*. 19(23), pp. 562-568

Stuyt, L.C.P.M., van Bakel, P.J.T., Delsman, J., Massop, H.T.L., Kselik, R.A.L., Paulissen, M.P.C.P., Oude Essink, G.H.P., Hoogvliet, M. en Schipper, P.N.M., 2012, *Zoetwatervoorziening in het*

Hoogheemraadschap van Rijnland; Onderzoek met hulp van €ureyeopener 1.0, 93 p. Alterra-rapport 2439.

TNO-GSN, in press, REGIS II v2.2, 3D hydrogeological reference model of the Netherlands, to be published at www.dinoloket.nl

Valleau N. 2000. HEM data processing – a practical overview. *Exploration Geophysics* 31, 584-594.

Van Rummelen, F.F.F.E., 1965. Zeeuwsch Vlaanderen, Bladen Zeeuwsch-Vlaanderen, West en Oost, Toelichting bij de Geologische Kaart van Nederland, 1 : 50.000. Rijks Geologische Dienst Haarlem, 79p.

Van Rummelen, F.F.F.E., 1972. Blad Walcheren, Toelichting bij de Geologische kaart van Nederland 1:50.000. Rijks Geologische Dienst, Haarlem, 120 pp.

Vernes, R.W., Hummelman, H.J. & Menkovic, A., 2010. REGIS Zeeland, Deelrapport B: Hydrogeologische opbouw en hydraulische eigenschappen van Holocene afzettingen. TNO, Report 034-UT-2010-01647/A, 74 pp.

Viezzoli A., Siemon B., Christiansen A.V. and Auken E. 2008. Spatially Constrained Inversion of HEM data: The Banda Aceh case study. In: *Proceeding on AEM2008 – 5th International Conference on Airborne Electromagnetics*, 28-30 May 2008, Haikko Manor, Finland.

Viezzoli, A., Christiansen, A. V., Auken, E., and Sørensen, K. I., 2008, Quasi-3D modelling of airborne TEM data by Spatially Constrained Inversion Geophysics, 73, F105-F113. [pdf](#)

Vignoli, G., Fiandaca, G., Christiansen, A. V., Kirkegaard, C., and Auken, E., 2015, Sharp spatially constrained inversion with applications to transient electromagnetic data *Geophysical Prospecting*, 63, 243-255. [pdf](#)

Vos, P. & S. de Vries 2013: 2e generatie palaeogeografische kaarten van Nederland (versie 2.0). Deltares, Utrecht. Op 9 mei 2017 gedownload van www.archeologieinnederland.nl

Wait J.R. 1982. *Geo-electromagnetism*. Academic Press, New York

Ward S.H. and Hohmann G.W. 1988. Electromagnetic theory for geophysical applications. In Nabighian M.N. (Eds.) *Electromagnetic methods in applied geophysics Vol. 1, Theory*. Society of Exploration Geophysics, IG no 3, Tulsa, 130-310.

Waxman, M., Smits, L., 1968. Electrical conductivities in oil-bearing shaly sands. *Soc. Pet. Eng. J.* 243, 107–122.

Zuurbier, 2016, Increasing freshwater recovery upon aquifer storage: A field and modelling study of dedicated aquifer storage and recovery configurations in brackish-saline aquifers, PhD thesis, TUDelft, 220 p.